Polymeric Excipients for the Enhanced Oral Delivery of Poorly Soluble Pharmaceutical Compounds

A DISSERTATION
SUBMITTED TO THE FACULTY OF
UNIVERSITY OF MINNESOTA
BY

Lindsay Michelle Johnson

IN PARTIAL FULFILLMENT OF THE REQUIREMENTS
FOR THE DEGREE OF
DOCTOR OF PHILOSOPHY

Marc A. Hillmyer, Advisor

March 2019

Acknowledgements

My time spent in graduate school has been era of great scientific, professional, and personal growth, and I would like to thank those in my life who have been a part of this process.

First and foremost, I would like to thank my advisor, Professor Marc Hillmyer, for his guidance through this experience. I learned a tremendous amount on how to be scientist through his insistence on scientific rigor and his instruction on the experimental process. I will always be grateful for the opportunity to learn, both directly and indirectly, from him.

I have also had the great fortune of learning from several professors, namely: Timothy Lodge, Theresa Reineke, and Frank Bates. Their scientific insights and helpful suggestions pushed my growth as a researcher, and I thank them for their time and encouragement.

My research was funded by The Dow Chemical Company, and for this collaboration, I thank Dr. William "Trey" Porter, Dr. Jodi Mecca, Dr. Timothy Young, Dr. Steven J. Guillaudeu, and Dr. Robert L. Schmitt. I enjoyed working alongside of many talented peers on this project, including: Dr. Ralm Ricarte, Ziang Li, Dr. Ligeng Yin, Anatolii Purchel, Dr. Jeffrey Ting, and Swapnil Tale, and others. This work was funded through agreement 22429AT with the University of Minnesota.

During my graduate school tenure, I was fortunate to mentor an undergraduate researcher, Andrew LaBelle. I would like to thank him for his work, and for the opportunity

he gave me to grow as a mentor. He was always ready to work, and ready to make work fun.

The graduate students, post-doctoral researchers, and staff members with whom I have shared time and space with have made my time in the program enjoyable and have contributed to my growth both as a scientist and as a person. In particular, a few people deserve a special thank you: Joahanna Macaranas, Dr. Megan Weisenberger, Dr. Victoria Szlag, Dr. Kailey Soller, Leon Lille, Derek Batiste, Dr. Mammad Nasiri, Annabelle Watts, Dr. Theodoros (Teddy) Vasilakopoulos, Dr. Benjamin Neisen, Dr. Alex Todd and Katie Zadrozny, Hussnain Sajjad, Craig Van Bruggen, Dr. James Gallagher, Ingrid Haugan, Dr. Stacey Saba, Stephanie Stathopoulos, and Dr. Letitia Yao.

Part of my time in graduate school included working closely with the American Chemical Society (ACS), and the ACS Graduate Education Advisory Board. For their support, and the opportunities they gave me to contribute to initiatives that were important to me, I thank: Dr. Joerg Schlatterer, Dr. Mary Kirchhoff, Nancy Bakowski, Dr. Steven Corcelli, Dr. Joseph Sostaric, Dr. Margaret Grow-Sadler, and Dr. Corrie Kuniyoshi.

I thank friends who lifted me up with laughter: Cordelia Weiss, Dara McCorkle, Trevor Johnson, Jubal Whitlock, Gini Thomas, and Joseph Dennis.

Finally, it is with the greatest love that I thank my father, David Johnson, and my grandmother, Valerie Johnson, for their support, encouragement, love, and senses of humor. They were always only a phone call away, even though that still felt too far sometimes.

Dedication

To all those suffering from disease, infection, illness, or injury

Abstract

The majority of the next generation of pharmaceutical actives that have been discovered to treat diseases, infections, and illnesses are poorly soluble in water, making their inherent bioavailability low and their effective delivery challenging. Poor solubility of a drug can be overcome by formulating the pharmaceutical active into solid dispersions with a polymeric excipient, improving the overall bioavailability of the drug. Excipient choice is paramount to the ultimate behavior of the polymer-drug solid dispersion, and the relationship between excipient properties and solid dispersion behavior is poorly understood. This dissertation describes a systematic evaluation of polymeric materials for the solubility enhancement of phenytoin, a poorly soluble antiepileptic. Through the synthesis and/or modification of polymers for use as excipients, several fundamental relationships between excipient structure and dispersion performance relationships were explored.

Table of Contents

List of Tables

List of Figures

List of Schemes

Chapter 1: Introduction

1.1 Motivation

In recent decades, pharmaceutical companies have incorporated combinatorial chemistries and high-throughput screening tools to uncover new active pharmaceutical ingredients.[1,2] An estimated 40 to 70% of these emerging pharmaceutical drugs, or "actives," suffer from poor aqueous solubility and require the development of solubility-enhancing formulation strategies to become efficacious in a clinical setting.[3,4,5] Thus, the need for improved absorption during oral delivery of these actives has driven research in this area for over a decade. Forming drug-polymer solid dispersions has been identified as a robust, reliable, and broadly applicable solubility-enhancement method that does not

compromise the active's intestinal permeability. Dispersing the active pharmaceutical amorphously within a polymeric excipient is a way to deliver the high-energy amorphous form of the drug; the higher theoretical solubility of this amorphous form can aid in accessing concentrations above the crystalline drug's solubility, or supersaturations. As a result of this apparent supersaturation, it is expected that oral absorption will increase as a function of increased flux of drug diffusing across the gastrointestinal membrane.[6] Unfortunately, the higher free energy of the amorphous compound encourages a thermodynamically favored transition to the crystalline drug. As such, the choice of a suitable excipient to stabilize the amorphous drug during dissolution, as well as the solid state during storage, is critical to the success of this solubilizing technology platform.

Despite industrial and academic efforts to predict successful active-excipient pairs, suitable polymeric excipients are often found through an Edisonian approach. Top-performing excipients often belong to the family of cellulosic esters because of their characteristically high T_gs, semi-rigid backbones, and the stable colloidal structures they form as a function of their amphiphilic nature and ionizable carboxylates.[7] Interestingly, hydroxypropyl methylcellulose acetate succinate (HPMCAS) commonly outperforms other excipients with respect to maintaining supersaturation in a broad range of actives.[7,8] Other studies have also identified a limited number of excipients that perform well with specific actives. However, a fundamental understanding of drug-polymer interactions is still absent during the initial design stages of these excipients, and good matches are often found through a serendipitous trial-and-error approach. Establishing relationships between the molecular properties of an excipient and the overall performance of the system is critical for directing the expanding field of polymeric solid dispersions excipients.

1.2 Background

1.2.1 Hydrophobic Pharmaceutical Solubilization Strategies

Oral drug absorption is inherently dictated by many complex factors – hydrophilicity and hydrophobicity, ionizability, melting point, hydrogen bonding ability, aromaticity, stereochemistry, etc. Efforts to simplify formulation considerations for drugs have reduced these complex factors down to two composite qualities: (1) the solubility of the drug in gastrointestinal (GI) milieu, and (2) the permeability of the drug through the GI membrane.[9,10] While this two-property approach is a considerable simplification of drug properties and behavior, these two parameters govern the placement of a drug within the Biopharmaceutical Classification System (BCS) as a predictor of inherent oral bioavailability. The BCS categorizes pharmaceutical actives across four classes (Figure 1.1): high solubility + high permeability (class I), low solubility + high permeability (class II), high solubility + low permeability (class III), and low solubility + low permeability (class IV). Guidance for defining the boundaries of different BSC classes are separately published by the United States Food and Drug Administration (USFDA),[11] the World Health Organization (WHO),[12] and European Medicines Evaluation Agency (EMEA).[13] However, it is generally accepted that the definition of 'high solubility' is when the highest strength dose is soluble in 250 mL of aqueous media across biorelevant pHs (~1-7.5).[14] 'High permeability' is generally defined as when the drug substance is absorbed in humans at a 90% mass balance of the administered dose. When considering formulations for oral delivery, each BCS category requires a formulation strategy designed to address solubility and/or permeability deficiencies, with the exception of Class I.[15]

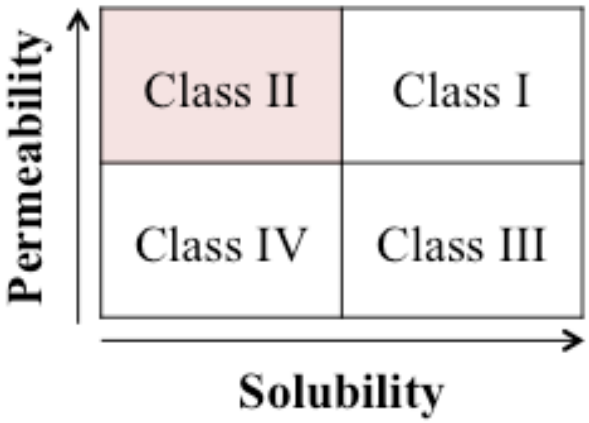

Figure 1.1. Biopharmaceutical Classification System scheme representing categorization of pharmaceutical actives.

With a desire to avoid chemical alterations (*i.e.*, prodrug modifications, salt formations, etc.) to Class II drugs, viable formulation options focus on apparent solubility-enhancing strategies. Historically, these strategies have included cosolvent systems,[16] cyclodextrin complexes,[17] surfactant-based emulsifiers,[18] and amorphous solid dispersions (Figure 1.2).[19] However, ultimately effective delivery of the drug requires there to be no appreciable sacrifice of intestinal permeability. In a comprehensive set of studies to evaluate each of the above-mentioned formulation strategies, Miller and coworkers evaluated each system's individual solubility enhancement/permeability interplay. Miller and coworkers uncovered that in cosolvent systems, despite increased apparent aqueous solubility, membrane permeability was decreased because of the decreasing apparent membrane/aqueous partitioning.[16] Cyclodextrin complexes are based on inclusion chemistries where the hydrophobic drug prefers association in the hydrophobic interior of the cyclic oligosaccharide; as such, the preference for the drug to remain in the hydrophobic pocket again reduces permeability.[17] Similarly, surfactant-based emulsifiers utilize amphiphilic molecules to create hydrophobic cores.[18] This option also decreases the free

fraction of drug available for transmembrane flux based on the inclusion/micellization structures.

In contrast, solid dispersions stabilize the drug in the higher free energy amorphous form and thereby, upon dissolution, rely on an increased *kinetic* solubility achieved via supersaturation achievement.[19] In contrast to the other strategies, Miller et al. found no negative effect on the GI permeability with increasing supersaturation concentrations of an active through solid dispersion, which thereby increased the transmembrane flux. The authors declare that solid dispersions are a "win-win," whereby the bioavailability of class II drugs is enhanced through increased kinetic solubility, and membrane permeability is not sacrificed. Indeed, many articles and reviews cover the benefits of solid dispersions as both an effective and FDA-friendly formulation strategy.[20]

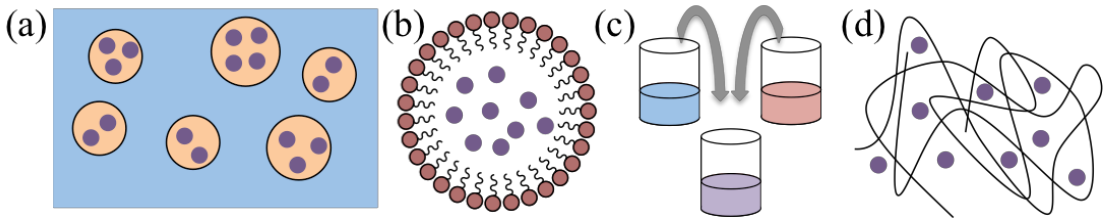

Figure 1.2. Schemes representing strategies for overcoming solubility issues of class II drugs: (a) emulsions, (b) micelles, (c) cosolvents, and (d) amorphous polymer-drug solid dispersions. Purple dots represent amorphous drug. Drawings are representative, not to relative scale.

1.2.2 Solid Dispersions as Formulations

In early literature, solid dispersions of a hydrophobic drug in a hydrophilic carrier were originally simple eutectic mixtures.[21, 22] When (hydrophobic) drug A and

(hydrophilic) carrier B are miscible as liquids and immiscible as solids, a specific A/B composition can be cooled from the liquid solution such that the compounds cocrystallize. When this complex is introduced to aqueous release media, the hydrophilic carrier B quickly dissolves and releases very fine crystals of drug. The increased dissolution of drug in this system is a function of the reduction of particle size.

Solid dispersions where the drug was *molecularly and amorphously* dissolved in a carrier excipient soon followed these eutectic mixtures.[23,24] Pharmaceutical excipients have historically included carbohydrates, lipids, proteins, sugars (sucrose, xylitol), organic acids, surfactants, polymers, and others.[25,26,27] Some amorphous dispersions are even formulated with more than one excipient (usually including at least one surfactant). While pharmaceutical literature covers systems that include many combinations of these excipients, simple binary mixtures of an active with a single polymeric excipient will be the focus of this discussion.

Polymers are chemically composed of a repeating unit structure, where molecular properties such as the repeating unit (monomer) functionality, total molecular mass, and end group identity can impart a wide range of physical properties across such characteristics as solubility (hydrophilic, hydrophobic, or amphiphilic character), polymer-solute interaction strength, chain mobility, and more.[28] Polymers can be classified by their chemical origins, as either natural (*e.g.* cellulose, starch), semisynthetic (*e.g.* hydroxypropyl methylcellulose), or synthetic (*e.g.* polystyrene, polyvinylpyrrolidone). Based on the packing abilities of the chains, polymers can also be classified as crystalline (near-complete long-range order), semi-crystalline (domains of long-range order), or amorphous. Similar to a glass, polymers that exist as amorphous solids have no long-range order or symmetry in the packing of the chains, and this solid state is closely related to the

disordered state of a liquid. Pharmaceutical actives can be trapped within a matrix of polymer excipient, where the distribution of polymer and active reflects that of the active being molecularly dissolved, or dispersed, within the polymer; these active/polymer blends are called amorphous solid dispersions.

The dissolution improvements of these polymer-based amorphous solid dispersion complexes over their predecessors is attributed to several factors.[29] First, reduction of the drug particle size to the molecular level maximizes the surface area of drug available for dissolution. If drug molecules are introduced to the release medium, there is no longer a significant crystal lattice energy barrier to overcome for dissolution. Secondly, upon dissolution, solid dispersions are designed to release the metastable amorphous form of the drug; in this regard, solid dispersions can achieve a supersaturation concentration in solution that the crystalline counterpart cannot access. The amorphous form of a drug has a higher enthalpy, higher entropy, higher free energy, and larger volume, as compared to the crystalline form. For these reasons, the solubility of the amorphous form is theoretically higher than the crystalline solubility. This difference in free energy allows for a prediction of the supersaturation level achievable when the solubility of the amorphous form ($S_{\text{amorphous}}$) is greater than the crystalline solubility ($S_{\text{crystalline}}$). In this regard,[30]

$$G_{\text{amorphous}} - G_{\text{crystalline}} \equiv \Delta G_{\text{a}\rightarrow\text{c}} \approx RT \ln \frac{S_{\text{amorphous}}}{S_{\text{crystalline}}} \tag{1.1}$$

where R is the gas constant, T is the temperature, $\Delta G_{\text{a}\rightarrow\text{c}}$ is the difference in free energy of the amorphous and crystalline forms; $\Delta G_{\text{a}\rightarrow\text{c}}$ can be estimated with the Hoffman equation[31] using the melting temperature, T_{m}, and the heat of fusion, H_{f}.

$$\Delta G_{a\rightarrow c} = \Delta H_f \frac{(T_m - T)T}{(T_m)^2} \quad (1.2)$$

Because the amorphous form of the drug is a higher free energy state than the crystalline form ($\Delta G_{a\rightarrow c} > 0$), there is always a thermodynamic driving force for crystallization. Small lipophilic molecules (*e.g.* BSC Class II pharmaceutical actives) present at supersaturation in aqueous media can form aggregates that may coalesce, increase in size, and crystallize.[32,33,34,35,36,37,38] However, polymeric excipients have been shown to stabilize supersaturation concentrations achieved from solid dispersions for timescales relevant to oral delivery (several hours). The biological relevance of supersaturation stems from, all other variables being constant, an increased concentration of dissolved active in the gastrointestinal tract, which is directly correlated to a higher flux of active across the gastrointestinal membrane, and thus, a presumed increase in oral bioavailability.

The effectiveness of polymers as solid dispersion excipients to inhibit crystallization of drug during dissolution is widely noted. The exact mechanism of this phenomenon remains unclear, though several have been proposed, including: limiting diffusion of drug by altering bulk solution viscosity, changing boundary layer properties at the hydrodynamic interface of solution and crystal surface, and creating amorphous nanoaggregates in solution.[7] Also, based on increased surface activities in the presence of a hydrophilic polymer, the amorphous drug is expected to exhibit improved wettability relative to its crystalline form. Additionally, it has been proposed that as polymers absorb onto a growing crystal surface, they may act as a physical barrier against solute incorporation into the crystal lattice.[39] Perhaps several of these mechanisms are at play, and perhaps the mechanism depends on details of the system.[40]

1.2.3 Solid Dispersion Preparation Techniques

Amorphous solid dispersions are typically prepared via melt or solvent evaporation processes.[41] For typical melt processing, the drug and excipient are heated to a molten state, mixed at a high rotational speed, extruded, cooled, and milled.[41] Melting methods possess the advantages of easy scale up and continuous operation. However, high processing temperatures may invoke degradation of thermally labile excipients or drugs. Incomplete mixing and incomplete conversion of the drug to the amorphous form may also occur because of poor drug-excipient miscibility and limited molecular mobility due to the high viscosity of the melted excipient. Further, melt extrusion often requires large quantities of material, which may not be amenable to the early stages of solid dispersion research.[42]

For solvent evaporation methods, the drug and excipient are dissolved in a volatile organic solvent, such as acetone, tetrahydrofuran, or methanol.[41] Rapid evaporation of the organic solvent ideally leaves the drug in the amorphous or near-amorphous state within the polymeric matrix, though small, residual crystalline particles may also be observed at high loadings of drug relative to polymer. One such method invokes the use of a spray nozzle, where the dissolved drug and excipient are forced through a small, heated orifice. Rapid evaporation of solvent from the sprayed droplets renders micron-sized solid particles, with the drug dispersed (hopefully molecularly and amorphously) within the matrix. The disadvantages of using evaporation methods include the high cost of organic solvents along with the difficulty of complete removal from the final solid. However, with advantages such as low operating temperature and solubility of hydrophobic actives in organic solvents, evaporation methods such as spray drying are well-suited for early-stage solid dispersion production and characterization.

All solid dispersion preparation techniques must consider the interplay between the economic and biological goal of maximized drug loading within a single dosage form, and the propensity of higher concentrations of drug to crystallize. Increased drug loading allows for smaller (or fewer) dosages to be delivered; however, there is often an observed maximum loading limit, above which solid-state stability is compromised within common storage times.

1.2.4 Evaluation Methods of Solid Dispersions

The ultimate goal of a solid dispersion is to deliver the poorly soluble drug in the supersaturated state with retarded crystallization (nucleation and growth) of the drug. Dissolution tests in physiological media are used to evaluate the *in vitro* ability of the solid dispersion to achieve and maintain supersaturation. Brouwers et al. likened solid dispersion dissolution profiles to a 'spring and parachute' mechanism.[43] When considering a dissolution concentration-vs.-time profile, the ability of an excipient to achieve a high 'spring' release and then interfere with crystallization to extend the 'parachute' (or induction) time provides the basis for comparing the performance of polymeric excipients (Figure 1.3). As these processes do not necessarily follow the same mechanisms, strong performers in each category ('spring' and 'parachute') may not be seen from the same excipient.[44] Spring release is related to the polymer's solubility and its ability to fully release the drug quickly. The parachute, however, is linked to crystallization (*i.e.* crystal nucleation and crystal growth) inhibition. As the achieved supersaturation is a *kinetic* rather than *thermodynamic* increase in the apparent solubility, the falling end of the parachute is observed when crystallization eventually does occur to bring the drug concentration to its inherent solubility.

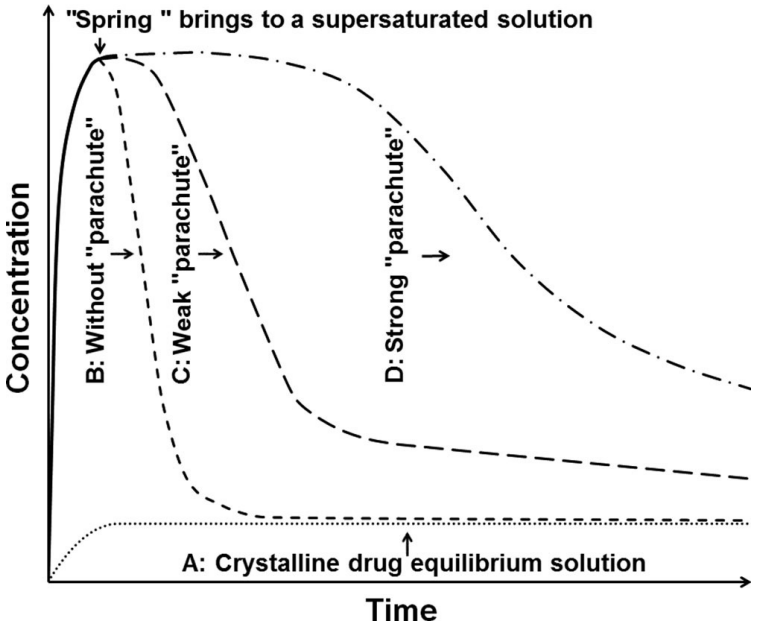

Figure 1.3. Representation of the "spring" and "parachute" mechanisms involved during drug supersaturation. Figure taken from reference 45.

A second goal of solid dispersions is to show stability against drug crystallization over relevant storage times prior to introduction into the body (up to 4 years). Solid-state properties are routinely measured upon manufacturing and over time by powder X-ray diffraction (PXRD), differential scanning calorimetery (DSC), and water uptake/humidity susceptibility[46] measurements. PXRD is used to identify the drug polymorphs present and detects drug crystallinity down to 5-10%. DSC quantitatively detects endothermic and exothermic transitions as a function of temperature.[21] These transitions can include crystallization, melting, and the onset of long-range segmental motion at the glass transition temperature (T_g) (the so called α-transition). A simple two-component blend with large domains of polymer and drug will display two T_g transitions, one for the drug ($T_{g,drug}$

), and one for the polymer ($T_{g,polymer}$). However, when the polymer and drug are intimately mixed (at the near-molecular level), the final mixture will show a single T_g transition, which can be estimated by the Gordon-Taylor[47] equation:

$$T_g = \frac{W_1 T_{g,drug} + K_G W_2 T_{g,polymer}}{W_1 + K_G W_2} \quad (1.3)$$

where T_g is the glass transition temperature of the final mixture; W_1 and W_2 are the weight fractions of the drug and polymer, respectively, and K_G is a constant that indicates the interaction between the polymer and drug. The T_g of the final solid dispersion can also be estimated by similar empirical equations, such as the Fox,[48] Couchman-Karasz,[49] or Kwei equations.[50] When lower-T_g drugs are mixed with higher-T_g polymers, plasticization occurs for the polymer (lowering of T_g), and antiplasticization occurs for the drug (raising of the T_g). This phenomenon helps with solid-state stability, as the carrier decreases the diffusion ability of the drug. For this reason, high-T_g polymers are often the most advantageous choices for solid dispersion formulation, such that the final T_g of the dispersion is 50 °C above the storage temperature (usually room temperature).

Secondary β-relaxations may also be detected using DSC. Bhattacharya and Suryanarayanan recently reviewed the importance of these β-relaxations in solid dispersions as local motions are, in certain cases, sufficient to allow critical nuclei to form, undermining the physical stability below the T_g.[51] Also from DSC, based on the enthalpies of drug crystallization and melting, the extent of crystallinity in a solid dispersion is detectable, typically down to 2%.[21] Finally, water uptake/humidity measurements are important as humidity-induced plasticization leads to increased mobility of the amorphous

drug at lower temperatures, making hydroscopic solid dispersions susceptible to humidity-induced crystallization.[52]

Recent, state-of-the-art advances in solid-state characterization techniques include transmission electron microscopy, electron energy-loss spectroscopy, and solid-state nuclear magnetic resonance.[53-55] Recent advances in solution state characterization include small-angle x-ray scattering, cryo-TEM, and fluorescence spectroscopy.[53,56,72-78] Atomic force spectroscopy has been utilized for model hydration studies, designed to mirror the dissolution process.[53] Relevant discussions of these techniques will be included in the related thesis chapters.

1.2.5 Excipients for Solid Dispersions

Common polymeric excipients for pharmaceutical solid dispersions span both synthetic and natural polymers. Among the fully-synthetic polymers, poly(vinyl pyrrolidone) (PVP) and its poly(vinyl acetate) copolymer (PVPVA) are used most frequently (Scheme 1.1). The extensive capability of PVP to act as a hydrogen-bond acceptor drives the use with a drug containing suitable hydrogen-bond donor moieties.[57] To its disadvantage, PVP has been shown to readily dissolve and release carried drug at gastric pH. [58] Upon dissolution in the stomach, crystallization may initiate, and supersaturation may never be achieved in the small intestine.

Scheme 1.1. Common synthetic excipients (a) poly(vinyl pyrrolidone) (PVP) and (b) poly(vinyl acetate) (PVPVA).

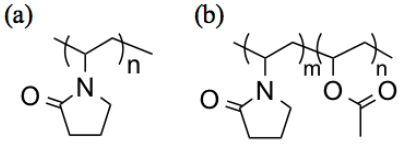

Within naturally derived polymers, the most studied and best performing materials for solid dispersions include ester- and/or ether-functionalized cellulose derivatives (Scheme 1.2).[29] These polysaccharides are excellent solid dispersion excipients based on their bioavailability, and their naturally integrated hydroxyls allow for easy structural modifications. Compared to their synthetic counterparts, the semi-rigid anhydrogluco-unit backbones are thought to advantageously facilitate more points of contact with crystal surfaces in solution.[44,59]

Scheme 1.2. Structures of common cellulosic excipients: (a) cellulose acetate phthalate (CAP), (b) cellulose acetate (CAT), (c) hydroxypropyl methylcellulose (HPMC), (d) hydroxylpropyl methylcellulose phathalate (HPMCP), and (e) hydroxylpropyl methylcellulose acetate succinate (HPMCAS).

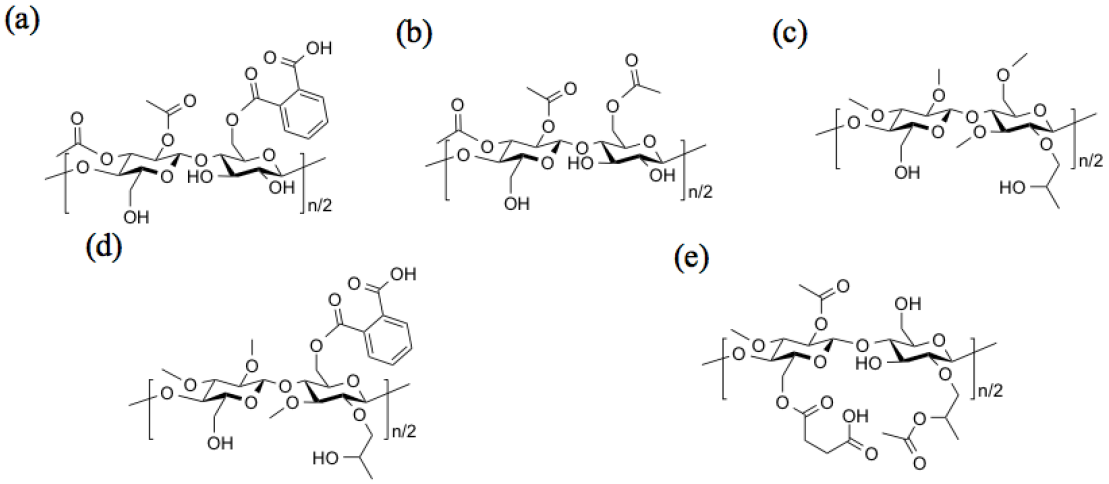

In an effort to guide the design of optimal drug-excipient pairs, the performances of over twenty-five commercially available polymers were evaluated for their ability as spray-dried dispersion matrices to achieve (‘spring’) and maintain (‘parachute’) supersaturation of nine hydrophobic drugs.[8] Curatolo et al. concluded that for drugs across a wide range of physical properties and chemical structures, hydroxypropyl

methylcellulose acetate succinate (HPMCAS) was a common top performer to the other polymers tested, including other cellulosics (Figure 1.4).

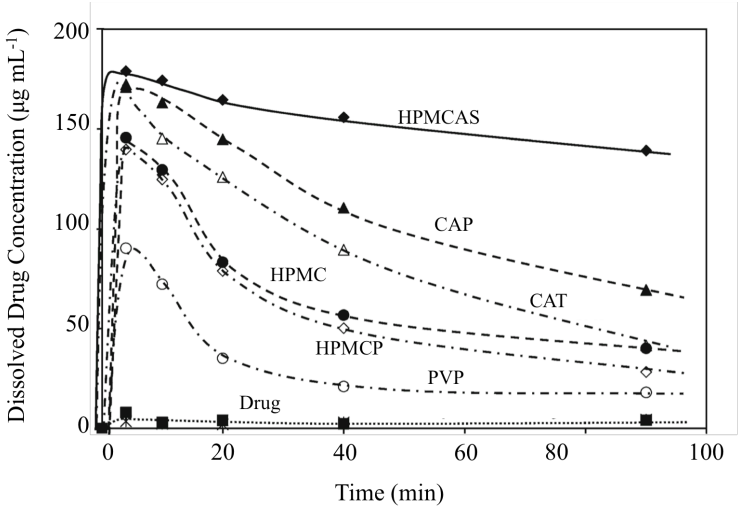

Figure 1.4. Dissolution performance of solid dispersions made from various polymers with 2-phenanthrenecarboxamide (solubility in water 0.0038 μg mL^{-1}) at 10 wt % drug loading. The target drug concentration for all samples was 200 μg mL^{-1}. Figure reproduced from reference 7.

The success of HPMCAS, relative to the other cellulosic materials, is thought to stem from its multifunctional, amphiphilic nature.[60] The statistically distributed methoxyl and acetate groups are relatively hydrophobic and may suitably interact with hydrophobic drug molecules. Furthermore, the free hydroxyls along the backbone and off the hydroxypropyl groups are hydrophilic and aid in dispersion of the polymer. At gastric pH (~1.2), the protonated succinic acids impart low solubility to the polymer and, in this form, protect the drug from release in the stomach.[61,62,63] The incorporated succinic acids become almost fully ionized at intestinal pH (~6.5), and it is thought that the resulting succinates stabilize colloidal polymer-drug nanostructures and nanoaggregates.[8] In solution, the drug

is stabilized within these colloidal structures, with hydrophobic polymer/drug interactions hindering the organization necessary for crystal nucleation and growth. Ilevbare et al. noted that decreasing the number of succinate groups per repeat unit on cellulosic polymers decreased the ability of the polymer to effectively retard crystal growth for ritonavir.[59] They argue that increasing the succinate levels leads to an extended polymer conformation (driven by charge repulsion), which may allow the polymer to better adhere to drug crystal surfaces and form more multi-point contacts at the polymer-drug interface.

The advantageous properties of HPMCAS for solid dispersions drove the design and discovery of other cellulose ethers and/or esters of moderate hydrophobicity. Edgar and colleagues expanded this space through the synthesis of novel cellulose ω-carboxyalkanoates with varying degrees of hydrophobicity (Scheme 1.3).[63,64,65] These polymers maintained the terminal carboxylate functionality through the addition of varying length carboxylic acids and retained the hydrophobic moieties through the addition of varying ester groups. The authors then calculated solubility parameters for over twenty polymers, including the novel esters mentioned, using a method proposed by Fedors.[44,66] Collaboration between the Taylor and Edgar research groups yielded in an enlightening series of publications describing the effect of the molecular properties of these polymers on crystal nucleation[44] and growth,[59,57] mostly with respect to three poorly water-soluble drugs (efavirenz, ritonavir, and celecoxib). They found that the *most* hydrophilic and *most* hydrophobic polymers were poor crystallization inhibitors. More hydrophilic polymers have a higher affinity for water molecules and promote polymer-solvent interactions, whereas more hydrophobic polymers will preferentially associate with themself. In both of these cases, the drug molecules are left to self-associate, order, and either nucleate or adsorb to a crystal surface. Consequently, the authors found that the greatest inhibition of

drug nucleation and growth was generally seen using moderately hydrophobic polymers where the polymer's solubility parameter roughly equaled that of the drug. As polymer-drug interactions using these excipients were mostly driven by non-specific hydrophobic interactions, an increase in the hydrophobicity of the drug shifted the optimal window of polymer hydrophobicity necessary for maximum drug stabilization in solution. Furthermore, although several synthetic polymers were within the optimal hydrophobic range for drug stabilization, these polymers were found to be ineffective at crystallization inhibition, suggesting the additional importance of other molecular properties.

Scheme 1.3. Cellulose ω-carboxyalkanoates.

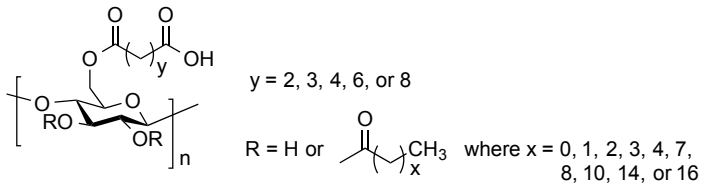

Polymer-drug interactions can expand beyond those solely driven by non-specific hydrophobic attractions. Polymers facilitating *specific* intermolecular interactions with drugs containing suitable donor or acceptor groups often show heightened stability in both the solid and solution states.[44,64] For example, when screening polymers for crystal growth inhibition of ritonavir in phosphate buffered saline, Ilevbare et al. found that the most effect inhibitor was poly(*N*-isopropylacrylamide) (PNiPAm).[59] The fast growing '*a*'-axis of ritonavir presents several carbonyl oxygens and thiazole functional groups, both of which are hydrogen-bond acceptors that can interact with the intermediately hydrophobic, hydrogen bond-donating and -accepting PNiPAm (Figure 1.5). Growing seed crystals of ritonavir in the presence of PNiPAm was found to significantly change the final crystal

aspect ratio (length/width) from 8.8 to 4.4, suggesting that inhibiting growth along this *a*-axis greatly contributed to the overall lowering of the growth rate.

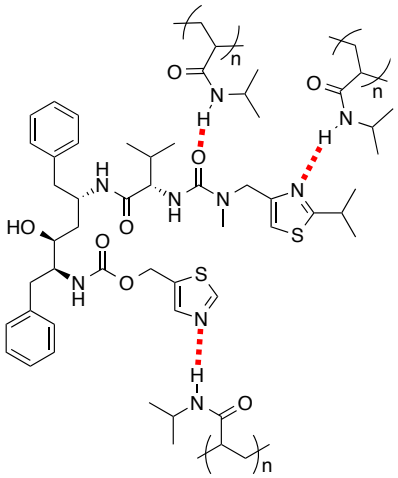

Figure 1.5. Representative hydrogen bond interactions (red) between ritonavir and PNiPAm; polymer-drug hydrogen bonding is posited to greatly inhibit growth of ritonavir in aqueous buffer.[59]

To expand the field of solid dispersion excipients, this thesis project examined several different polymeric excipient platforms. With synthetic control over each excipient, we had full freedom to independently probe the validity of already-established designed principles, as well as generate and test new theories on fundamental relationships between polymer and drug.

1.2.6 Solid Dispersion Dissolution Enhancement Mechanisms

One of the key assumptions of solid dispersion literature is that there will be an *in vitro-in vivo* correlation of dispersion performance. Perhaps this is presumptuous, as the dissolution kinetics of a solid dispersion in buffer may be an oversimplification of the complex processes involved with gastrointestinal absorption. However, several studies and

analytical techniques have recently indicated promise in the correlation between *in vitro* supersaturation and *in vivo* bioavailability enhancements. This limited understanding is further complicated by the apparent non-universal mechanisms of supersaturation achievement and maintenance from system to system. Most researchers recognize the spring and parachute concept,[43] where the drug and polymer are introduced to buffer concurrently, and the dissolved polymer delays the induction time of crystal nucleation and/or growth; however, this model is an oversimplification of the swelling, devitrifying, disentangling, and dissolving processes involved as the glassy polymer/drug dispersion releases the drug into solution.[67] Additionally, this process changes from system to system; for example, at higher hydrophobic drug loadings, even with the same excipient, the dissolution rate of the solid dispersion decreases.[68,69,70] Dissolution processes also change with differing *in vitro* biorelevant media.[71]

Further complicating our understanding, the mechanisms of the parachute delay have been attributed to several different things. For example, some posit that the solid dispersion excipient adsorbs to drug molecules, nuclei, and crystals in a way that inhibits further association and incorporation of drug. There are others, most notably Taylor and colleagues, who have proposed the formation of amorphous, drug-rich nanodroplet reservoirs, through a mechanism of liquid-liquid phase separation (LLPS).[72 - 78] The excipient polymers are then responsible for the stability of these nanodroplets, preventing coalescence and drug crystallization. Recent studies have validated this relatively new hypothesis within the field, even when studying the often-researched excipient, hydroxypropyl methylcellulose acetate succinate.[56] However, again, the overall performance of these solid dispersions is dependent on the polymer and drug pairing, and the interaction between the binary components is complex and not easily understood.[79] To

the best of our understanding, any one excipient could act by one or more of these mechanisms; the field does not have the appropriate analytical tools developed yet to be able to understand this yet.

1.3 Objective

The objective of this thesis research is to understand the relationship between excipient molecular properties and final solid dispersion performance. Through the design, synthesis, and testing of tailored polymeric excipients, we will determine what key formulation elements dictate active supersaturation attainment and maintenance during dissolution, as well as amorphous drug stability in the solid state. Furthermore, characterizing the solution structures made during dissolution will help enlighten the contributions of hydrophobic domains and ionizable groups on aqueous dispersion stability. Through this work, we hope to shed light on mechanism within a defined class of excipients and actives. Ultimately, we will deliver a validated design strategy based on structure-property relationships to direct excipient choice and development.

1.4 Dissertation Approach

1.4.1 Iterative Design of Studies

The goal of this project was to enable the targeted and rational design of future excipients. We sought to build a fundamental understanding of excipient-active behavior through a hypothesis-driven, iterative approach. This iterative cycle approach cycled through four stages:

(1) synthesizing novel solid dispersion excipients,

(2) screening performance behavior with a model active,

(3) probing physical properties to identify the relevant performance-enhancing characteristics, and

(4) using an overall understanding of the system to guide the next generation of solid dispersions.

This iterative approach described above was always centered around a defined engineering target, and, for many of the studies described here, that engineering target was the solubility enhancement of phenytoin, a model BCS Class II pharmaceutical active. By continuously expanding on knowledge gained through multiple iterative studies, we discovered and validated several fundamental relationships between the molecular properties of a polymer and its performance as a solid dispersion excipient.

1.4.2 Outline of Thesis

Each chapter in this thesis summarizes a study that was specifically designed to build a fundamental understanding of how to design excipients to enhance the solubility of model hydrophobic drugs, primarily phenytoin.

- *Chapter 2: Synthesis of Hydrophobically Modified Hydroxypropyl Methylcellulose (HPMC) Esters for the Dissolution Enhancement of Phenytoin*

  This study expanded on published work on HPMC esters that was performed by Yin and Hillmyer.[80] By making similar modifications on a different starting HPMC material, we assessed additional HPMC-based excipients with the same cyclohexyl succinic acid chemical functionalities.

- *Chapter 3: Synthesis of Low-Molar-Mass Poly(*N*-Isopropyl Acrylamide)s for the Dissolution Enhancement of Phenytoin*

This study followed a serendipitously discovered high-performing excipient described in Appendix 1. By varying end groups and molar mass, this work illuminated the influence of those molecular properties in poly(*N*-isopropyl acrylamide)-based excipients for the dissolution behavior with phenytoin.

- *Chapter 4: Micelles and Blends*

  This chapter was our final investigation, and was motivated to explicitly probe the generalizability of our findings to date. Working to answer specific, hypothesized-based questions, we expanded our knowledge of the mechanism by which several of our high-performing excipients achieved and maintained supersaturation of phenytoin, through the investigation into micelle-forming excipients and blends of those excipients.

- *Appendix 1: HPMC grafts and Blends*

  This appendix was a brief study of novel HPMC graft polymers, and blends of synthetic homopolymers with HPMC.

1.5 References

(1) Lipinski, C. A. *J. Pharmacol. Toxicol. Methods* **2001**, *44*, 235–249.

(2) Lipinski, C. A.; Lombardo, F.; Dominy, B. W.; Feeney, P. J. *Adv. Drug Deliv. Rev.* **2001**, *46*, 3–26.

(3) Ku, M. S. *AAPS J.* **2008**, *10*, 208–212.

(4) Ku, M. S.; Dulin, W. *Pharm. Dev. Technol.* **2012**, *17*, 285–302.

(5) Babu, N. J.; Nangia, A. *Cryst. Growth Des.* **2011**, *11*, 2662–2679.

(6) Raina, S. A.; Zhang, G. G. Z.; Alonzo, D. E.; Wu, J.; Zhu, D.; Catron, N. D.; Gao, Y.; Taylor, L. S. *Journal of Pharmaceutical Sciences* **2014**, *103* (9), 2736–2748.

(7) Friesen, D. T.; Shanker, R.; Crew, M.; Smithey, D. T.; Curatolo, W. J.; Nightingale, J. A. S. *Mol. Pharm.* **2008**, *5*, 1003–1019.

(8) Curatolo, W.; Nightingale, J. A.; Herbig, S. M. *Pharm. Res.* **2009**, *26*, 1419–1431.

(9) Amidon, G. L.; Lennernäs, H.; Shah, V. P.; Crison, J. R. *Pharm. Res.* **1995**, *12*, 413–420.

(10) Waldmann, S.; Almukainzi, M.; Bou-Chacra, N. A.; Amidon, G. L.; Lee, B.-J.; Feng, J.; Kanfer, I.; Zuo, J. Z.; Wei, H.; Bolger, M. B.; Löbenberg, R. *Mol. Pharm.* **2012**, *9*, 815–822.

(11) Center for Drug Evaluation, USFDA. Guidance for industry: Waiver of *In vivo* bioavailability and bioequivalence for immediate release solid oral dosage forms based on a biopharmaceutics classification system. August 2000.

(12) Multisource (generic) pharmaceutical products: Guidelines on registration requirements to establish interchangeability. In: WHO Expert Committee on

Specifications for Pharmaceutical Preparations, Fortieth Report. Geneva, World Health Organization. WHO Technical Report Series, No. 937, Annex 7: 2000. p. 347-390.

(13) Committee for Medicinal Products for Human Use. Guideline on the Investigation of Bioequivalence (CPMP/EWP/QWP/1401/98 Rev. 1), July 2008.

(14) Chavda, H.; Patel, C.; Anand, I. *Systematic Reviews in Pharmacy* **2010**, *1* (1), 62–69.

(15) Kawabata, Y.; Wada, K.; Nakatani, M.; Yamada, S.; Onoue, S. *Int. J. Pharm.* **2011**, *420*, 1–10.

(16) Miller, J. M.; Beig, A.; Carr, R. A.; Webster, G. K.; Dahan, A. *Mol. Pharm.* **2012**, *9*, 581–590.

(17) Miller, J. M.; Dahan, A. *Int. J. Pharm.* **2012**, *430*, 388–91.

(18) Miller, J. M.; Beig, A.; Krieg, B. J.; Carr, R. A.; Borchardt, T. B.; Amidon, G. E.; Amidon, G. L.; Dahan, A. *Mol. Pharm.* **2011**, *8*, 1848–1856.

(19) Miller, J. M.; Beig, A.; Carr, R. A.; Spence, J. K.; Dahan, A. *Mol. Pharm.* **2012**, *9*, 2009–2016.

(20) Jermain, S. V.; Brough, C.; Williams, R. O. *International Journal of Pharmaceutics* **2017**.

(21) Leuner, C.; Dressman, J. *Eur. J. Pharm. Biopharm.* **2000**, *50*, 47–60.

(22) Sekiguchi, K.; Obi, N. *Chem. Pharm. Bull. (Tokyo)* **1961**, *9*, 866–872.

(23) Kanig, J. L. *J. Pharm. Sci.* **1964**, *53*, 188–92.

(24) Levy, G. *Am. J. Pharm. 1835-1936* **1963**, *135*, 78–92.

(25) Baghel, S.; Cathcart, H.; O'Reilly, N. J. *Journal of Pharmaceutical Sciences* **2016**, *105* (9), 2527–2544.

(26) Laitinen, R.; Löbmann, K.; Grohganz, H.; Priemel, P.; Strachan, C. J.; Rades, T. *International Journal of Pharmaceutics* **2017**, *532* (1), 1–12.

(27) Dengale, S. J.; Grohganz, H.; Rades, T.; Löbmann, K. *Advanced Drug Delivery Reviews* **2016**, *100* (Supplement C), 116–125.

(28) Hiemenz, P. C.; Lodge, T. P. *Polymer Chemistry*, 2nd ed.; Boca Raton, Fl, 2007.

(29) Warren, D. B.; Benameur, H.; Porter, C. J. H.; Pouton, C. W. *J. Drug Target.* **2010**, *18*, 704–731.

(30) Hancock, B. C.; Parks, M. What is the true solubility advantage for amorphous pharmaceuticals? *Pharm. Res.* **2000,** *17*, (4), 397–404.

(31) Hoffman, J. D. Thermodynamic driving force in nucleation and growth processes. *J. Chem. Phys.* **1958,** *29*, 1192–3.

(32) Frenkel, Y.V.; Clark, A.D.; Das, K.; Wang, Y-H.; Lewi, P.J.; Janssen, P.A.J.; Arnold, E. *J Med Chem.* **2005**, *48* (6), 1974–1983.

(33) Coan, K.E.D.; Shoichet, B.K. *J. Am. Chem. Soc.* **2008**, *130* (29), 9606–9612.

(34) Coan, K.E.D; Maltby, D.A.; Burlingame, A.L; Shoichet, B.K. *J. Med. Chem.* **2009**, *52* (7), 2067–2075.

(35) Brick, M.C.; Palmer, H.J.; Whitesides, T.H. *Langmuir* **2003**, *19* (16), 6367–6380.

(36) Pacheco, L.F.; Carmona-Ribeiro, A.M. *J. Colloid Interface Sci.* **2003**, *258* (1), 146–154.

(37) Seidler, J.; McGovern, S.L.; Doman, T.N.; Shoichet, B.K. *J. Med. Chem.* **2003**, *46* (21), 4477–4486.

(38) Feng, B.Y.; Simeonov, A.; Jadhav, A.; Babaoglu, K.; Inglese, J.; Shoichet, B.K.; Austin, C.P. *J. Med. Chem.* **2007**, *50* (10), 2385– 2390.

(39) Fleer, G. J.; Cohen Stuart, M. A.; Scheutjens, M. H. M.; Cosgrove, T.; Vincent, B. *Polymers at Interfaces*; 1st ed.; Chapman & Hall: London, 1993.

(40) Sun, D. D.; Lee, P. I. *Journal of Controlled Release* **2015**, *211* (Supplement C), 85–93.

(41) Vasconcelos, T.; Sarmento, B.; Costa, P. *Drug Discov. Today* **2007**, *12*, 1068–1075.

(42) Padden, B. E.; Miller, J. M.; Robbins, T.; Zocharski, P. D.; Prasad, L.; Spence, J. K.; LaFountaine, J. Amorphous Solid Dispersions as Enabling Formulations for Discovery and Early Development http://www.americanpharmaceuticalreview.com.

(43) Brouwers, J.; Brewster, M. E.; Augustijns, P. *J. Pharm. Sci.* **2009**, *98*, 2549–2572.

(44) Ilevbare, G. A.; Liu, H.; Edgar, K. J.; Taylor, L. S. *Cryst. Growth Des.* **2013**, *13*, 740–751.

(45) He, Y.; Ho, C. *Journal of Pharmaceutical Sciences* **2015**, *104* (10), 3237–3258.

(46) Lehmkemper, K.; Kyerematen, S. O.; Heinzerling, O.; Degenhardt, M.; Sadowski, G. *Mol. Pharmaceutics* **2017**.

(47) M. Gordon, J. S.; Taylor, *J. Appl. Chem.* **1952**, *2* (9), 493–500.

(48) Tian, B.; Wang, X.; Zhang, Y.; Zhang, K.; Zhang, Y.; Tang, X. *Pharm Res*. **2015**, *32*, 840–851.

(49) Song, Y.; Yang, X.; Chen ,X.; Nie, H.; Byrn, S.; Lubach, J. *Mol Pharm.* **2015**, *12*, 857–866.

(50) Prudic, A.; Lesanik, A.; Ji, Y.; Sadowski, G. *Eur J Pharm Biopharm.* **2015**, *93*, 88–94.

(51) Bhattacharya, S.; Suryanarayanan, R. *J. Pharm. Sci.* **2009**, *98*, 2935–2953.

(52) Chen, H.; Pui, Y.; Liu, C.; Chen, Z.; Su, C.-C.; Hageman, M.; Hussain, M.; Haskell, R.; Stefanski, K.; Foster, K.; Gudmundsson, O.; Qian, F. *Journal of Pharmaceutical Sciences* **2017**.

(53) Mugheirbi, N. A.; Marsac, P. J.; Taylor, L. S. *Mol. Pharmaceutics* **2017**.

(54) Ricarte, R. G.; Lodge, T. P.; Hillmyer, M. A. *Mol. Pharmaceutics* **2015**, *12* (3), 983–990.

(55) Ricarte, R. G.; Lodge, T. P.; Hillmyer, M. A. *Langmuir* **2016**, *32* (29), 7411–7419.

(56) Ricarte, R. G.; Li, Z.; Johnson, L. M.; Ting, J. M.; Reineke, T. M.; Bates, F. S.; Hillmyer, M. A.; Lodge, T. P. *Macromolecules* **2017**, *50* (8), 3143–3152.

(57) Ilevbare, G. A.; Liu, H.; Edgar, K. J.; Taylor, L. S. *Mol. Pharm.* **2013**, *10*, 2381–2393.

(58) Li, B.; Wegiel, L. A.; Taylor, L. S.; Edgar, K. J. *Cellul. Dordr. Neth.* **2013**, *20*, 1249–1260.

(59) Ilevbare, G. A.; Liu, H.; Edgar, K. J.; Taylor, L. S. *Cryst. Growth Des.* **2012**, *12*, 3133–3143.

(60) Chen, R. *Int. J. Polym. Anal. Charact.* **2009**, *14*, 617–630.

(61) Li, B.; Liu, H.; Amin, M.; Wegiel, L. A.; Taylor, L. S.; Edgar, K. J. *Cellul. Dordr. Neth.* **2013**, *20*, 2137–2149.

(62) Li, B.; Konecke, S.; Harich, K.; Wegiel, L.; Taylor, L. S.; Edgar, K. J. *Carbohydr. Polym.* **2013**, *92*, 2033–2040.

(63) Liu, H.; Ilevbare, G. A.; Cherniawski, B. P.; Ritchie, E. T.; Taylor, L. S.; Edgar, K. J. *Carbohydr. Polym.*

(64) Edgar, K. J.; Li, B.; Taylor, L.; Ilevbare, G.; Williams, S. M.; Liu, H. Cellulose derivatives for inhibiting crystallization of poorly water-soluble drugs. WO 2013/106433, July 18, 2013.

(65) Liu, H.; Kar, N.; Edgar, K. J. *Cellulose* **2012**, *19*, 1279–1293.

(66) Fedors, R. F. *Polym. Eng. Sci.* **1974**, *14*, 147–154.

(67) Narasimhan, B.; Peppas, N. A. *J. Pharm. Sci.* **1997**, *86*, 297–304.

(68) Simonelli, A. P.; Mehta, S. C.; Higuchi, W. I. *J. Pharm. Sci.* **1969**, *58*, 538–549.

(69) Alonzo, D. E.; Gao, Y.; Zhou, D.; Mo, H.; Zhang, G. G. Z.; Taylor, L. S. *J. Pharm. Sci.* **2011**, *100*, 3316–3331.

(70) Jackson, M. J.; Kestur, U. S.; Hussain, M. A.; Taylor, L. S. *Mol. Pharm.* **2016**, *13*, 223–231.

(71) Elkhabaz, A.; Sarkar, S.; Dinh, J. K.; Simpson, G. J.; Taylor, L. S. *Mol. Pharmaceutics* **2017**.

(72) Hsieh, Y.L.; Ilevbare, G.A.; Van Eerdenbrugh, B.; Box, K.J.; Sanchez-Felix, M.V.; Taylor, L.S. *Pharm. Res.* **29**, *2012*, 2738–2753.

(73) Ilevbare, G. A.; Liu, H.; Pereira, J.; Edgar, K. J.; Taylor, L. S. *Mol. Pharm.* **2013**, *10*,

3392–3403.

(74) Mosquera-Giraldo, L. I.; Taylor, L. S. *Mol. Pharm.* **2015**, *12*, 496–503.

(75) Indulkar, A. S.; Box, K. J.; Taylor, R.; Ruiz, R.; Taylor, L. S. *Mol. Pharm.* **2015**, *12*, 2365–2377.

(76) Jackson, M. J.; Kestur, U. S.; Hussain, M. A.; Taylor, L. S. *Mol. Pharm.* **2016**, *13*, 223–231.

(77) Almeida e Sousa, L.; Reutzel-Edens, S. M.; Stephenson, G. A.; Taylor, L. S. *Mol. Pharm.* **2015**, *12*, 484–495.

(78) Raina, S.; Alonzo, D.; Zhang, G.Z.; Gao, Y.; Taylor, L. *Pharm. Res.* **2015**, *32,* 3660-3673.

(79) Purohit, H. S.; Taylor, L. S. *Pharm Res* **2017**, 1–20.

(80) Yin, L.; Hillmyer, M. A. *Mol. Pharm.* **2014**, *11* (1), 175–185.

Chapter 2: Hydroxypropyl Methylcellulose Esters of Substituted Succinates for Phenytoin Dissolution Enhancement

2.1 Introduction

Array-style screening studies have attempted to elucidate key molecular structure-performance relationships that could be used to predict beneficial active-excipient pairings for the achievement and maintenance of active supersaturation in aqueous media.[1,2] While the potential of any particular active-excipient blend to achieve and maintain supersaturated concentrations of the drug remains relatively unpredictable, one cellulosic ester material, hydroxypropyl methylcellulose acetate succinate (HPMCAS), has been

found to enhance the performance of a wide variety of actives. In this project, we functionalized hydroxypropyl methylcellulose (HPMC) to generate novel excipients with molecular structures akin to the uniquely high-performing HPMCAS (Scheme 2.1). Modification of HPMC with substituted succinic anhydrides provided a simple and effective way to add ester substituents with desirable functionalities at targetable substitution levels. Previous studies showed that an HPMC ester containing a hydrophobic cyclohexylthioether moiety was an effective solid-dispersion excipient with respect to achieving and maintaining supersaturation concentrations of phenytoin, a model hydrophobic drug, at low drug loadings (10 wt %).[3] We have supplemented these studies by expanding our library of materials to include more hydrophilic polymers with the same substituent; this was achieved by starting from an HPMC material with lower methyl ether substitution. By evaluating the fine points of the dissolution profiles of all these materials, we elucidated key relationships between the molecular properties of the excipient and its performance in a solid dispersion with phenytoin.

Scheme 2.1. Molecular structures of hydroxypropyl methycellulose acetate succinate (HPMCAS), hydroxylpropyl methylcellulose (HPMC), and phenytoin. The cellulosic structure is representative, where actual placement of all substituents is without regioselective control, and the degree of substitution of each functionality can be independently varied. Further, crosslinking may happen during substitution processes.

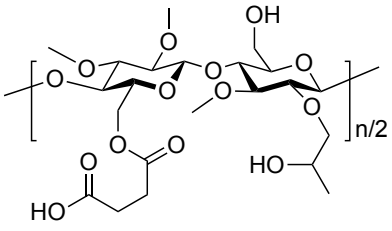

HPMCAS

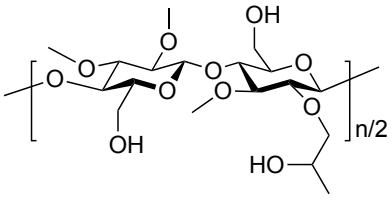

HPMC

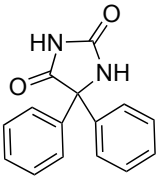

Phenytoin

2.2 Etherification and Esterification of Cellulose

Etherification and esterification methods are commonly employed to functionalize cellulose at its hydroxyl positions.[4,5,6,7,8] In industrial practice, etherification of cellulose to yield HPMC begins with a caustic treatment of cellulose, followed by the addition of methyl chloride and propylene oxide.[9] This treatment breaks up the extensive hydrogen-bonding network of cellulose and eliminates its crystallinity. These methyl and hydroxypropyl ether substituents can be added at varying ratios to control hydrophobicity, solubility, and other performance properties of the final polymer.

The most popular cellulose esterification methods include the use of acid chlorides or anhydrides.[5,6,7] Based on the form of the acid chloride (mono- or di-) or anhydride (linear or cyclic), the resultant ester moiety will be terminated with either a hydrophobic alkyl group or a pH-responsive carboxylic acid. Other esterifying regents such as benzyl monoesters of an acid chloride have been used to add functionalities with terminal carboxylates without the use of cyclic anhydrides or crosslinking diacids.[10] Depending on the desired functionality, etherification and esterification reactions may be performed in sequence to yield combined cellulose ether esters, such as HPMCAS.

2.3 Previous HPMC Esters for Phenytoin Dissolution Enhancement

Previous work by Yin and Hillmyer[3] focused on the modification of HPMC with substituted succinate esters for the dissolution enhancement of the hydrophobic model drug phenytoin. These HPMC ester materials maintained the rich functionality and semi-rigid backbone of the parent HPMC, and were therefore analogous to the commercially available, high-performing HPMCAS. The simple, one-step treatment of HPMC with a modified succinic anhydride was modularized to allow the addition of an alkyl, aryl,

alklythio or arylthio group. The hydrophobic moiety was hypothesized to limit crystallization of phenytoin from solution through interactions with either dissolved drug or growing crystal surfaces. Using the five-membered cyclic maleic anhydride as a template allowed for the facile addition of succinates, whose terminal carboxylic acids, nearly fully ionized at intestinal pH, are expected to impart the same colloidal stability as they do for HPMCAS. The free HPMC hydroxyls serve to ring open the modified anhydride; as such, the final pH-responsive carboxylate and the hydrophobic R group were incorporated at the prescribed one-to-one ratio, and these groups were fixed in close proximity (Scheme 2.2).

Scheme 2.2. Novel HPMC esters previously synthesized for solid dispersion excipients.[3] The cellulosic structure is representative, where actual placement of all substituents is without regioselective control. The degree of substitution (DS) for each group is defined as the average number of substituents per repeat unit, which was determined by ^{1}H NMR.

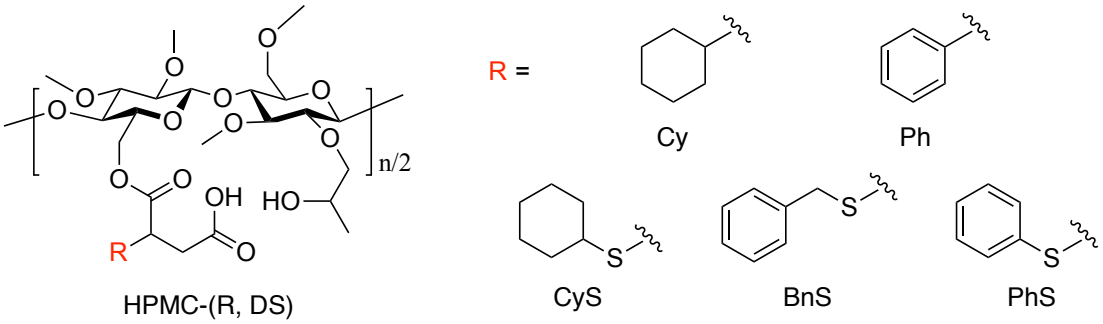

All of the HPMC esters from Yin and Hillmyer[3] were synthesized from a starting HPMC material with a degree of methyl ether substitution of 1.91, a hydroxypropyl ether substitution of 0.25, and a free hydroxyl substitution of 1.09. For clarity of comparison later, all esters from this series are denoted by the grade of the commercially-available

starting HPMC used, METHOCEL™ E (a trademark of The Dow Chemical Company), where 'E' grade is associated to the ether substitution levels above. For example, E-HPMC-(CyS, DS) denotes a HPMC ester from E grade HPMC, functionalized with cyclohexylthio (CyS) succinate at some degree of substitution (DS).

After functionalization with the substituted succinic anhydride, the resulting HPMC esters and phenytoin were spray dried from acetone to form solid dispersions. Phenytoin, a BCS class II anticonvulsant, is a relatively lipophilic compound with an octanol-water partition coefficient (log *P*) value of 1.9 and solubility in water of 27.1 μg mL^{-1}.[11] Furthermore, hydrogen-bonding and π-π interactions[12] make the crystal form very stable as indicated by its high melting point of 296 °C and heat of fusion, ΔH_f, of 158 J g^{-1}. Based on equations 1.1 and 1.2, the solubility of amorphous phenytoin is estimated at 1,300 μg mL^{-1}.[3] These physical characteristics make incorporation into solid dispersion an ideal formulation approach for the drug.

As an indirect measure of the potential of the novel esters to enhance oral bioavailability *in vivo*, the ability of each solid dispersion to achieve and maintain high phenytoin supersaturation was studied over 6 h. The integrated area under the curve over the 6 h (AUC_{6h}) of these concentration-vs.-time dissolution profiles served to quantitatively compare excipient performance through an *in vitro* screening method. The AUC_{6h} of the solid dispersions can then be compared against the AUC_{6h} observed for crystalline phenytoin, and ultimately presented as an enhancement factor (EF), where:

$$EF = \frac{AUC_{6h,\ \text{solid dispersion}}}{AUC_{6h,\ \text{phenytoin}}} \tag{2.1}$$

The $AUC_{6h,\ solid\ dispersion}$ can also be related to the maximum release potential based on the total loaded concentration of the drug over the studied time. This fraction of the engineering target (F_{ET}) release is defined as:

$$F_{ET} = \frac{AUC_{6h,\ solid\ dispersion}}{[\text{phenytoin}]_{loaded} \bullet 6\ h} \tag{2.2}$$

At a degree of substitution (DS) of ~ 0.6, HPMC cyclohexylthio (CyS) succinate outperformed the other polymers and HPMCAS with respect to supersaturation enhancement of phenytoin at 10 wt % loading, based on their relative AUC_{6h}s, EFs, and F_{ET}s (Figure 2.1A). After observing the heightened performance of the HPMC-CyS succinates, a series varying the CyS DS from 0.42 to 0.99 was made (Figure 2.1B). At 10 wt % the best performance was seen at a CyS DS of 0.57. To study the affect of relative phenytoin to polymer in the solid dispersions further, solid dispersions at 25 wt % drug loading were studied while using the same engineering protocols, such that the same maximum enhancement factor could be achieved (Figure 2.1C and 2.1D). Little differentiation between samples was seen at the higher drug loading.

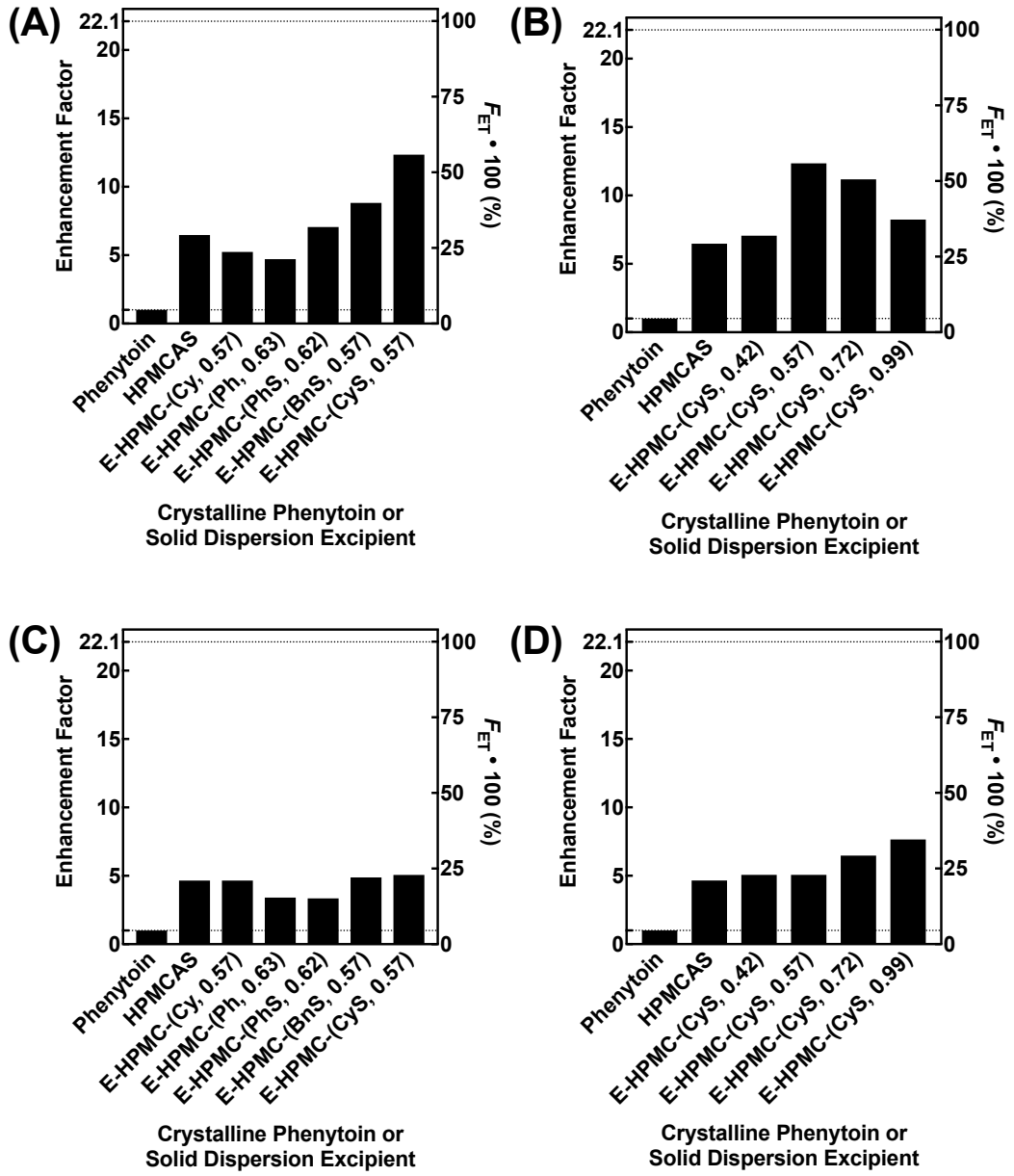

Figure 2.1. A comparison of the enhancement factors (EFs) (left axis) measured during dissolution over 6 h for different spray-dried dispersions and crystalline phenytoin, as defined in equation (2.1). Solid dispersions are loaded at 10 wt% in (A) and (B); solid dispersions are loaded at 25 wt% in (C) and (D). All dissolution studies were performed with a phenytoin target concentration of 1000 μg mL^{-1}, and the maximum EF possible under these conditions was 22.1. Also shown are the related percentages of the engineering target achieved, as defined in equation (2.2) (right axis).

To analyze the success of the HPMC-CyS excipients further, and to further compare this performance to HPMCAS, dissolution profiles are shown at both drug loadings (Figure 2.2). The dissolution profiles are separated into rough categories based on the apparent induction time of phenytoin, where crystallization from solution is evident by a decrease in the concentration. Samples that peak quickly followed by a rapid decline in under 20 min were categorized as 'spring-loaded' and possessing a 'type I' dissolution profile. Samples that extended this induction time to 90 min were categorized as exhibiting a 'type II' release. Finally, dissolution profiles where no decrease in the phenytoin concentration achieved was seen over the full 6 h were categorized as 'type III' release.

In solid dispersions at 10 and 25 wt % phenytoin loadings, HPMCAS was able to 'spring' to high supersaturation concentrations of phenytoin, but the nearly immediate and rapid induction of crystallization from solution showed its limited ability to stabilize the drug after dissolution (Figure 2.2A). Alternatively, several of the novel HPMC esters (Figures 2.2B and 2.2C) were able to both achieve and maintain supersaturation levels that exceeded what was seen for HPMCAS.

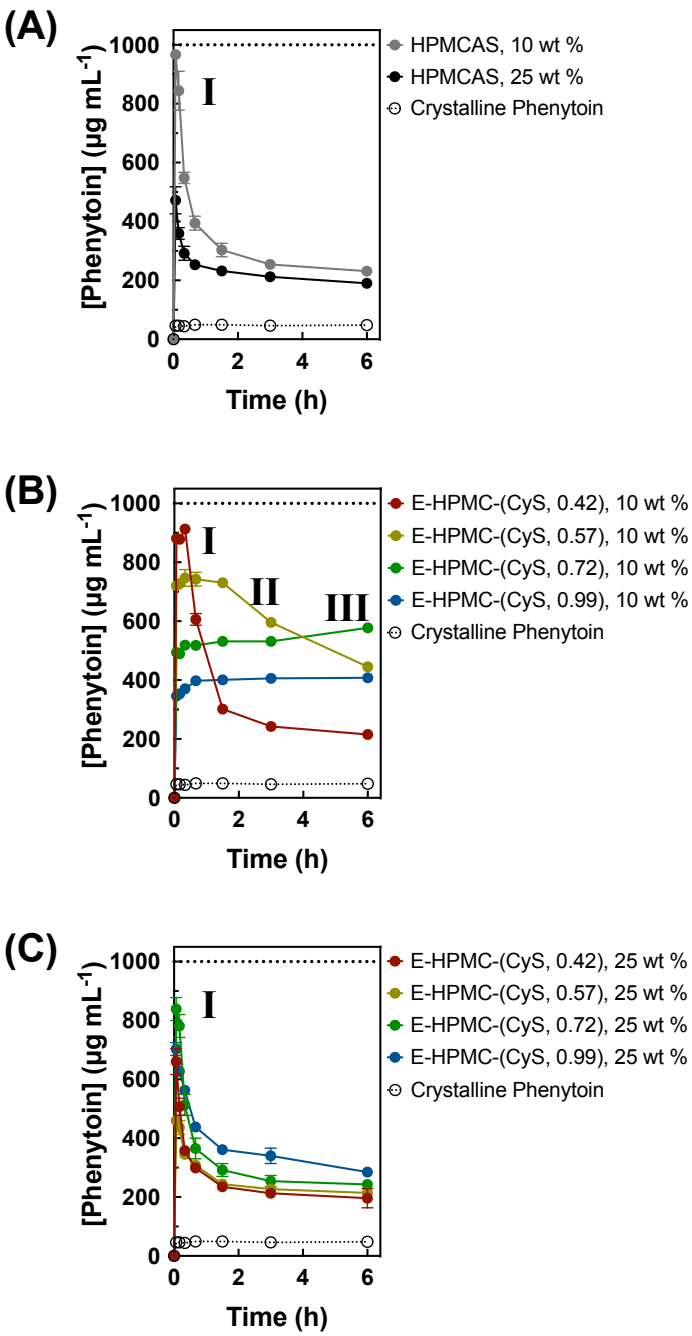

Figure 2.2. Dissolution profiles of phenytoin and the series of (A) solid dispersions from HPMCAS at 10 and 25 wt % phenytoin, and the solid dispersions from HPMC cyclohexythio succinates at (B) 10 wt % and (C) 25 wt % phenytoin. Samples are named E-HPMC-(CyS, DS) where the E represents the commercially-available starting grade of HPMC used, METHOCEL™ E, a trademark of The Dow Chemical Company, and DS is

the degree of substitution of the CyS substituent. Solid dispersions were added at a concentration to give a total amount of phenytoin of 1000 μg mL^{-1}.

At 10 wt % loading, the differences of performance are evident across all three dissolution profile types (Figure 2.2B). The lowest CyS substitution of 0.42 yielded a 'type I' release while further increasing the substitution to 0.57 extended the induction time to give a 'type II' profile. Solid dispersions made from the two highest CyS substitution levels of 0.72 and 0.99 showed no decrease in the concentration of phenytoin achieved over the 6 h and were categorized as 'type III'. On the contrary, at 25 wt % drug (Figure 2.2C), all excipients show fast induction times of less than 4 min and all gave 'type I' profiles.

There are two stages evident in these dissolution tests: (1) immediate release and (2) either the sustainment or the decrease of the achieved supersaturation level. The first stage, immediate release, or the spring, is governed by the solubility of the polymer, which dictates the maximum phenytoin concentration achievable. As the substitution levels increase across the series, the polymer solubility of these materials in PBS decreases from >9000 to 7000 to 3000 to 2000 μg mL^{-1} and therefore the maximum phenytoin concentration is progressively reduced, as exemplified at 10 wt %. At solid dispersion loadings of 25 wt %, the lower substitution levels of the HPMC CyS esters appear to achieve a lower maximum phenytoin concentration than the two highest substitution levels. However, this apparent discrepancy is likely due to the limited resolution at the early time points, where phenytoin may have already crystallized from solution by the 4 min time point for the most soluble dispersions (DS = 0.42).

The previous second stage, or the parachute, is governed by the ability of the polymer to stabilize the supersaturation level of drug that was reached during the spring. Here differences arise in the shape and the duration of a plateaued concentration of

phenytoin, ultimately determining the release type. If specific intermolecular interactions between the hydrophobic CyS groups and the phenytoin molecules stabilize the drug in solution against crystallization, higher substitutions will yield the best performance with respect to maintaining their achieved supersaturation levels. Indeed, this is seen as better performance at 10 wt % is (with respect apparent with lengthening induction times) a function of increasing substitution. The enhanced performances at higher substitutions at 25 wt % are seen as increasing pseudo-plateau concentrations at the highest substitutions.

These studies demonstrated two important qualities that an ideal excipient must posses to perform well: (1) an appropriately high solubility polymer, and (2) the ability to form enough polymer-drug intermolecular interactions to stabilize the supersaturation level attained during the immediate release. Ergo, to improve the performance of solid dispersions made from the highest-performing E-HPMC-CyS esters, we enacted an excipient design strategy that targeted simultaneously strengthening both of these important qualities.

Our excipient design strategy for this study followed a rationale of orthogonal control. While keeping the CyS functionality, we sought to change other molecular properties of the excipient to probe their independent control on performance, and this was accomplished by adjusting the starting grade of HPMC. Switching to a lower methoxyl ether content in the starting HPMC material increases the free hydroxyls present. More free hydroxyls per anhydroglucose repeat unit independently allow two things:

(1) a higher overall achievable CyS DS, and,

(2) a more hydrophilic material at the same CyS DS of an analogous E-grade based excipient, based on the hydrophilic nature of the remaining unsubstituted hydroxyls.

Thus, the hypothesis of the work presented in this chapter is that improving the solubility of the HPMC esters while achieving high cyclohexylthio succinate degrees of substitution will lead to enhancements in the release of phenytoin over previous work.

2.4 Synthesis of HPMC Esters of Substituted Succinates

A series of four HPMC-CyS succinate esters were prepared as depicted in Scheme 2.3. The esterification proceeded in glacial acetic acid in the presence of catalytic sodium acetate. The reaction time remained constant and the degree of substitution of the cyclohexylthio succinate group was controlled by varying the molar ratio of initial free hydroxyls on the cellulosic backbone to the anhydride (Table S2.1).

Scheme 2.3. Synthesis of HPMC esters of substituted succinates via simple anhydride chemistry.[13]

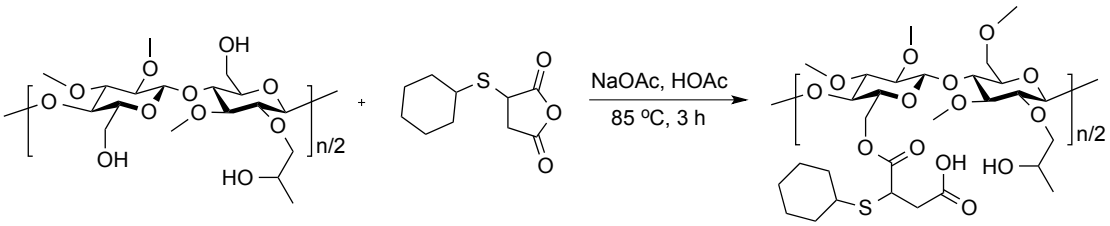

HPMC HPMC-(CyS, DS)

Cyclohexylthio succinic anhydride was synthesized by a thio-ene reaction of cyclohexylthiol with maleic anhydride. Catalytic weak base deprotonates the thiol, which allows for anionic addition across the alkene bond (Scheme 2.4).

Scheme 2.4. Anionic thio-ene reaction of cyclohexylthiol with maleic anhydride in the presence of catalytic triethylamine.

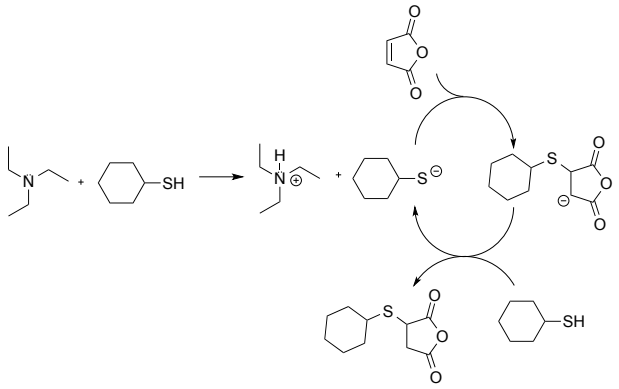

The starting more-hydrophilic HPMC material of this work had methyl ether and hydroxypropyl ether degrees of substitution of 1.41 and 0.23, respectively. Thus, again including the secondary hydroxyls on the HPO substituents, each HPMC repeat unit possessed 1.59 free hydroxyls (on average, and assuming no HPO oligomers) for substitution. The previous work used an HPMC with only 1.09 free hydroxyls per repeat unit. This starting HPMC material was again from the commercially available METHOCEL™ product line, and was generously donated by The Dow Chemical Company. Analogous to the previously used HPMC being of the METHOCEL™ 'E' grade, this HPMC was of the METHOCEL™ 'K' grade, and all samples will be denoted with a prefix 'K'. We chose to use this specific grade of HPMC because, compared to the 'E' grade, the methyl ether substitution level was lower (1.43 vs. 1.91) while hydroxypropyl ether substitution level was similar (0.23 vs. 0.25). This lowering of the hydrophobic methyl ether content freed a higher number of initial hydroxyls, which was directly in accordance with our strategy for accessing both higher ester functionality and more hydrophilic character.

By varying the initial ratio (Table S2.1) of free hydroxyls from HPMC to substituted succinic anhydride, CyS succinate substitution levels were achieved between 0.42 and 1.41. As before, the final HPMC esters are named with starting grade of HPMC, the substituent on the succinate ester, and the degree of substitution. For example, K-HPMC-(CyS, 0.42) refers to HPMC cyclohexylthio succinate at a CyS DS of 0.42, produced from the starting HPMC METHOCEL™ K.

Thermal and molecular weight data of the starting HPMC and the four HPMC succinates are summarized in Table 2.1. Molecular weight determination by size exclusion chromatography (SEC) in aqueous medium gave a number-average molecular weight of 24 kg mol^{-1} and a weight-average molecular weight of 31 kg mol^{-1}. Approximate dn/dc values were determined by the *d*RI signal assuming 100% mass recovery and utilized for the multi-angle light scattering signal. Molecular weights of the HPMC CyS succinate esters ranged from M_n = 22 to 34 and M_w = 30 to 50 kg mol^{-1}. The discrepancy between the lower M_n of the unsubstituted HPMC and the higher M_n of the K-HPMC-(CyS, 0.42) sample was likely a function of using two SEC mobile phases for the HPMC and HPMC esters. No significant crosslinking occurred during esterification as evident by the solubility of the resulting product, though the dispersity did increase after ester substitution.

Table 2.1. Thermal and molecular characteristics of the starting K-HPMC and the K-HPMC-CyS esters.

Polymer Sample	CyS DS[a]	T_g (°C)[b]	M_n SEC (kg mol^{-1})[c]	M_w SEC (kg mol^{-1})[c]	$Đ$[c]	dn/dc (mL mg^{-1})[c]
K-HPMC	–	144	24	31	1.26	0.140
K-HPMC-(CyS, 0.42)	0.42	89	22	30	1.36	0.086
K-HPMC-(CyS, 0.86)	0.86	88	25	38	1.50	0.098
K-HPMC-(CyS, 1.23)	1.23	82	29	43	1.48	0.102
K-HPMC-(CyS, 1.41)	1.41	63	34	50	1.46	0.093

[a]Degree of substitution for cyclohexylthio succinates as determined by ^{1}H NMR.
[b]Glass transition temperatures determined by differential scanning calorimetry (DSC).
[c]Number-average molecular weight, weight-average molecular weight, and dispersity as determined by SEC. Starting HPMC was dissolved in a mobile phase of 0.1 M Na_2SO_4 with 1% acetic acid. HPMC succinates were dissolved in a mobile phase of tetrahydrofuran (THF). SEC instruments were equipped with LS and *d*RI detectors. dn/dc values were determined by the *d*RI signal assuming 100% mass recovery.

The glass transition temperatures (T_gs) of the HPMC succinates were between 60 and 90 °C. The T_g decreased with increasing substitution, with all esters exhibiting a T_g about 60 to 80 °C lower than the starting HPMC. Plasticization likely occurred from the incorporation of the bulky ester substituents,[14] which increased the spacing between cellulose chains and therefore increase chain mobility.

We compared the solid dispersion performance of the novel HPMC esters against a sample of AFFINISOL™ HPMCAS with methyl ether, hydroxypropyl ether, acetate, and succinate substitutions of 1.94, 0.25, 0.57, and 0.28 respectively. This sample falls within a relative medium ('M') Ac to Su ratio range. This M grade HPMCAS was determined by The Dow Chemical Company to outperform all other HPMCAS substitution levels as a solid dispersion excipient for phenytoin at a loading of 10 wt % over 6 h.

2.5 Spray-dried Dispersions of HPMC Esters with Phenytoin

Spray drying is a simple method for preparing solid dispersions of a polymer and drug. THF was determined to be a suitable common solvent for phenytoin and the HPMC esters of substituted succinates. Spray-dried samples were made at lab scale using a mini spray drier from Bend Research, Inc. Organic solutions of the HPMC esters and phenytoin were sprayed from a 2.0 wt % total solids solution. Drug/polymer compositions are expressed as wt % drug, where a 10 wt % sample contains 1:9 (w/w) drug/polymer. Samples were made at 10 wt % and 25 wt % phenytoin. The organic solution of drug and polymer was introduced into the spray-drying apparatus against heated nitrogen via syringe pump; rapid evaporation of the solvent at the spray nozzle left a white powder that collected on a filter. The powders were dried under vacuum overnight. Processing parameters such as inlet temperature, solution flow rate, and nitrogen flow rate were kept constant (see Supplementary Information).

Scanning electron microscopy (SEM) images of the particles were taken of both 10 and 25 wt % samples (Figures 2.3 and 2.4, respectively). The size distributions of the spray-dried particles are broad and roughly bimodal, with a population centered around 1-10 μm in diameter and a population centered around 100 – 200 nm. No substantial differences in bulk morphologies were seen between drug loadings. For the HPMCAS and HPMC-(CyS, 0.42) samples, the spray-dried particles appeared as collapsed spheres. However, at higher CyS substitution levels more spherical particles were observed.

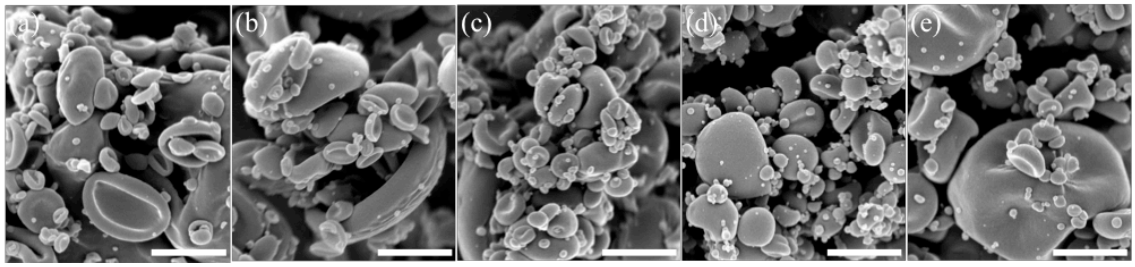

Figure 2.3. Representative SEM images of spray-dried dispersions at 10 wt% phenytoin with (a) HPMCAS, (b) K-HPMC-(CyS, 0.42), (c) K-HPMC-(CyS, 0.86), (d) K-HPMC-(CyS, 1.23), (e) K-HPMC-(CyS, 1.41). Scale bars represent 1.5 μm.

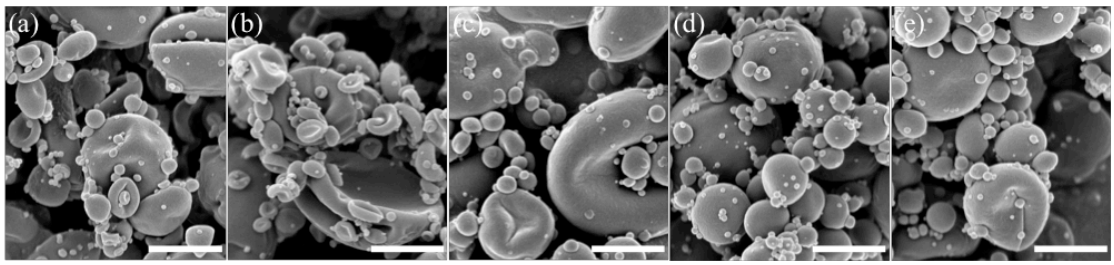

Figure 2.4. SEM images of spray-dried dispersions at 25 wt% phenytoin with (a) HPMCAS, (b) K-HPMC-(CyS, 0.42), (c) K-HPMC-(CyS, 0.86), (d) K-HPMC-(CyS, 1.23), (e) K-HPMC-(CyS, 1.41). Scale bars represent 1.5 μm.

Wide-angle powder X-ray diffraction (PXRD) was carried out on the spray-dried solid dispersions and phenytoin, as received. For phenytoin as received, characteristic peaks at 11.2, 16.5, and 20.2, and 22.3° on the 2θ scale were indicative of crystalline phenytoin. High purity of the drug was supported by an endothermic peak melting temperature of 296 °C by differential scanning calorimetry (DSC). All spray-dried dispersions exhibited broad, featureless XRD patterns (Figure S2.1), indicating the samples are substantially amorphous.

Complementary to XRD, DSC is often employed to determine the crystallinity of spray-dried dispersions, where the percent crystalline drug in the spray-dried samples can

be determined based on the enthalpies of melting, crystallization, and fusion (Equation 2.3).

$$\% \ crystalline = \frac{\Delta H_m - \Delta H_c}{\Delta H_f}\left(\frac{1}{fraction\ drug}\right) \bullet 100 \tag{2.3}$$

Unfortunately, in these systems, the T_m of phenytoin exceeds the temperature of degradation for cellulosic materials. Thus, analyses of thermal stability are restricted to the information that can be deduced from the solid dispersion's tendency to crystallize upon heating. The cold crystallization peak temperature (T_c) seen for pure phenytoin was 157 °C. Spray-dried samples at 10 wt % did not show a crystallization peak in the range of 22 °C to 180 °C (Figure S2.2). Therefore, it is posited that the 10 wt % samples are predominantly thermally-stable, homogeneous amorphous dispersions. In contrast, the 25 wt % dispersions exhibited cold crystallization peaks upon heating, as seen in Figure 2.5, indicative of reduced thermal stability compared to the 10 wt % samples.

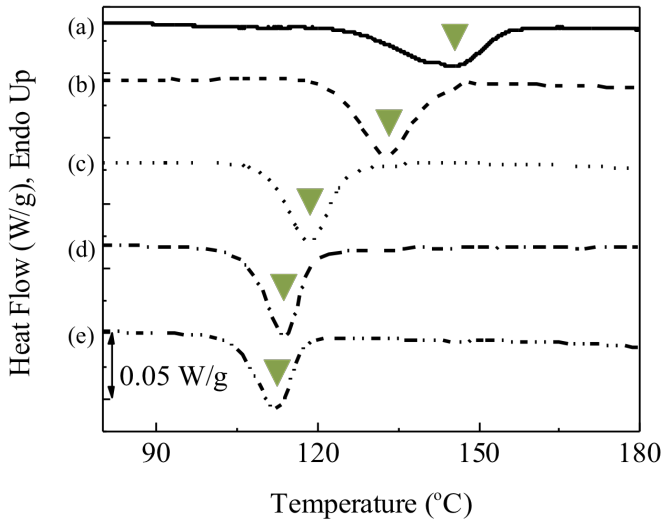

Figure 2.5. DSC traces of 25 wt% phenytoin dispersions with (a) HPMCAS, and K-HPMC-(CyS, DS) where DS = (b) 0.42, (c) 0.86, (d) 1.23, (e) 1.41. Triangles mark cold crystallization exotherms.

The enthalpies of cold crystallization for the solid dispersions (J g^{-1} of spray-dried dispersion) were converted to enthalpies of phenytoin in the sample (J g^{-1} of phenytoin) (Table 2.2). The fraction of loaded drug that crystallized (F_c) during this heat is also given. As pictured in Figure 2.5, the cold crystallization temperatures for the 25 wt % spray-dried dispersions decreased with increasing DS of CyS succinates. Increasing the bulky substituents on the polymer presumably enables molecular mobility of the polymer at lower temperatures, as indicated by lower T_g values, allowing the drug to crystallize at lower temperatures. While the fraction of loaded phenytoin that underwent cold crystallization decreased with increasing CyS succinate substitution levels, the point that a third or so of the loaded drug crystallizes on thermal treatment will likely limit practical loading below this 25 wt %.

Table 2.2. Cold crystallization data for phenytoin and 25 wt % spray-dried solid disperions.

Sample	wt % phenytoin[a]	T_c (°C)[b]	ΔH_c (J g^{-1} phenytoin)[b]	T_m (°C)[c]	F_c[d]
Phenytoin	—	157	—	296	—
HPMCAS	25	145	49	—	0.31
K-HPMC-(CyS, 0.42)	25	133	68	—	0.43
K-HPMC-(CyS, 0.86)	25	119	57	—	0.36
K-HPMC-(CyS, 1.23)	25	114	59	—	0.37
K-HPMC-(CyS, 1.41)	25	112	45	—	0.28

[a]Weight % of the drug in the solid dispersions.

[b]Peak crystallization temperatures and enthalpies as shown by DSC (1st heat cycle). Calculated as ΔH_c (J g^{-1} phenytoin) = ΔH_c (J g^{-1} solid dispersion) / 0.25 (g phenytoin g^{-1} solid dispersion).

[c]Peak melting temperature of pure phenytoin as determined by DSC.

[d]The fraction of phenytoin incorporated in the dispersion that crystallized upon heating. Calculated as ΔH_c (J g^{-1} phenytoin) / ΔH_f (J g^{-1} phenytoin), where ΔH_f of pure phenytoin is 158 J g^{-1}.

To test the effectiveness of these K-HPMC esters at achieving and maintaining supersaturation of phenytoin, dissolution studies were performed with the 10 and 25 wt % spray-dried samples. For all dissolution studies, enough spray-dried dispersion was added such that, if dissolved, all loaded phenytoin would yield a 1000 μg mL^{-1} total concentration. At set time points over 6 h, ultracentrifugation was used to separate undissolved matter from free drug in solution. An aliquot of the supernatant was taken and the concentration of drug in the supernatant was measured by HPLC. Dissolution profiles for the 10 and 25 wt % samples are shown in Figures 2.6 and 2.7, respectively. Performance characteristics such as the maximum concentration reached over the 6 h study (c_{max}), the concentration at the 6 h time point (c_{6h}), and the total area under the curve over the 6 h (AUC_{6h}) are detailed in Table 2.3.

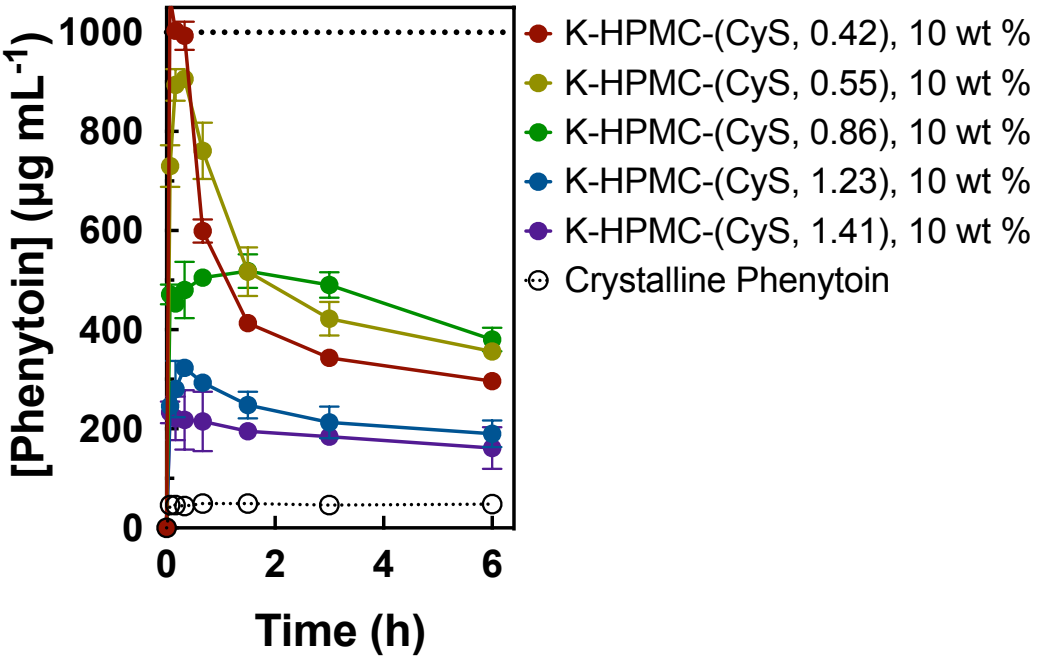

Figure 2.6. Dissolution studies of spray-dried dispersions at 10 wt % phenytoin from K-HPMC-(CyS, DS) solid dispersions. Target phenytoin concentration was 1000 µg mL^{-1}. Tests were run in triplicate. Error bars mark the standard deviation.

Table 2.3. Dissolution performance characteristics for 10 and 25 wt % samples.

Sample	wt % phen-ytoin	c_{max} (μg mL^{-1})[a]	c_{6h} (μg mL^{-1})[b]	AUC_{6h} (μg•h mL^{-1})[c]	EF	F_{ET} • 100 (%)[d]
Phenytoin	—	50	50	2.8×10^2	1.0	5
HPMCAS	10	1000	300	1.8×10^3	6.5	31
K-HPMC-(CyS, 0.42)	10	1000	300	2.5×10^3	8.8	42
K-HPMC-(CyS, 0.55)	10	910	360	3.0×10^3	11	50
K-HPMC-(CyS, 0.86)	10	520	380	2.8×10^3	10	47
K-HPMC-(CyS, 1.23)	10	320	190	1.4×10^3	4.9	23
K-HPMC-(CyS, 1.41)	10	230	160	1.1×10^3	3.9	19
HPMCAS	25	390	120	1.3×10^3	4.6	22
K-HPMC-(CyS, 0.42)	25	430	120	1.0×10^3	3.6	17
K-HPMC-(CyS, 0.55)	25	700	140	1.1×10^3	3.9	18
K-HPMC-(CyS, 0.86)	25	710	190	1.6×10^3	5.6	27
K-HPMC-(CyS, 1.23)	25	370	280	1.6×10^3	5.8	27
K-HPMC-(CyS, 1.41)	25	370	280	1.1×10^3	3.9	19

[a]Maximum concentration of phenytoin achieved.

[b]Concentration of phenytoin at 6 h.

[c]Area under the curve over 6 h dissolution profile.

[d]F_{ET} is the fraction of the engineering target $AUC_{6h(max)}$ achieved, where $AUC_{6h(max)} = 6 \times 10^3$ μg•h mL^{-1}, as if 1,000 μg mL^{-1} phenytoin was immediately achieved and maintained over the full 6 h.

The early-time spring stage of dissolution of the spray-dried particles is directly influenced by polymer solubility. Targeting a 1,000 μg mL^{-1} total drug concentration at 10 wt % phenytoin, the polymeric excipient is added at a concentration of 9,000 μg mL^{-1}. At 25 wt %, the polymer is added at 3,000 μg mL^{-1}. It follows that if the polymer's solubility is significantly below these loadings, in either case, partial dissolution of the polymer will restrict dissolution of the drug. Alternatively, to determine the approximate solubilties of each polymer, polymer solutions were made in PBS, and the concentrations at which the solutions became optically clear were taken as crude polymer solubilities (Table 2.4). Solubility decreased with increasing DS CyS succinate substitution, suggesting that,

although each CyS group also adds an ionizable carboxylate, the hydrophobic CyS moiety dominates solubility.

Table 2.4. Polymer solubilities in PBS.

Polymer	Solubility in PBS (μg mL^{-1})
HPMCAS	> 9,000
K-HPMC-(CyS, 0.42)	> 9,000
K-HPMC-(CyS, 0.55)	7,000
K-HPMC-(CyS, 0.86)	2,000
K-HPMC-(CyS, 1.23)	< 1,000
K-HPMC-(CyS, 1.41)	< 1,000

Evaluating the AUC_{6h}s of the 10 wt % spray-dried dispersions, those made with K-HPMC esters at a CyS DS of 0.42, 0.55, and 0.86 outperformed the HPMCAS dispersions by 35, 61, and 52%, respectively. At this loading, clear differences in the dissolution profiles make it possible to relate the fine elements of the performance parameters to the molecular properties of the HPMC ester excipients. The c_{max} was directly related to polymer solubility as it consistently decreased with decreasing solubility. At the lowest CyS substitution of 0.42, the polymer was completely soluble (*i.e.* solubility is higher than polymer concentration loaded for dissolution), and full release of phenytoin from the solid dispersion was immediately achieved followed by rapid crystallization from solution ('type I' release). However, at the higher CyS degrees of substitution, starting with 0.86, polymer loadings exceeded the polymers' solubilities. In these dissolution studies, release was only achieved to some lower extent and the concentration is maintained at that level over the 6 h (all 'type III' release). Increasing hydrophobicity progressively limited the achieved drug concentration.

When directly comparing the 10 wt % K-HPMC series against the previously studied E-HPMC series, at the same CyS DS of 0.42, the K-HPMC-(CyS, 0.42) sample

had a 30% higher AUC_{6h} than its E-HPMC-(CyS, 0.42) counterpart. Overall, a higher c_{max} was achieved during the initial time points of dissolution for K-HPMC-(CyS, 0.42) (1000 μg mL^{-1} vs. 890 μg mL^{-1}). We hypothesize that the increased hydrophilicity of the starting K-HPMC material directly increased the solubility at this same CyS DS, and therefore increased the achieved supersaturation concentration of phenytoin.

Comparing the best performing of the E-HPMC series, E-HPMC-(CyS, 0.57), to the analogous K-HPMC-(CyS, 0.55), the overall performance with respect to EF and F_{ET} decreased when using the more hydrophilic K-HPMC starting material. This result was contrary to our hypothesis that the increased hydrophilicity at the same substitution level would increase overall supersaturation enhancement of phenytoin in the same dissolution conditions. Under closer examination of the dissolution profiles, the increased hydrophilicity of the K- sample relative to the E- sample switched the release profile from type II to type I. While the solid dispersion from the K-HPMC-(CyS, 0.55) sample reached a higher initial concentration, dissolved phenytoin underwent rapid crystallization. Compared to the delayed induction seen for the E-HPMC-(CyS, 0.57), this type I profile meant that sustainment of high phenytoin concentrations was not achieved, and thus the overall, time-dependent enhancement of phenytoin solubility was lessened.

Comparing across the E- and K- series, at a higher substitution level, the ***K***-HPMC-(CyS, ***0.86***) sample gave a 'type III' dissolution profile with a c_{max}, c_{6h}, AUC_{6h}, and F_{ET} between the ***E***-HPMC-(CyS, ***0.72***) and ***E***-HPMC-(CyS, ***0.99***) profiles. At the highest CyS substitutions (***1.23*** and ***1.41***) of the K series, the c_{max}, c_{6h}, AUC_{6h}, and F_{ET} were all *lower* than what we seen for the E-HPMC-(CyS, ***0.99***) sample. The hydrophobicity of these highly substituted samples limits the potential of these HPMC esters for excipients of solid

dispersions, as phenytoin release continues to decrease from 0.99 to 1.23 to 1.41 across both HPMC grades.

From these dissolution plots, we have determined that the overall dissolution profile character (type I, type II, type III, etc.) across both the E- and K- series is both a function of the substitution level and the starting HPMC. With increasing CyS substitution, the transition from type I to II to III is evident and related to decreased solubility of the polymer. Separately, at the same substitution, the hydrophilic/hydrophobic character of the starting HPMC can drastically change the dissolution profile. Of particular significance is that this evidence suggests that sustainment of supersaturation is not only related to the number of stabilizing pendants (CyS groups), but also related to the overall nature of the excipient and its behavior in aqueous buffer.

Considering both series, the best performance of all HPMC esters was seen for samples with substitutions between 0.55 and 0.86. Each of these gave EFs above 10; HPMCAS gave an EF of 6.5. We hypothesize that within this DS 'sweet spot,' the polymer is at a hydrophilic/hydrophobic ratio that promotes the polymer to interact with phenytoin while still allowing the polymer to mostly dissolve in solution (releasing a significant fraction of the drug). Further, while we recognize that there is a detrimental DS CyS-solubility interplay, it appears that, at this substitution, there are enough CyS groups to significantly stabilize the amount of phenytoin initially introduced into solution at the 10 wt % to minimize crystallization for several hours.

The dissolution profiles of the solid dispersions at 25 wt % phenytoin (Figure 2.7) exhibited a great deal of overlap and made differentiating success of the samples difficult. At this drug loading, the sulfur to phenytoin ratio is significantly reduced (Table 2.5) and, as a result, so is the potential for CyS-drug intermolecular interactions, which have been

suggested to be important in supersaturation achievement and maintenance. Interestingly, at 25 wt %, a profile switch is observed for the higher substitution K-HPMC esters. At 25 wt %, no excipients were seen to significantly outperform HPMCAS. Enhancement factors for both 10 and 25 wt % are summarized in Figure 2.8.

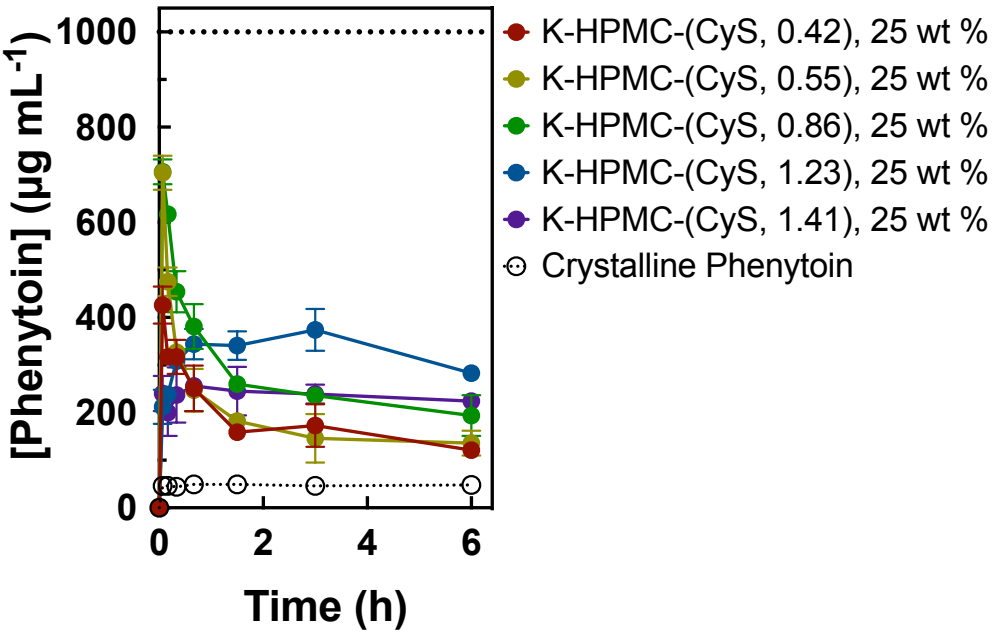

Figure 2.7. Dissolution studies of spray-dried dispersions at 25 wt % phenytoin from K-HPMC-(CyS) solid dispersions. Target phenytoin concentration was 1000 µg mL^{-1}. Tests were run in triplicate. Error bars mark the standard deviation.

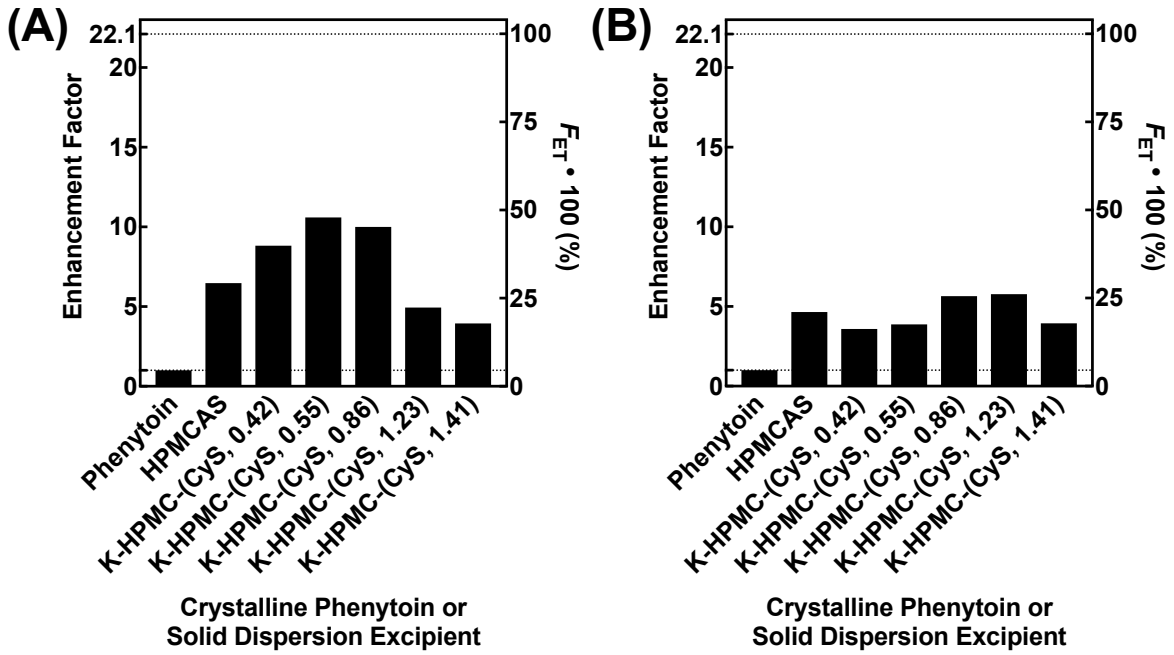

Figure 2.8. A comparison of the enhancement factors (EFs) (left axis) measured during dissolution over 6 h for crystalline phenytoin and different spray-dried dispersions loaded at (A) 10 wt % phenytoin and (B) 25 wt% phenytoin, as defined in equation (2.1). All dissolution studies were performed with a phenytoin target concentration of 1000 μg mL^{-1}, and the maximum EF possible under these conditions was 22.1. Also shown are the related percentages of the engineering target achieved, as defined in equation (2.2) (right axis).

Table 2.5. Ratios of sulfur to loaded phenytoin[a] based on solid dispersion drug loading and CyS substitution of the HPMC esters.

Polymer	10 wt % phenytoin	25 wt % phenytoin
K-HPMC-(CyS, 0.42)	3.3	1.1
K-HPMC-(CyS, 0.86)	5.0	1.7
K-HPMC-(CyS, 1.23)	6.0	2.0
K-HPMC-(CyS, 1.41)	6.3	2.1

[a]These are the same ratios of carboxylates to phenytoin, as the CyS and acid functionalities are added on the same substituent. An analogous table for the E-HPMC ester series can be found in Table S2.2.

In conclusion, we have utilized two HPMC-CyS ester series made from different starting HPMC materials to evaluate how the molecular properties of the excipient affect solid dispersion performance. The spring mechanism was enhanced in the K series by increasing the hydrophilicity of the excipient, as evident by the higher c_{max} phenytoin concentrations seen for K-HPMC-(CyS, 0.42) and K-HPMC-(CyS, 0.55) relative to E-HPMC-(CyS, 0.42) and E-HPMC-(CyS, 0.57) at 10 wt %. The dissolution parachute was a function of the stabilizing interactions between phenytoin and the CyS group, where increasing CyS substitution levels led to better stability of the maximum concentration of phenytoin achieved (less crystallization evident over the 6 h, as would be seen by a decrease in concentration). However, with higher CyS substitution levels, the maximum concentration was lowered as the polymer's hydrophobicity restricted its dissolution.

2.6 Supplemental information

Materials

All chemicals were used as received: cyclohexanethiol (Aldrich, 97%), triethylamine (Sigma-Aldrich, 99.0+%), sulfuric acid (BDH, 95.0-98.0%), maleic anhydride (Fluka, 99+%), phenytoin (Sigma, 99+%), toluene (Sigma-Aldrich, anhydrous, 99.8%), acetic acid (Sigma-Aldrich, 99.7+%), sodium acetate (Sigma-Aldrich, 99.0+%), hydroxypropyl methylcellulose (METHOCEL™ K3 Premium LV, The Dow Chemical Company), hydroxypropyl methylcellulose acetate succinate (AFFINISOL™ HPMCAS 912 G, The Dow Chemical Company), simulated intestinal fluid powder (Biorelevant), chloroform-*d* (Aldrich, 99.96% atom D) and dimethyl sulfoxide-d_6 (Cambridge Isotope Laboratories, 99.9% D).

Molecular Characterization

Nuclear magnetic resonance (NMR) was performed on a 500 MHz Varian INOVA-500 spectrometer in chloroform-*d* or DMSO-d_6.

Size exclusion chromatography (SEC) was performed on the starting HPMC using an aqueous Agilent 1260 Infinity system equipped with Eprogen (Downers Grove, IL) columns [CATSEC-1000 (1000 Å, 7 μm, 50 × 4.6), CATSEC-100 (100 Å, 5 μm, 250 × 4.6), CATSEC-300 (300 Å, 5 μm, 250 × 4.6), CATSEC-1000 (1000 Å, 7 μm, 250 × 4.6) columns, a Wyatt Dawn Heleos-II light scattering detector and an Optilab T-rEX refractometer. The mobile phase was Millipore water with 0.1 M Na_2SO_4 supplemented with 1% acetic acid at a flow rate of 0.4 mL min^{-1}.

SEC was performed on the HPMC cyclohexylthio succinates using an Agilent 1260 liquid chromatograph with THF as the mobile phase. The SEC houses a Waters Styragel guard column and three separation columns that cover an effective molecular weight range of 100– 10,000,000 g mol^{-1}. The system is equipped with an Agilent 1260 VWD UV-Vis detector, a Wyatt Dawn Heleos II light scattering detector, and a Wyatt Optilab T-rEX refractometer.

Synthesis of Cyclohexylthiosuccinic Anhydride

Synthesis of cyclohexylthiosuccinic (CyS) anhydride followed a method previously developed in our group.[43] Cyclohexylthiol (11.3 mL, 9.2 × 10^{-2} mol), maleic anhydride (9.0 g, 9.2 × 10^{-2} mol), and triethylamine (128 μL, 9.2 × 10^{-4} mol) was added to 75 mL of toluene at 70 °C and reacted for 3.0 h. Concentrated sulfuric acid (150 μL) was added in slight excess to quench the reaction. The dark brown mixture was filtered and concentrated under vacuum. The crude product was purified by column chromatograph in 8/2 (v/v) hexanes/ethyl acetate (R_f = 0.49) and fractional distillation (b.p. = 105 °C at 7

mTorr) to give a light-yellow oil that crystallized upon storage in the refrigerator (99% conversion by ^{1}H NMR, 61% yield). ^{1}H NMR (500 MHz, Chloroform-*d*) δ 4.03 (dd, 1H), 3.40 (dd, 1H), 3.14 (m, 1H), 2.83 – 2.70 (dd, 1H), 2.12 (m, 1H), 1.92 (m, 1H), 1.87 – 1.70 (m, 2H), 1.65 (d, 1H), 1.34 (m, 5H).

Synthesis of HPMC Cyclohexylthiosuccinates

The synthesis of HPMC-(CyS, 0.42) is given as a representative example. HPMC (2.0 g, 1.6×10^{-2} mol pendant hydroxyls), acetic acid (20 mL), sodium acetate (2.7 g, 3.2×10^{-2} mol) was allowed to dissolve and brought to 85 °C. Cyclohexylthiosuccinic anhydride (1.7 g, 8.1×10^{-3} mol) was added and the reaction proceeded for 3 h. Unreacted anhydride was quenched with the addition of DI H_2O. The reaction mixture was precipitated into 2 L DI H_2O, collected, redissolved in THF and precipitated at least twice more. The final product was dried for two days under vacuum at room temperature. The product was fibrous with an increasing yellow color at higher degrees of substitution.

Spray Drying

Spray-dried dispersions were made at lab scale using a Mini-spray dryer (Bend Research, Bend, OR). At a total solids loading of 2.0 wt %, polymer and drug were magnetically stirred in tetrahydrofuran overnight. Samples were loaded into a 20 mL syringe and fastened to a syringe pump. The inlet temperature (68 °C), N_2 flow rate (12.8 sL min^{-1}), and solution flow rate (0.65 mL min^{-1}) were kept constant. Spray-dried dispersions were collected on a filter, left under a grounded, anti-static wand and dried under vacuum (less than 20 mTorr) for 24 h. Samples were stored at room temperature in a vacuum desiccator.

Dissolution Studies

Dissolution studies were performed in phosphate buffered saline (PBS, 82 mM sodium chloride, 20 mM sodium phosphate dibasic, 47 mM potassium phosphate monobasic, 0.5 wt% simulated intestinal fluid powder, adjusted to pH 6.5 with 0.1 M NaOH) solutions at 37 °C. In a 1.5-mL microcentrifuge tube, an appropriate amount of spray-dried dispersion and PBS was added to target a total drug concentration of 1000 μg mL^{-1} (1.00 mg mL^{-1}). For example, for dispersions of 25 wt% phenytoin, 6.0 mg of spray-dried dispersions (6.0 ×0.25 = 1.5 mg phenytoin) was diluted with 1.5 mL of PBS. Samples were vortexed for 1 min and set in an isothermal sample holder at 37 °C (t=0). At set time points (4, 10, 20, 40, 90, 180, 360 min), the samples were centrifuged at 13,000 g for 1 min, a 50-μL aliquot was removed and diluted with 250 μL of HPLC grade methanol. The samples were then vortexed for 30 sec to resuspend the dispersion and returned to the isothermal sample holder. The drug concentration was determined by reverse phase high performance liquid chromatography (HPLC) in 60/40 (v/v) H_20/MeCN. Samples were analyzed on an Agilent 1260 liquid chromatograph with a multi-wavelength UV-Vis detector, 1260 MWD, at 240 nm. Separation occurred on an Agilent Poroshell 120 EC-C18 column with 120 Å pores. A calibration was made from 12.5 to 500.0 μg mL^{-1} with an R^2 = 0.9999.

Powder X-ray Diffraction (Powder XRD)

Spray-dried dispersion samples were examined by PXRD using a Bruker-AXS D5005 Diffractometer. Samples (~50 mg) were packed in a 0.5-mm-deep zero-background holder. Using a Cu- Kα X-ray source (λ=1.54 Å, 45 kV and 40 mA), data was collected from 5° to 40° on the 2θ scale at a step size of 0.02° with a dwell time of 1 s $step^{-1}$.

Differential Scanning Calorimetry (DSC)

DSC analyses were performed using a Discovery DSC (TA Instruments) equipped with a refrigerated cooling system. Samples (2 – 8 mg) were packed in TZero aluminum pans. A dry N_2 purge flowed through the cell at 50 mL min^{-1}. Pure polymer was loaded into standard pans and ramped through a heat/cool/heat cycle between 22 °C and 180 °C at 10 °C min^{-1}. T_gs were taken from the 2nd heating cycle. Spray-dried dispersions were packed in hermetically-sealed pans and heated from 22 °C to 180 °C at 2.5 °C min^{-1}. Cold crystallization enthalpies are reported from the 1st heat. Phenytoin was packed in a hermetically-sealed pan and run through a heat/cool/heat cycle between -20 °C and 300 °C at 10 °C min^{-1}. All analyses were carried through TA Trios software version 3.0.

Scanning Electron Microscopy (SEM)

SEM images were taken on a Hitachi S-900 field emission gun SEM using a secondary electron detector operating at an accelerating voltage of 3.0 kV. Magnification was between 5,000 and 20,000 magnification. Prior to imaging, spray-dried dispersions were sprinkled on to conductive carbon tape (Ted Pella Inc.) and sputter coated with 10 nm of Au/Pd (60/40) to limit sample charging.

Table S2.1. HPMC ester substitution levels as a function of the ratio of free HPMC hydroxyls to anhydride.

Sample	**[HPMC OH]$_0$:[Anhydride]$_0$**[a]	**DS**[b]
K-HPMC-(CyS, 0.42)	1:0.5	0.41
K-HPMC-(CyS, 0.55)	1:0.75	0.57
K-HPMC-(CyS, 0.86)	1:1	0.86
K-HPMC-(CyS, 1.23)	1:2	1.23
K-HPMC-(CyS, 1.41)	1:3	1.41

[a]The initial ratio of free hydroxyls on HPMC to the cyclohexylthio succinic anhydride.

[b]The degree of substitution as determined by ^{1}H NMR.

Table S2.2. Ratios of sulfur[a] to loaded phenytoin based on solid dispersion drug loading and CyS substitution of the HPMC esters for the E series samples.

Polymer	10 wt % phenytoin	25 wt % phenytoin
E-HPMC-(CyS, 0.42)	3.3	1.1
E-HPMC-(CyS, 0.57)	4.0	1.3
E-HPMC-(CyS, 0.72)	4.6	1.5
E-HPMC-(CyS, 0.99)	5.4	1.8

[a]These are the same ratios of carboxylates to phenytoin, as both functionalities are included on the same substituent.

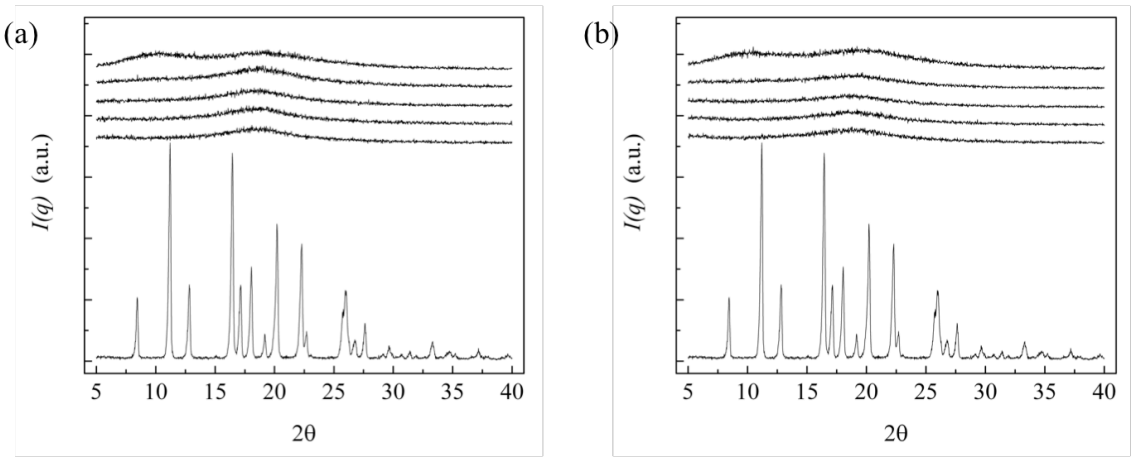

Figure S2.1. PXRD patterns of spray-dried dispersions loaded at (a) 10 wt % and (b) 25 wt % phenytoin. In both patterns, the excipients are HPMCAS, K-HPMC-(CyS, 0.42), K-HPMC-(CyS, 0.86), K-HPMC-(CyS, 1.23), K-HPMC-(CyS, 1.41) from top down with crystalline phenytoin at the bottom. All solid dispersion patterns appear broad and featureless.

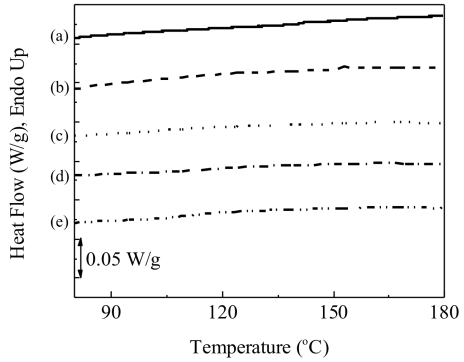

Figure S2.2. Representative DSC traces of spray-dried dispersions loaded at 25 wt% phenytoin with (a) HPMCAS, (b) K-HPMC-(CyS, 0.42), (c) K-HPMC-(CyS, 0.86), (d) K-HPMC-(CyS, 1.23), (e) K-HPMC-(CyS, 1.41).

2.7 References

(1) Friesen, D. T.; Shanker, R.; Crew, M.; Smithey, D. T.; Curatolo, W. J.; Nightingale, J. A. S. *Mol. Pharm.* **2008**, *5*, 1003–1019.

(2) Curatolo, W.; Nightingale, J. A.; Herbig, S. M. *Pharm. Res.* **2009**, *26*, 1419–1431.

(3) Yin, L.; Hillmyer, M. A. *Mol. Pharm.* **2014***, 11* (1), 175–185.

(4) Fox, S. C.; Li, B.; Xu, D.; Edgar, K. J. *Biomacromolecules* **2011**, *12* (6), 1956–1972.

(5) Philipp, B.; Wagenknecht, W.; Wagenknecht, M.; Nehis, I.; Klemm, D.; Stein, A.; Heinze, T.; Heinze, U.; Helbig, K.; et, al. *Papier (Darmstadt)* **1995**, *49* (Copyright (C) 2017 American Chemical Society (ACS). All Rights Reserved.), 3–7.

(6) Philipp, B.; Klemm, D.; Wagenknecht, W. *Papier (Darmstadt)* **1995**, *49* (Copyright (C) 2017 American Chemical Society (ACS). All Rights Reserved.), 58–64.

(7) Philipp, B.; Klemm, D.; Stein, A. *Papier (Darmstadt)* **1995**, *49* (Copyright (C) 2017 American Chemical Society (ACS). All Rights Reserved.), 102–103, 106–108.

(8) Klemm, D.; Heinze, T.; Stein, A.; Liebert, T. *Macromol. Symp.* **1995**, *99* (1), 129–140.

(9) Using Dow Excipients for Controlled Release of Drugs in Hydrophilic Matrix Systems **2006**.

(10) Kar, N.; Liu, H.; Edgar, K. J. *Biomacromolecules* **2011**, *12*, 1106–1115.

(11) Mithani, S. D.; Bakatselou, V.; TenHoor, C. N.; Dressman, J. B. *Pharm. Res.* **1996**, *13*, 163–167.

(12) Zipp, G. L.; Rodriguez-Hornedo, N. *J. Phys. Appl. Phys.* **1993**, *26*, B48.

(13) Zienty, F. B.; Vineyard, B. D.; Schleppnik, A. A. *J. Org. Chem.* **1962**, *27*, 3140–3146.

(14) Liu, H.; Kar, N.; Edgar, K. J. *Cellulose* **2012**, *19*, 1279–1293.

Chapter 3: Impact of Molar Mass and End Groups of Poly(*N*-Isopropyl Acrylamide)-Based Excipients for Phenytoin Dissolution Enhancement

3.1 Introduction

Several general guiding principles for designing successful excipients have been established from the combination of serendipitously discovered high performing excipient-drug combinations and expansive polymer-screening studies.[1-6] However, exceptions to these design guides remain prevalent, and appropriate polymer-drug matches are still often only found through a laborious and inefficient screening process. In this study, we aimed to systematize the evaluation of excipient candidates in order to provide guiding principles for future directions in excipient science. Specifically, we explored the influence of molar mass and polymer end group identity on the efficacy of solid dispersion excipients to

increase hydrophobic drug solubility. Although it is well known that polymer end group and molar mass can significantly alter solution properties, such as solubility and solution assembly,[7,8] the aforementioned excipient design principles were often based on studies that did not emphasize these molecular details. In this work, we investigated the role of these polymeric excipient molecular characteristics (*i.e.*, molar mass and end groups) in order to clarify our understanding of structure-performance relationships, and to increase our ability to predictively design amorphous solid dispersion excipients for pharmaceutical formulations. We prepared poly(*N*-isopropylacrylamide)-based excipients of varying molar mass and with various end group identities, and examined their ability to improve the aqueous solubility of the Biopharmaceutical Class System Class II drug, phenytoin. Solid dispersions of these excipients and phenytoin were prepared at 10 wt% drug loading. Performance, as determined by apparently solubility enhancement, depended largely on the tendency of the polymer excipient to form micellar aggregates in aqueous buffer. We present several systems that achieved significant improvement of phenytoin solubility, with no indication of drug crystallization over 6 h. This is among the highest enhancement factors seen for phenytoin in literature, and the success of these systems is preliminarily ascribed to the added micelle-forming character of these solid dispersions.

3.2 Synthesis Strategy to Control and Vary End Group and Molar Mass

To systematically study the effect of end groups and molar mass on the performance of an excipient, we chose a single monomer from which to synthesize several series of polymeric materials for solid dispersion excipients with phenytoin (Figure 3.1a). Poly(*N*-isopropylacrylamide) (PNiPAm) is a hydrophilic thermoresponsive polymer, (Figure 3.1b) and was chosen as the studied excipient because it possesses an amide group on each

monomer that could potentially participate in hydrogen bonding with phenytoin. In fact, PNiPAm homopolymer, poly(*N*-isopropylacrylamide-*co*-vinylpyrrolidone) copolymers, poly(*N*-isopropylacrylamide-*co*-dimethylacrylamide) copolymers, and PNiPAm-based blends have been studied as solid dispersion excipients with much success in enhancing supersaturation of phenytoin.[9,10]

We prepared NiPAm-based polymers via reversible addition-fragmentation chain transfer (RAFT) polymerization, and studied their ability as excipients to maintain high levels of supersaturation of phenytoin.[11] By synthesizing these materials via RAFT polymerization, we gained facile end-group selection and precise control over molar mass. Trithiocarbonate chain transfer agents (CTAs) are readily synthesized, and numerous structural variations are commercially available. Additionally, polymers synthesized by RAFT inherit both polymer ends directly from the CTA. By independently adjusting the functionalities of the α-end group (the CTA R-group) and the ω-end group (the alkyl chain from the CTA Z-group), we probed the impact of each chain end on excipient solution behavior and solid dispersion dissolution performance. Changing the CTA can also be a facile method for controlling the solubility of the final polymer, in low molar mass samples in particular, and hydrophobic ω-end groups was varied to induce self-assembly of hydrophilic polymers in aqueous solution.[12]

Inherent to RAFT polymerizations, the trithiocarbonate moiety is incorporated into the final polymer. Fairbanks *et al.* reviewed biomedical application studies of polymers derived by RAFT, and while there are a variety of synthetic methods to remove the trithiocarbonate functionality, removal does not appear to be necessary for this application of solid dispersions.[13] Indeed, Pissuwan *et al.* and Chang *et al.* report that the trithiocarbonate moiety does not invoke cytotoxicity.[14,15] Thus, while the trithiocarbonate

is included in all of the polymers generated in this study, we did not find a strong motivation to modify it. Additionally, while the trithiocarbonate is molecularly incorporated into all of the polymers studied here, we have focused on only denoting and differentiating based on the α- and ω- groups, as they differ across the samples (Figure 3.1b).

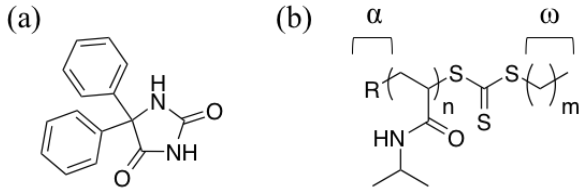

Figure 3.1. Structures of (a) BCS Class II model drug phenytoin, and (b) PNiPAm from a trithiocarbonate RAFT CTA with a linear alkyl thiol Z group. The α- and ω-end groups are labeled.

3.3 Synthesis of poly(*N*-isopropylacrylamide)s

Seventeen poly(*N*-isopropylacrylamide) samples with varying end groups were synthesized by RAFT polymerization. End group identities were inherited from the starting RAFT CTAs, which were either commercially available or synthesized from an alkyl thiol precursor. To independently probe the effects of the α-group and the ω-group, ten different RAFT CTAs were utilized (Scheme 3.1).

Scheme 3.1. Synthesis of PNiPAm samples from various RAFT agents

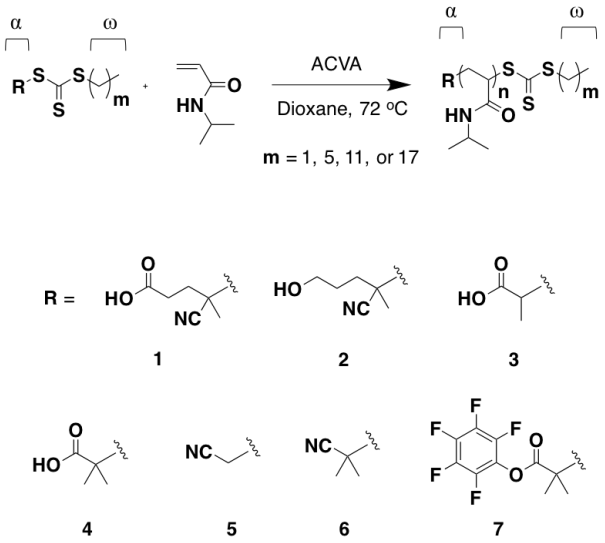

Poly(*N*-isopropylacrylamide) was synthesized from each CTA (Scheme 3.1), and samples are named as PNiPAm-(α, ω, M), where α represents the RAFT CTA R group (**1**–**7**), ω is the Z-end terminus alkyl thiol length (C_2, C_6, C_{12}, or C_{18}) (excluding the sulfur attached to the thioester that is typically included in trithiocarbonate RAFT CTA Z-group nomenclature), and M is the PNiPAm M_n (by NMR spectroscopy) in kg mol^{-1}. The molecular characteristics and thermal data for these samples are summarized in Table 3.1. Low molar masses of PNiPAm were targeted to enhance the observed influence of the end groups. All of the samples showed monomodal elution curves by SEC in THF with light scattering detection, with $Đ$ values ranging from 1.02 to 1.14. DSC thermograms of the polymers displayed a single T_g value between 70 and 114 °C; representative traces are displayed in Figure S3.1. The polymers were hydroscopic and readily absorbed atmospheric water, as shown in water uptake studies (Table S3.1). The hydroscopic nature of these excipients would likely warrant specific future formulation considerations to prevent a plasticizing effect from the absorption of atmospheric moisture.

Table 3.1. Molecular and thermal characteristics of PNiPAm samples.

Sample	M_n NMR[a] (kg mol^{-1})	M_n SEC[b] (kg mol^{-1})	M_w SEC[b] (kg mol^{-1})	$Đ$[b]	T_g[c] (°C)	Solubility[d]
PNiPAm-(**1**, C_{12}, 1.3)	1.3	2.0	2.0	1.02	70	++
PNiPAm-(**2**, C_{12}, 1.3)	1.3	2.1	2.2	1.08	74	++
PNiPAm-(**3**, C_{12}, 1.5)	1.5	2.0	2.2	1.10	75	+
PNiPAm-(**4**, C_{12}, 1.6)	1.6	1.9	2.2	1.10	80	+
PNiPAm-(**5**, C_{12}, 1.5)	1.5	5.7	6.0	1.06	72	–
PNiPAm-(**6**, C_{12}, 1.4)	1.4	4.7	5.3	1.14	70	–
PNiPAm-(**7**, C_{12}, 1.5)	1.5	2.7	2.9	1.08	79	–
PNiPAm-(**1**, C_2, 1.8)	1.8	2.3	2.6	1.13	98	++
PNiPAm-(**1**, C_2, 3.9)	3.9	3.9	4.0	1.02	102	+
PNiPAm-(**1**, C_6, 2.1)	2.1	2.6	2.8	1.08	95	++
PNiPAm-(**1**, C_6, 3.8)	3.8	4.6	4.8	1.02	101	+
PNiPAm-(**1**, C_{18}, 1.4)	1.4	2.2	2.4	1.09	75	+
PNiPAm-(**1**, C_{18}, 4.6)	4.6	4.8	5.0	1.05	98	++
PNiPAm-(**1**, C_{12}, 4.4)	4.4	4.5	4.6	1.03	101	+
PNiPAm-(**1**, C_{12}, 22.0)	22	21	22	1.04	114	–
PNiPAm-(**1**, C_{18}, 6.0)	6.0	6.0	6.1	1.02	96	++
PNiPAm-(**1**, C_{18}, 8.0)	8.0	8.1	8.3	1.02	111	++

[a] M_n NMR determined by ^{1}H NMR spectroscopy in d_6-DMSO.

[b] M_n SEC, M_w SEC, and $Đ$ determined by SEC using a light-scattering detector.

[c] Glass transition temperatures (T_gs) as determined by DSC in the second heating cycle at a heating rate of 10 °C min^{-1}.

[d] (++) represents solubility in PBS greater than 9 mg mL^{-1}, (+) represents solubility in PBS between 3 mg mL^{-1} and 9 mg mL^{-1}, (–) represents solubility in PBS less than 3 mg mL^{-1}.

The first series of PNiPAm samples varied the α-end group (**1**–**7**) while keeping the ω-end group (C_{12}) and molar mass (1.3–1.6 kg mol^{-1}) approximately constant. The second series varied molar mass (1.3, 4.4, 22.0 kg mol^{-1}) while keeping the α-end group (**1**) and ω-end group (C_{12}) constant. The third series varied the alkyl length on the ω-end group (C_2, C_6, C_{12}, and C_{18}) while keeping the α-end group (**1**) and molar mass (3.8–4.6 kg mol^{-1}) approximately constant. A fourth series was also studied where the α-end group was constant (**1**), an alternate ω-end group alkyl length of C_{18} was constant (similar to the second series using C_{12}), and molar mass was varied (4.6, 6.0, and 8.0 kg mol^{-1}).

3.4 Spray-Dried Dispersions with Phenytoin

The bulk spray-dried dispersions were evaluated by scanning electron microscopy (SEM), powder X-ray diffraction (PXRD), thermogravimetric analysis (TGA), and differential scanning calorimetry (DSC). By SEM, all bulk, spray-dried samples appeared as collapsed and wrinkled particles ranging from ~50 nm to 10 μm in size (Figure 3.2) with no indication of crystalline phenytoin structures (Figure S3.1). PXRD data on the bulk spray-dried samples were broad and essentially featureless (Figure S3.2), indicating that the dispersions were largely amorphous, within the detection limits of the PXRD analysis.[16]

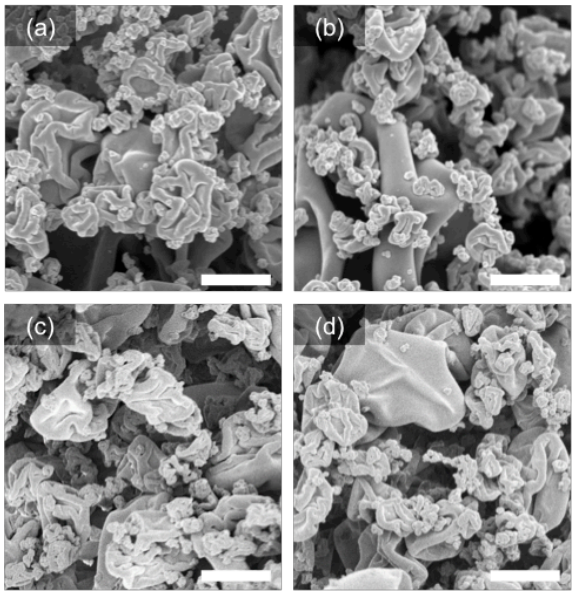

Figure 3.2. Representative SEM images of spray-dried dispersions of (a) pure polymer, PNiPAm-(**1**, C_{12}, 1.3), (b) PNiPAm-(**1**, C_{12}, 1.3) and phenytoin at 10 wt% drug loading, (c) PNiPAm-(**2**, C_{12}, 1.3) and phenytoin at 10 wt% drug loading, and (d) PNiPAm-(**7**, C_{12}, 1.3) and phenytoin at 10 wt% drug loading. Scale bars indicate 1 μm.

Thermal analysis of the dispersions by TGA in nitrogen showed 5 wt% mass loss temperatures ($T_{d,5\%}$) between 181 and 216 °C (Table 3.2). DSC thermograms of the solid dispersions were taken after vacuum drying. Although thermal cycling is typically utilized

to remove thermal history of a sample,[17] first-heat T_g values for the dispersions are reported as a more direct measure of the bulk property in the immediate, as-processed state. The thermograms revealed broad T_g values in the range of 46 to 98 °C, and no evidence of phenytoin cold crystallization was observed (Figure S3.3). Dispersions made with polymers of molar masses above 3.8 kg mol^{-1} showed T_g values above 91 °C. Nearly all T_g values of the ASDs were lower than the T_g values of the polymers alone, which can be attributed to the plasticizing effect of dispersed drug in the polymeric matrix.

Table 3.2. Thermal and dissolution characteristics of spray-dried dispersions loaded with 10 wt% phenytoin.

Dispersion matrix	$T_{d,5\%}$ (°C)[a] (TGA)	T_g (°C)[b] (DSC)	c_{max} (μg mL^{-1})[c]	c_{6h} (μg mL^{-1})[c]	AUC_{6h} (μg h mL^{-1})[c]	EF (%)[d]	
PNiPAm-(**1**, C_{12}, 1.3)	207	78	910	870	5250	19	(87%)
PNiPAm-(**2**, C_{12}, 1.3)	201	66	810	800	4800	17	(80%)
PNiPAm-(**3**, C_{12}, 1.5)	202	70	630	620	3700	13	(62%)
PNiPAm-(**4**, C_{12}, 1.6)	198	70	210	200	1210	4.3	(20%)
PNiPAm-(**5**, C_{12}, 1.5)	181	49	110	100	620	2.2	(10%)
PNiPAm-(**6**, C_{12}, 1.4)	209	65	110	100	560	2.0	(9%)
PNiPAm-(**7**, C_{12}, 1.5)	213	46	110	100	540	1.9	(9%)
PNiPAm-(**1**, C_2, 1.8)	210	89	520	490	2040	7.2	(34%)
PNiPAm-(**1**, C_2, 3.9)	209	93	170	130	820	2.9	(14%)
PNiPAm-(**1**, C_6, 2.1)	198	84	380	320	3020	11	(50%)
PNiPAm-(**1**, C_6, 3.8)	203	91	240	150	1130	4.1	(19%)
PNiPAm-(**1**, C_{18}, 4.6)	204	96	926	913	5360	19	(90%)
PNiPAm-(**1**, C_{12}, 4.4)	202	97	335	293	1830	6.5	(31%)
PNiPAm-(**1**, C_{12}, 22.0)	201	98	180	150	510	2.8	(13%)
PNiPAm-(**1**, C_{18}, 6.0)	216	94	780	780	4520	16	(75%)
PNiPAm-(**1**, C_{18}, 8.0)	202	97	380	190	1290	4.6	(22%)

[a] Temperature at 5 wt% mass loss by thermogravimetric analysis in nitrogen.

[b] Glass transition temperatures (T_gs) of the solid dispersions as determined by DSC in the second heating cycle at a heating rate of 10 °C min^{-1}.

[c] Dissolution performance metrics, where c_{max} is the maximum phenytoin concentration achieved over the 6-h study, c_{6h} is the final concentration at the 6 h time point, AUC_{6h} is the area under the concentration-time curve over the 6 h study.

[d] The enhancement factor (EF) is defined as EF = AUC_{6h}(solid dispersion)/AUC_{6h}(phenytoin). Based on these studies, if all loaded drug was released completely and sustained at 1000 μg mL^{-1}, the maximum EF possible is 21. The parenthetical percentage (%) is the percentage of the max possible enhancement factor (21) based on drug loading.

The dissolution performance of a solid dispersion loaded with drug reveals how well the matrix excipient is able to achieve and maintain an *in vitro* supersaturation concentration of the loaded drug in solution. For drugs with high permeability and low solubility (primarily BCS Class II drugs), bioavailability can often be enhanced by raising

the concentration of dissolved drug in solution. Thus, the use of solid dispersion excipients that achieve a high drug supersaturation concentration may translate to an increase in bioavailability of the drug upon administration.

In all dissolution tests, the solid dispersions were added to an aqueous solution that mimics the intestinal lumen (PBS buffer, pH 6.5). At this pH, most carboxylic acid end groups are ionized. Undissolved solids were removed from solution by microcentrifugation at a 13,000 rpm for 1 min, and the concentration of dissolved drug was determined by HPLC. Phenytoin was loaded in these *in vitro* tests at 1,000 μg mL^{-1}, slightly below the theoretical amorphous solubility of phenytoin in DI water[18] of 1,300 μg mL^{-1}, and thus in so-called "non-sink" conditions.[19] At non-sink conditions, near the solubility of the drug, the most discriminating dissolution curves can be obtained.[19]

The maintenance of steady-state supersaturation was largely ascribed to effective crystallization inhibition, where the micellar structures formed by these excipients did not allow for the formation or growth of phenytoin crystals. The dissolution profiles are shown in Figure 3.3, and key metrics such as the maximum concentration reached (c_{max}), the concentration at 6 h (c_{6h}), and the area under the curve over the full 6-hour study (AUC_{6h}) are summarized in Table 3.2. Additionally, the enhancement factors, defined as the AUC_{6h}(solid dispersion)/AUC_{6h}(phenytoin), are included in Table 3.2.

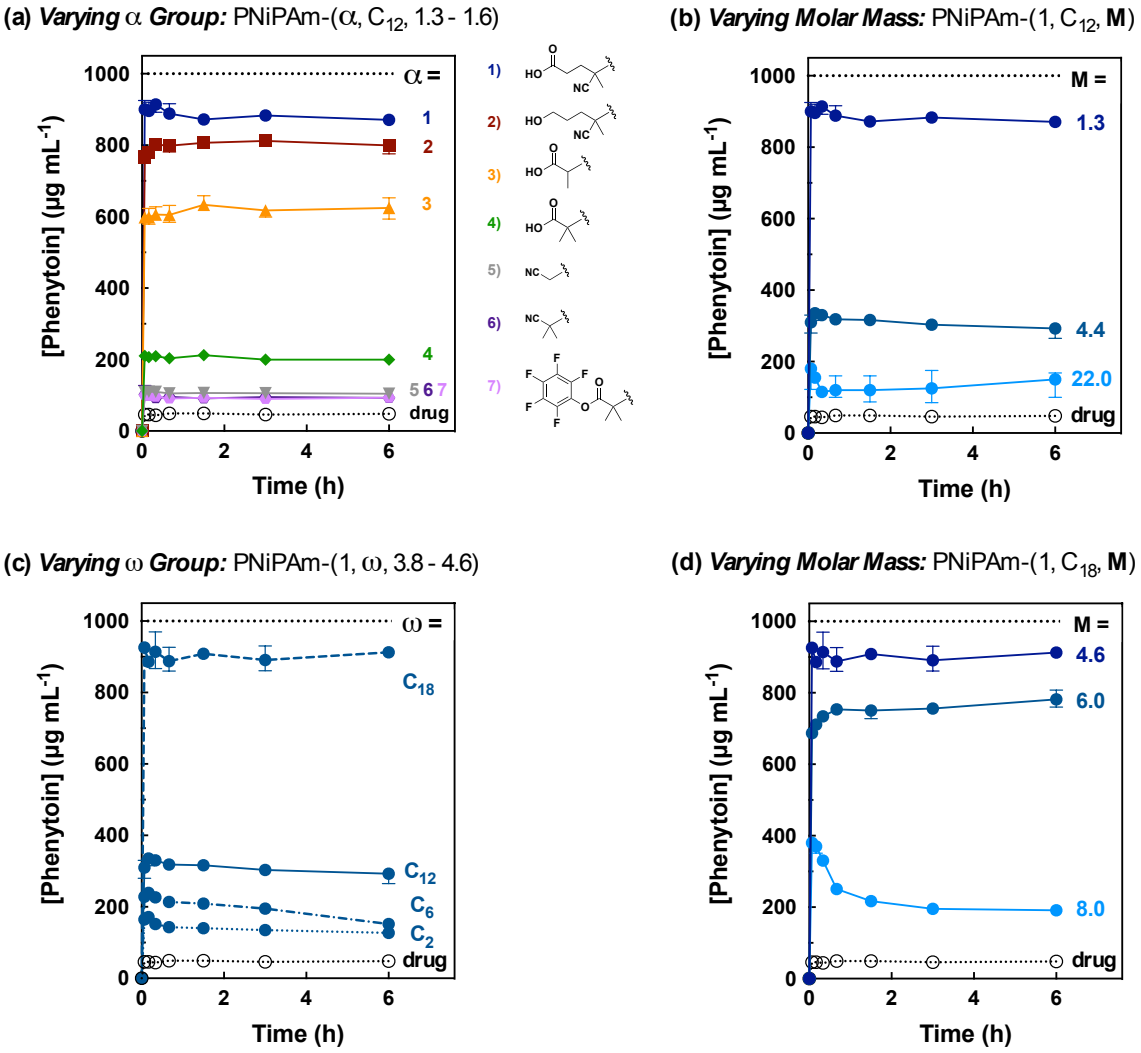

Figure 3.3. Dissolution profiles of spray-dried dispersions at 10 wt% phenytoin loading, as a function of (a) α-end group, (b) molar mass with C_{12} ω-end group, and (c) ω-end group alkyl chain length, and (d) molar mass with C_{18} ω-end group. In all plots, the dissolution profile of crystalline phenytoin was also included as a reference (dots, open circles, labeled 'drug'). The loaded concentration of phenytoin was 1,000 μg mL^{-1}. Dissolution was run in triplicate. The data shown are the mean values, and the error bars represent the range of data.

3.5 Varying α-End Group

The first series (Figure 3.3a) of excipients varied the chemical nature of the α-end group (**1**–**7**) while keeping the ω-end group (C_{12}) fixed and the molar mass (1.3–1.6 kg mol^{-1}) approximately constant. From this series, we identified a strong dependence of the solid dispersion performance on the α-end group. The CTA α-end groups are assigned from **1** to **7** based on increasing elution times of the CTAs by reverse-phase HPLC using the same mobile phase, a measure of increasing hydrophobicity (Table S3.3). Based on the phenytoin loading and target concentration, the polymer matrices were added to the dissolution media at 9 mg mL^{-1}. Qualitatively, the relative solubility of the corresponding PNiPAm homopolymers at 9 mg mL^{-1} in PBS w/ SIF powder agreed with the order (**1** to **7**) assigned from the solubilities of the CTAs: PNiPAm-(**1**, C_{12}, 1.3) and PNiPAm-(**2**, C_{12}, 1.3) gave clear, yellow solutions, PNiPAm-(**3**, C_{12}, 1.5) gave a slightly yellow, cloudy solution with small undissolved particulates, PNiPAm-(**4**, C_{12}, 1.6) gave a pale yellow, hazy solution with particulates, and PNiPAm-(**5**, C_{12}, 1.5), PNiPAm-(**6**, C_{12}, 1.4), PNiPAm-(**7**, C_{12}, 1.5) all gave clear, colorless solutions with larger chunks of undissolved polymer. The solubilities of CTAs **5**, **6**, and **7** in PBS were too low to be quantified by the saturation-centrifugation method.

All dispersions in this first series achieved a burst (immediate) release of phenytoin, and roughly maintained the concentration seen at 4 min over the 6-h course of the experiment. Crystallization of phenytoin would be seen as a decrease in drug concentration over the allotted time, which was not observed. These excipients are thus considered to yield apparent steady-state supersaturations. Based on this series of solid dispersions, it is hypothesized that increasing the hydrophilicity of the excipient α-end group facilitates higher supersaturation of phenytoin.

3.6 Varying Molar Mass Using ω = C_{12}

In the second series of excipients, we explored the molar-mass dependence of the best performing polymer from the first series. Therefore, this second series maintained the same hydrophilic α-end group (**1**) and hydrophobic alkyl ω-end group (C_{12}), while varying molar mass (1.3, 4.4, 22.0 kg mol^{-1}). At low molar masses, the α-end and ω-end groups contribute significantly more of the overall weight fraction of the polymer chain (Table 3.3). As seen in Figure 3.3b (α = **1**, ω = C_{12}), there is a significant influence of excipient molar mass on solid dispersion performance. The greatest level of supersaturation is achieved when using the lowest molar mass excipient (1.3 kg mol^{-1}). At progressively higher molar masses (to 4.4 and 22.0 kg mol^{-1}), the steady-state supersaturation level seen is considerably reduced.

Table 3.3. **Weight percent of the α-end group and ω-end group components for the two PNiPAm molar mass series.**

Sample	***α-end wt%***	***ω-end wt%***
PNiPAm-(**1**, C_{12}, 1.3)	10	13
PNiPAm-(**1**, C_{12}, 4.4)	2.9	3.8
PNiPAm-(**1**, C_{12}, 22.0)	0.6	0.8
PNiPAm-(**1**, C_{18}, 4.6)	2.7	5.5
PNiPAm-(**1**, C_{18}, 6.0)	2.1	4.2
PNiPAm-(**1**, C_{18}, 8.0)	1.6	3.2

3.7 Varying ω-End Group

The third series of excipients varied the alkyl length of the ω-end group across ethyl (C_2), hexyl (C_6), dodecyl (C_{12}), and octadecyl (C_{18}) linear hydrocarbons, while keeping the hydrophilic α-end group (**1**) that gave the highest performance at low molar mass. We chose to focus this series around an intermediate molar mass (3.8–4.6 kg mol^{-1}) to better identify potential differences in dissolution behavior. As shown in Figure 3.3c, dissolution of the corresponding solid dispersions was greatly impacted by the hydrocarbon chain length. While each excipient maintained the initially achieved phenytoin concentration with little to no evidence of crystallization over 6 h, a significant increase in the plateau supersaturation concentration was seen with increasing alkyl chain length. This same trend was observed with excipients of lower molar masses (between 1.3 and 2.5 kg mol^{-1}) (Figure S3.4). However, the low T_g of the octadecyl (C_{18}) derivative in this molar mass range prohibited effective spray drying.

3.8 Varying Molar Mass Using ω = C_{18}

The fourth series of excipients returned to the effect of molar mass, this time maintaining the best-performing C_{18} alkyl ω-end group and the most hydrophilic α-end group **1** (over a more limited molar mass range, and only down to 4.6 kg mol^{-1} due to spray drying difficulties as a result of low T_gs). Again, the performance was inversely related to increasing molar mass, as seen in the C_{12} series. Of note, when comparing the performance of the lowest-molar-mass samples in the C_{12} and C_{18} series, higher molar masses can achieve near-full release when ω = C_{18}. This is seen when comparing PNiPAm-(**1**, C_{12}, 1.3) and PNiPAm-(**1**, C_{18}, 4.6), both with enhancement factors of 19. Using a higher molar mass

may be advantageous in preventing the undesired absorption of the excipient,[20] and also in achieving a higher solid dispersion T_g, which is beneficial for solid-state stabilization.

3.9 Supersaturation Maintenance of Drug in Pre-Dissolved Polymers

In addition to analyzing the ability of a solid dispersion formulation to increase the supersaturation of phenytoin upon dissolution, the ability of pre-dissolved polymer to maintain supersaturation of phenytoin was also probed. This was accomplished by doping a polymer solution with a concentrated solution of drug in a water-miscible organic solvent (methanol). The free drug concentration vs. time behavior was compared to the dissolution performance of the analogous solid dispersion. Figure 3.4 shows representative graphs (all the data are shown in Figure S3.5). Three types of supersaturation maintenance behaviors were observed and were directly related to polymer solubility:

(I) As exemplified by one of the top performers, PNiPAm-(**1**, C_{12}, 1.3), several pre-dissolved polymers sustained high steady-state supersaturations at concentrations that were slightly lower than the concentrations achieved from spray-dried dispersions (Figure 3.4). The polymers that displayed this behavior had solubilities above the loaded threshold (9 mg mL^{-1}), indicating that all loaded polymer was available in solution to slow nucleation and/or crystal growth. The slightly lower concentrations seen in these series are possibly due to rapid crystallization during the initial doping step before the polymer and drug are mixed through vortexing. After being mixed, dissolved polymer is able to maintain the high steady-state concentration of free phenytoin as if polymer and drug had been dissolved concurrently (as from the solid dispersion experiments). PNiPAm-(**2**, C_{12}, 1.3), PNiPAm-(**1**, C_{18}, 4.6), and PNiPAm-(**1**, C_{18}, 6.0) behaved similarly (Figure S3.5).

(II) As exemplified by the more hydrophobic PNiPAm-(**4**, C_{12}, 1.6), the second behavior type manifests as slow crystallization of phenytoin. This suggests that the crystallization of free phenytoin in solution is kinetically hindered by the fraction of polymer that is dissolved in solution. PNiPAm-(**1**, C_2, 3.9), PNiPAm-(**1**, C_6, 3.8), and PNiPAm-(**1**, C_{12}, 4.4) also exhibited this behavior. These polymer excipients were only partially soluble in PBS at the loaded threshold. During dissolution studies of the spray-dried dispersions formulated with these polymers, the fraction of phenytoin released was likely limited to the equivalent fraction of polymer that dissolved. In the supersaturation maintenance study, the full loading of free drug was added to solution, but only the soluble fraction of the polymer was readily able to stabilize phenytoin. Thus, as the amount of dissolved polymer is equal in both cases, both studies give a very similar final drug concentration.

(III) For type III, poorly performing solid dispersions were matched with poorly performing supersaturation maintenance studies. These excipients are minimally soluble, and cannot effectively prevent phenytoin from crystallization. No induction period was observed, indicating rapid crystallization of phenytoin from solution, even before the first 4-min time point. PNiPAm-(**4**, C_{12}, 1.5), PNiPAm-(**6**, C_{12}, 1.4), PNiPAm-(**7**, C_{12}, 1.5), and PNiPAm-(**1**, C_{12}, 22.0) showed type III behavior.

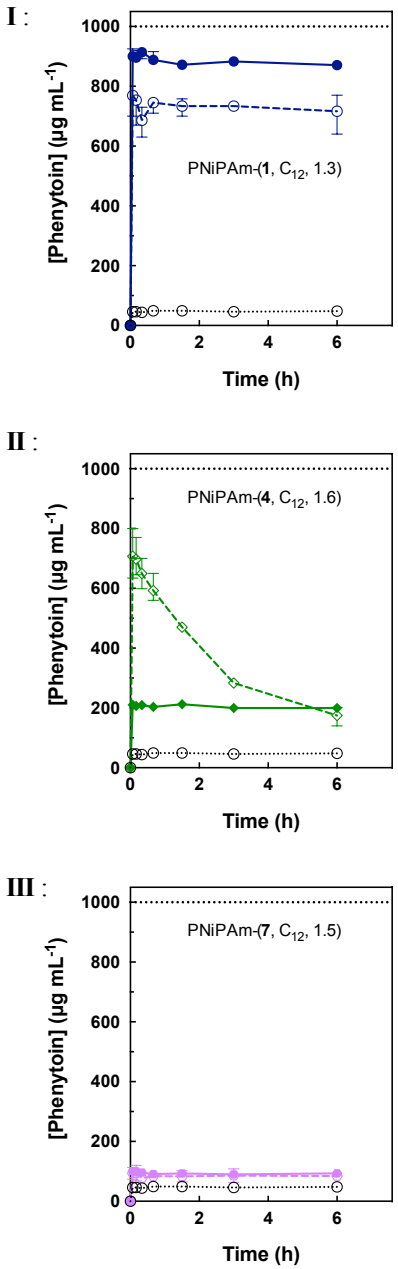

Figure 3.4. Representative examples of solid dispersion dissolution performance vs. supersaturation maintenance as a function of polymer. Dissolution studies are shown with a solid line, and supersaturation maintenance studies are shown with a dashed line. All tests were performed with 9 mg mL^{-1} polymer and 1,000 µg mL^{-1} phenytoin. In all plots, the dissolution profile of crystalline phenytoin was included as a reference (open circles, dotted line). Tests were run in triplicate. The data shown are the mean values, and the error bars represent the range of data.

3.10 Dynamic Light Scattering

Dynamic light scattering (DLS) was used probe the existence, size, and size distribution of solution structures that the excipients form in PBS, based on the length of the alkyl ω-end group and the polymer molar mass. Key results from the DLS studies in PBS are summarized in Table 3.4. The scattering data at 90° angle was analyzed using the Laplace inversion routine REPES (Figure S3.7). Based on the number of populations seen in the REPES analysis, the normalized autocorrelation functions of the scattered light intensity at five angles from 60° to 120° were fitted to either a second-order cumulant expansion model or a double exponential decay model (Figure S3.8). The random residuals (Figure S3.9) indicated the reliability of the fitting model chosen. Plots of the mean decay rates (Γ) versus q^2 (Figure S3.10, Figure S3.11) are linear and the intercepts are near zero, which is consistent with both relaxation processes being diffusive. For samples displaying two peaks by REPES, the intensity of the two peaks were approximately equal, suggesting a much higher numerical concentration of the smaller population.

We compared R_h values from the DLS analyses to those determined for free chains ($R_{h,\text{ free chain}}$) using an empirical formula developed previously for PNiPAm, based on M_w in water (Table 3.4).[21] This empirical formula was based on high-molar-mass PNiPAm samples in the range of 138 – 9,100 kg mol^{-1}. As such, application of this scaling law to lower molar mass samples in PBS buffer has limitations; nonetheless, we compared the relative ratios between the experimental R_h values to those calculated for free chains as a way to analyze relative solution behavior.

Table 3.4. Hydrodynamic Radius (R_h) values determined by DLS in PBS buffer (pH 6.5).

Polymer	Experimental R_h (nm)	Average μ_2/Γ^2	Calculated $R_{h,\text{ free chain}}$ (nm)[a]	Ratio of smallest R_h to $R_{h,\text{ free chain}}$
PNiPAm-(**1**, C_{12}, 1.3)[b]	4, 39		1.0	4
PNiPAm-(**2**, C_{12}, 1.3)[b]	4, 33		1.0	4
PNiPAm-(**1**, C_2, 3.9)[c]	2	0.42	1.4	1
PNiPAm-(**1**, C_6, 3.8)[c]	10	0.38	1.6	6
PNiPAm-(**1**, C_{12}, 4.4)[b]	7, 51		1.6	4
PNiPAm-(**1**, C_{18}, 4.6)[c]	5	0.03	1.5	3
PNiPAm-(**1**, C_{12}, 22.0)[c]	13	0.05	3.6	4
PNiPAm-(**1**, C_{18}, 6.0)[c]	7	0.15	1.8	4
PNiPAm-(**1**, C_{18}, 8.0)[c]	9	0.10	2.1	4

[a] Calculated from scaling law as $R_h = 0.16 \times M_w^{0.54}$ (nm), using M_w by SEC.[21]

[b] Determined by fitting with a double exponential decay function.

[c] Determined by fitting with a second-order cumulant expansion.

In all samples, there are small aggregates that gave ratios of R_h to $R_{h,\text{ free chain}}$ of 3 or greater, except for the PNiPAm-(**1**, C_2, 3.9) sample, which gave a ratio of 1. In three samples, there are aggregates with R_h greater than 30 nm. Ratios greater than 1 suggest that these samples aggregated into micelles, except for the PNiPAm-(**1**, C_2, 3.9) sample, which existed as free chains only. Presumably the short C_2 alkyl chain was not able to drive association of the ω-end groups. With respect to dissolution enhancement, this free-chain PNiPAm-(**1**, C_2, 3.9) sample was the least effective, fully soluble excipient, suggesting that the free chains in solutions were unable to sufficiently stabilize phenytoin as compared to the micelle-forming samples.

Solutions of the excipients of the three best performing solid dispersions, PNiPAm-(**1**, C_{12}, 1.3), PNiPAm-(**2**, C_{12}, 1.3), and PNiPAm-(**1**, C_{18}, 4.6), were optically hazy and bluish-tinged, suggesting the presence of aggregates. Considering these data along with the respective dissolution profiles, the presence of aggregates contributes significantly to the

dissolution enhancement behavior. In fact, dissolution enhancement appears to be directly related to the tendency of the polymeric sample to form aggregates in solution.

For the PNiPAm-(**1**, C_{12}, 1.3), PNiPAm-(**2**, C_{12}, 1.3), and PNiPAm-(**1**, C_{12}, 4.4), REPES analyses of these samples show that the majority of aggregates present are of the smaller-sized R_h value. Thus, for the samples that show two populations, we hypothesize that the smaller aggregates determine dissolution performance. Further experimental studies and computation modeling that probe the shape character and concentrations of each population size and their respective influence on performance are ongoing.

3.11 Discussion

Through this systematic study of polymer excipients for solid dispersions with phenytoin, we were able to isolate structure-performance relationships based on polymer end group identity and molar mass. The spray-dried dispersions appeared as collapsed spheres with diameters of 10 μm or less. The high surface area of such small particles could allow for drug release performance that is either excipient-dissolution-limited or drug-diffusion-limited.[22] In support of the first mechanism being the most relevant with these solid dispersions, no indication of gradual release was seen. Rather, the supersaturation level achieved at early times (~4 min) was maintained over 6 h, showing that a steady-state solubility of polymer and drug was quickly reached during dissolution. Assuming that drug is evenly distributed in the solid dispersions,[23] the fraction of loaded drug released into the dissolution media will be roughly equivalent to the fraction of polymer that dissolved.

The strong dependence of dissolution performance on excipient solubility is evident across the first series studied as a function of the α-end group. By varying the polymer α-end functionality (the CTA R groups), the influence of this end group was isolated from

that of molar mass and the nature of the ω-end group. Polymers with the two most hydrophilic CTA α-end groups performed exceptionally well as solid dispersion excipients with phenytoin. Rather than being functional-group-specific, this increase in performance is hypothesized to be due to the resultant increase in the overall solubility of the final polymer, rather than any specific interactions between the drug and the end group. However, not all of the highly soluble polymeric excipients, *e.g.,* PNiPAm-(**1**, C_2, 1.8), showed the same performance level, indicating that other factors beyond solubility play a role in determining supersaturation achievement and maintenance.

Studying the influence of molar mass served as an indirect method for evaluating the overall contribution of end groups to excipient performance. At high molar mass, the impact of polymer end group is reduced. However, in the oligomeric regime, a significant fraction of the total molar mass comes from the starting CTA (Table 3.3). For example, PNiPAm-(**1**, C_{12}, 1.3) is 31 wt% starting CTA (including the trithiocarbonate moiety). Based on dissolution performance, even a small increase of molar mass comparing PNiPAm-(**1**, C_{12}, 1.3) ($n \approx 8$) to PNiPAm-(**1**, C_{12}, 4.4) ($n \approx 36$) significantly decreased the supersaturation level achieved and the resultant enhancement factor, from 19 to 6.5. Increasing the molar mass further, PNiPAm-(**1**, C_{12}, 22.0) gives only a slight enhancement factor of 2.8 over crystalline drug. Similar to the PNiPAm-(**1**, C_{12}, M) series, solid dispersion performance from the PNiPAm-(**1**, C_{18}, M) series was also seen to be inversely related to molar mass; increases from 4.6 to 6.0 to 8.0 kg mol^{-1} in this series also yielded a decrease in the observed enhancement factor. As the alkyl chain fraction of the polymer decreased, performance also decreased. These two series certainly highlight the importance of the ω-end group identity. Of particular note, when compared against the C_{12} series, the C_{18} series allowed higher molar mass excipients to be used without sacrificing dissolution

performance. For example, PNiPAm-(**1**, C_{18}, 4.6) gave an enhancement factor of 19, where as PNiPAm-(**1**, C_{12}, 4.4) gave an enhancement factor of only 6.5.

Because of our ability to separately vary the length of the inherited alkyl chain ω-end group, the tendency of the polymer chains to associate based on hydrophobic interactions of the polymer tail was controlled.[12, 24] The improved performance with increasing excipient tail length is attributed to the appearance of micellar aggregates in solution. At low molar masses (1.3 to 2.1 kg mol^{-1}), increased performance was seen going from ω = C_2 to C_6 to C_{12}. This same trend was observed at higher molar mass (3.8 to 4.6 kg mol^{-1}) going from ω = C_2 to C_6 to C_{12} to C_{18}. In PBS, the best performers formed hazy, bluish solutions, which is evidence of a high concentration of aggregates in solution. Small aggregates with R_h values of 4 to 10 nm are proposed to be responsible for the dissolution enhancement behavior of these excipients.

Self-assembly of the hydrophobic hydrocarbon ω-end group (the CTA Z-group tail) yields a NiPAm-rich local environment in the corona. In a similar system, Li et al. describe NiPAm-phenytoin interactions in the micelle corona, as seen by Nuclear Overhauser effect spectroscopy (NOSEY), where the corona chains are hypothesized to promote favorable, specific polymer-drug interactions.[25] Self-assembly of the hydrophobic hydrocarbon ω-end group yields a NiPAm-rich local environment in the corona that we hypothesize favors polymer-drug interactions.[25] Most micelle-based ASD systems load drug in the hydrophobic core of either a small-molecule surfactant or an amphiphilic block polymer.[26] For core-loaded systems, drug release is a function of diffusion from the micelle core, which can compromise the permeation of the drug through the gastrointestional membrane.[27] Rarely are corona-loaded systems used in self-aggregating excipients, though Dalsin et al. showed promising results in support of such excipients for drug delivery.[28]

Indeed, of the systems described here, the best-performing solid dispersions were bluish and hazy-tinged during dissolution. In parallel to what has been documented for cellulosic systems[11,29] and others,[28] the presence of drug-polymer nanoaggregates is advantageous in disrupting crystallization of these hydrophobic drugs from solution.

Based on the trends of enhancement factors seen across each of the four series (Figure S3.6), we identified design principles from this system that have the potential to translate to improved delivery of other small molecules. Collectively, low-molar-mass samples with sufficiently long alkyl groups that drive self-aggregation of the polymer chains perform the best as solid dispersion excipients. Some of the solid dispersions shown here are among the best formulations designed to date with respect to increasing supersaturation of phenytoin.[10,18,30,31] The highest enhancement factor has been described by Ting et al. using an excipient of PNiPAm-*co*-poly(dimethylacrylamide) that gives an enhancement factor up to 20.7.[10] Additionally, Li et al., using a blend of PNiPAm and hydroxypropyl methylcellulose acetate succinate, have achieved dissolution enhancement factors up to 19.2.[25] Another high-performing system was found by Yin et al., where hydroxypropyl methylcellulose esters of substituted succinates gave an enhancement factor up to 13.[18] Our systems are among these top performers, and gave a maximum enhancement factor of 19 (90% of the maximum release achievable), with five excipients achieving enhancement factors above 15.

We posit here that the high-performing systems from this study form nanoaggregates in solution that are primarily responsible for retarding the crystallization of phenytoin in solution over 6 h. Although larger-sized aggregates were detected in some cases, the relative intensity of the distributions by REPES suggests that they were present in very low concentrations with respect to the smaller-sized aggregates.[17] Also, we see no

evidence of crystallization, which would be perceivable as a decrease in free drug concentration. This suggests that nucleation and/or crystallization mechanisms may be disrupted by the association of free phenytoin molecules with the NiPAm-based micelles in such a manner that does not allow drug-drug association and packing to occur at the length scale of critical nucleation.[25] Crystal growth could also be limited, possibly by polymer molecules adhered to the surface of the growing crystal in a way that does not allow for additional packing of free phenytoin, and/or by immobilizing phenytoin sufficiently in the NiPAm-rich polymer space so that it is not able to readily pack along a crystal surface.

3.12 Conclusion

In summary, the α- and ω-end groups of low-molar-mass polymeric excipients were tailored to maximize the *in vitro* performance of the final solid dispersion loaded with a model BCS Class II drug, phenytoin. We presented low-molar-mass NiPAm-based polymers that gave up to a 19-fold improvement of phenytoin solubility with no indication of drug crystallization over 6 h, among the highest enhancement factor seen for phenytoin to date. The best excipients were highly soluble and possessed long alkyl tails that drove aggregation of polymer chains in solution. The association of the hydrophobic alkyl component is posited to create micelles with NiPAm-rich coronas in solution. The ample opportunity for amide-amide NiPAm-phenytoin interactions may then disrupt the ability of phenytoin to crystallize from solution. Molar mass was inversely related to performance, where a lower excipient molar mass yielded better solid dispersion performance. Despite the strong crystallization tendency of phenytoin, these micellizing solid dispersions maintained the drug supersaturation established after initial burst release. This maintenance

of steady-state supersaturation was largely ascribed to effective crystallization inhibition, where the micellar structures formed by these excipients were able to limit the formation and/or growth of phenytoin crystals.

3.12 Supplemental Information

Reagents

All commercial chemicals were reagent grade, purchased from Sigma-Aldrich, and used without further purification unless otherwise noted. 4-Cyano-4-[(ethylsulfanylthiocarbonyl) sulfanyl]pentanoic acid was purchased from STREM Chemicals, Inc. Simulated intestinal fluid (SIF) powder (FaSSIF) was purchased from Biorelevant.

Molecular Characterization

^{1}H NMR and ^{13}C NMR spectroscopy experiments were performed on a Bruker Avance III HD 500 with a 5-mm Prodigy TCI cryoprobe at 500 MHz and 125 MHz, respectively. NMR samples were dissolved in DMSO-d_6 or $CDCl_3$. SEC was carried out in THF on an Agilent 1260 liquid chromatograph. The SEC instrument housed three Phenomenex Phenogel-5 columns in series, and solvent ran at a flow rate of 1 mL min^{-1} at 25 °C. The detectors included an Agilent 1260 VWD UV-Vis detector, a Wyatt Dawn DSP Heleos II multi-angle light scattering (MALS) detector, and a Wyatt Optilab T-rEX refractive-index detector. Elemental analysis was performed by Atlantic Microlab, Inc (Norcross, GA). High-resolution mass spectrometry was performed on a Bruker BioTOF II instrument using a mixture of poly(ethylene glycol)s as the internal calibrant.

Synthesis of 4-Cyano-4-[(octadecylsulfanylthiocarbonyl)sulfanyl]pentanoic acid

The synthesis of 4-cyano-4-[(octadecylsulfanylthiocarbonyl)sulfanyl]pentanoic acid was adapted from a procedure by Moad et al.[32] 1-Octadecanethiol (21.78 g, 76 mmol) was dissolved in 200 mL of diethyl ether, and was added over 10 min to a stirred suspension of sodium hydride (60% in oil) (3.15 g, 79 mmol) in diethyl ether (250 mL) at 5 °C. Evolution of hydrogen was observed as the suspension developed into a thick, white slurry. The reaction mixture was cooled to 0 °C and carbon disulfide (6.0 g, 79 mmol) was added, turning the slurry to a bright yellow color. The reaction stirred overnight. The solids were collected by filtration and used without purification.

A suspension of sodium *S*-octadecyl trithiocarbonate (39.24 g, 102 mmol) in diethyl ether (400 mL) was treated by portion-wise addition of solid iodine. The reaction stirred for 1 h at room temperature. Sodium iodide and unreacted *S*-octadecyl trithiocarbonate were removed by filtration, redissolved in diethyl ether, treated with additional solid iodine for 1 h, and filtered again. The yellow-brown filtrates were combined, and washed with aqueous sodium thiosulfate until the organic layer was clear and yellow. The organic layer was collected, dried over sodium sulfate, filtered, and evaporated to leave a bright yellow powder of bis(octadecylsulfanylthiocarbonyl) disulfide.

A solution of bis(octadecylsulfanylthiocarbonyl) disulfide (16.0 g, 22.1 mmol) and 4,4'-azobis(4-cyanopentanoic acid) (9.31 g, 33.2 mol) in ethyl acetate (450 mL) was heated at reflux for 20 h. After removal of volatiles under reduced pressure, the crude product was rinsed 5 times with 400 mL DI water, to remove water-soluble side products. The crude mixture was evaporated down, re-dissolved in minimal ethyl acetate, and purified by column chromatography on silica with a 75/25 hexanes/ethyl acetate mobile phase supplemented with 1% acetic acid (R_f = 0.2). The fractions were combined and evaporated

to a crude solid. The solid was then dissolved in ethyl acetate and extracted into an aqueous phase of $NaHCO_3$. After isolation of the aqueous phase, the compound was extracted back into an organic phase of ethyl acetate through slow acidification of the aqueous layer with 1 M HCl. The organic phase was evaporated to yield a pure product of 4-cyano-4-[(octadecylsulfanylthiocarbonyl)sulfanyl]pentanoic acid. Elemental analysis calculated for $C_{25}H_{45}NO_2S_3$: C, 61.55; H, 9.30; N, 2.87; S, 19.72. Found: C, 61.43; H, 9.37; N, 2.96; S, 18.48. HRMS (ESI-TOF) m/z: $[M+Na]^+$ calculated for $C_{25}H_{45}NO_2S_3Na$: 510.2510; Found: 510.2511.

Synthesis of 4-Cyano-4-[(hexylsulfanylthiocarbonyl)sulfanyl]pentanoic acid

The synthesis of 4-cyano-4-[(hexylsulfanylthiocarbonyl)sulfanyl]pentanoic acid followed as described above. Elemental analysis analytically calculated for $C_{13}H_{21}NO_2S_3$: C, 48.87; H, 6.63; N, 4.38; S, 30.10. Found: C, 48.89; H, 6.61; N, 4.19; S, 29.13. HRMS (ESI-TOF) m/z: $[M+Na]^+$ calculated for $C_{13}H_{21}NO_2S_3Na$: 342.0632; Found: 342.0627.

Synthesis of PNiPAm series

The synthesis of PNiPAm homopolymers followed a similar procedure; a polymerization using 4-cyano-4-[(octadecylsulfanylthiocarbonyl)sulfanyl]pentanoic acid is given here as an example. NiPAm (1.275 g, 0.01127 mol), 4-cyano-4-[(octadecylsulfanylthiocarbonyl) sulfanyl]pentanoic acid (0.500 g, 0.00102 mol), and 4,4′-azobis(4-cyanopentanoic acid) (0.0286 g, 0.000102 mol) were added to a round-bottom flask. Dioxane (25 mL) was added. The reaction mixture was sparged with nitrogen gas for 45 minutes, and then placed in an oil bath at 72 °C. After at least 7 h, the reaction was quenched by cooling to 0 °C and opening the flask to air. The resultant polymer was isolated and purified by precipitation into a 75/25 v/v mixture of hexanes/diethyl ether

(2X). The polymer was dried under vacuum at 40 °C overnight to yield the final polymer (87% yield). Approximate solubility of the polymers in phosphate buffered saline (PBS), pH 6.5, was tested by visually examining solutions at 3 mg mL^{-1} and 9 mg mL^{-1}.

Spray-Dried Dispersion Preparation

Spray-dried dispersions were prepared at lab-scale using a Mini-spray dryer (Bend Research, Bend, OR). Solid dispersions were made at 10 wt% and 25 wt % drug (90 and 75 wt % polymer, respectively). At a total solids loading of 2.0 wt%, drug and polymer were dissolved in a 90/10 v/v MeOH/H_2O solution, unless otherwise specified. Samples were sprayed at a constant inlet temperature (75 °C), N_2 flow rate (28.6 sL min^{-1}), and solution flow rate (1.3 mL min^{-1}). Spray-dried dispersions were collected and immediately dried under vacuum overnight, and further stored at room temperature in a vacuum desiccator.

Scanning Electron Microscopy

SEM images were taken on a Hitachi S-4700 field emission gun SEM using a secondary electron detector operating at an accelerating voltage of 3.0 kV. Magnification was between 5,000× and 20,000×. Prior to imaging, spray-dried dispersions were sprinkled on to conductive carbon tape (Ted Pella Inc.) and sputter coated with 10 nm of Pt in a VCR Group IBS TM200S Ion Beam Sputterer.

Powder Wide-Angle X-ray Diffraction (PXRD)

Powder spray-dried dispersion samples were examined by PXRD using a Bruker-AXS D5005 Diffractometer. Samples were packed in a zero-background holder and analyzed using a Cu-Kα X-ray source (λ=1.54 Å, 45 kV and 40 mA). Data were collected from 5° to 40° on the 2θ scale at a step size of 0.02° with a dwell time of 1 s $step^{-1}$.

Thermal Analysis

Thermogravimetric analysis (TGA) was performed on a Q500 (TA Instruments, New Castle, DE) at a heating rate of 10 °C min^{-1} under N_2. Differential scanning calorimetry (DSC) was performed on a Discovery DSC (TA Instruments, New Castle, DE) equipped with a refrigerated cooling system. A dry N_2 purge flowed through the cell at 50 mL min^{-1}, and samples were run in hermetically sealed TZero aluminum pans. Polymer samples were dried under vacuum before DSC analysis; samples (2-10 mg) were heat-cool-heat cycled at 10 °C min^{-1} between −85 and 150 °C. T_g values were taken from the second heating scan. Spray-dried dispersions were dried under vacuum before DSC analysis; samples (2-6 mg) were ramped at 5 °C min^{-1} from −85 and 210 °C. Cold crystallization analyses and T_g values were taken from the first heating scan.

Dissolution Tests

Dissolution tests were performed as described previously,[18] in phosphate buffered saline solution (PBS, 82 mM sodium chloride, 20 mM sodium phosphate dibasic, 47 mM potassium phosphate monobasic) with 0.5 wt % simulated intestinal fluid (SIF) powder (FaSSIF, Biorelevant) at 37 °C. In a 1.5-mL microcentrifuge tube, an appropriate amount of spray-dried dispersion and PBS was added to target a total drug concentration of 1,000 μg mL^{-1}. Samples were vortexed (Scientific Industries Vortex-Genie 2 on a setting of 10) to suspend all solids for 1 min and immediately set in an isothermal sample holder held at 37 °C (t = 0). At set time points (4, 10, 20, 40, 90, 180, 360 min), the samples were centrifuged at 13,000 g for 1 min, a 50-μL aliquot was removed from the supernatant, and the aliquot was diluted with 300 μL of HPLC-grade methanol. The samples were then vortexed for 30 s to re-suspend the centrifuged solids, and the tubes were returned to the isothermal sample holder. The drug concentration was determined by reverse-phase high

performance liquid chromatography in 60/40 (v/v) H_2O/MeCN. Samples were analyzed on an Agilent 1260 liquid chromatograph with a multi-wavelength UV-Vis detector, 1260 MWD, at 225 nm. A calibration curve from 12.5 μg mL^{-1} to 500 μg mL^{-1} was prepared, with an R^2 value of 0.9986. Separation occurred on an Agilent Poroshell 120 EC-C18 column with 120 Å pores.

Supersaturation Maintenance of Drug in Predissolved Polymer Solutions

The ability of predissolved polymer to maintain a supersaturation of drug was tested by adding a concentrated stock solution of phenytoin in organic solvent (methanol) to a microcentrifuge tube with polymer predissolved in PBS (w/ SIF powder). To match dissolution concentration conditions from solid dispersions with 10 wt% drug, polymers were added at a loading of 9 mg mL^{-1} (9,000 μg mL^{-1}) and drug was added at a loading of 1 mg mL^{-1} (1,000 μg mL^{-1}). Polymer (~12 - 13 mg) was added to a 1.5-mL microcentrifuge tube, and an appropriate amount of PBS w/ 0.5 wt% SIF was added to reach a 9 mg mL^{-1} solution of polymer. The tube was vortexed on a Scientific Industries Vortex-Genie 2 on a setting of 10 for 1 min and then set in an isothermal sample holder at 37 °C for 30 min. Separately, a stock solution of phenytoin was prepared in methanol at 0.02 mg μL^{-1}. After the 30 min equilibration, the solution of polymer was revortexed for 1 min, and then the amount of phenytoin stock solution necessary to reach 1 mg mL^{-1} was added. The solution was vortexed for 1 min and returned to the isothermal sample holder. Time points were taken as described earlier for dissolution testing (4, 10, 20, 40, 90, 180, and 360 min). Concentrations were determined by HPLC as described in the Dissolution Tests section.

Dynamic Light Scattering

Dynamic light scattering (DLS) measurements were conducted using a Brookhaven Instruments BI-200SM light scattering system equipped with a 637-nm laser. Samples

were prepared at a concentration of 10 mg mL^{-1} polymer in phosphate buffered saline (PBS). Samples were passed through a 0.2-μm filter to remove dust, loaded into glass tubes, and placed in a temperature-controlled, index-matching bath. For samples that were not fully soluble at 10 mg mL^{-1}, the supernatant was studied, after being passed through a 0.2-μm filter. The temperature was held at 22 °C during measurements. Intensity autocorrelation functions spanning 1 μs to 1 s were collected at five scattering angles of 60°, 75°, 90°, 105°, and 120°, with an acquisition time of 10 min per angle. For each sample, a REPES analysis was performed on the autocorrelation function from 90°. The autocorrelation functions for samples that showed a single population by REPES were fitted to a second-order cumulant model, and for samples that showed two populations by REPES were fitted to a double exponential decay model. Residuals between the intensity correlation functions and the selected fits were random. The mutual diffusion coefficient, D_m, was extracted from linear fits of the mean decay rate (Γ) vs q^2. Mean hydrodynamic radii (R_h) were obtained via the Stokes-Einstein relationship. Dispersities for the samples fit to a second-order cumulant model are given as μ_2/Γ^2.

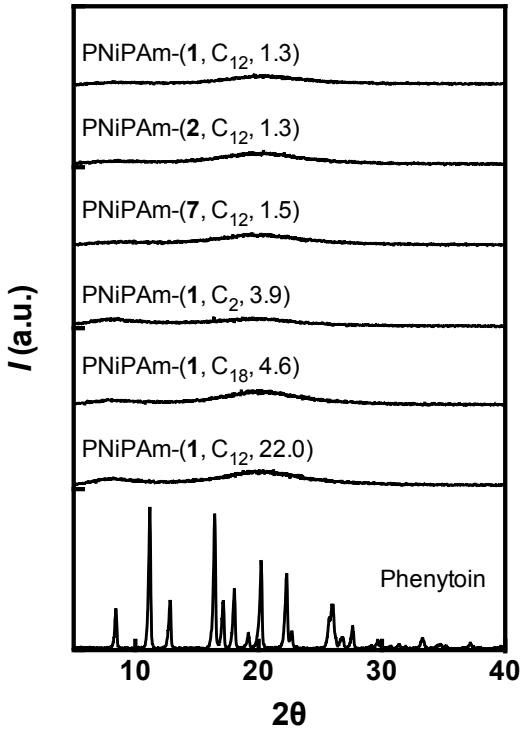

Figure S3.1. Representative powder wide-angle X-ray scattering (PXRD) patterns of solid dispersions. All patterns, including phenytoin, are plotted on the same scale, and dispersions are vertically shifted.

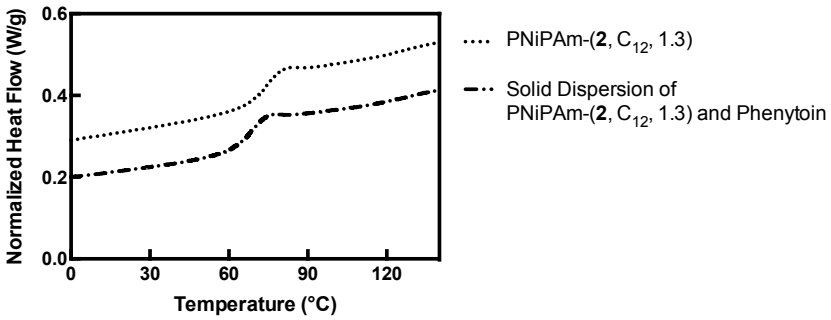

Figure S3.2. Differential Scanning Calorimetry (DSC) scans of polymeric excipient, PNiPAm-(**2**, C_{12}, 1.3) and solid dispersion PNiPAm-(**2**, C_{12}, 1.3). Polymer samples were dried before analysis; samples (2-10 mg) were heat-cool-heat cycled at 10 °C min^{-1} between −85 and 150 °C. T_g values were taken from the second heating scan. Spray-dried dispersions were dried under vacuum before DSC analysis; samples (2-6 mg) were ramped at 5 °C min^{-1} from −85 and 210 °C. T_g values were taken from the first heating scan.

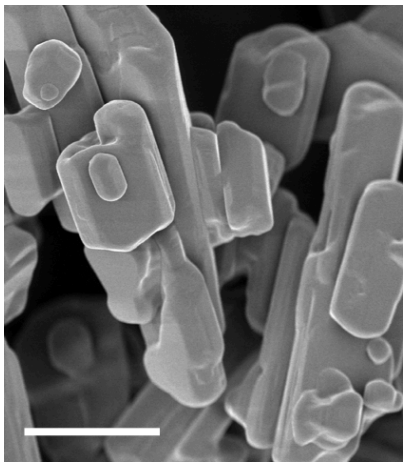

Figure S3.3. Scanning Electron Microscopy (SEM) of crystalline phenytoin, as received. Image taken at 5,000× magnification; scale bar represents 6 μm.

Varying* ω *Group: PNiPAm-(1, ω, 1.3 - 2.1)

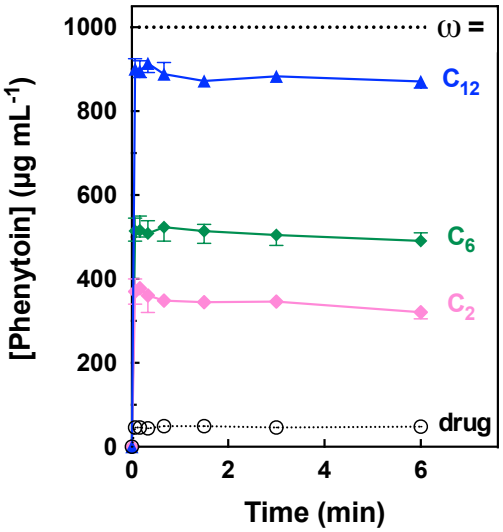

Figure S3.4. Dissolution profiles of spray-dried dispersions at 10 wt % phenytoin loading, as a function of ω-end group alkyl chain length using molar mass of 1.3 – 2.1 kg mol^{-1}. PNiPAm-(**1**, C_{18}, 1.4) did not spray dry due to a prohibitively low T_g. The dissolution profile of crystalline phenytoin was also included as a reference (dots, open circles, labeled 'drug'). The loaded concentration of phenytoin was 1,000 µg mL^{-1}. Dissolution was run in triplicate. The data shown are the mean value, and the error bars represent the range of data.

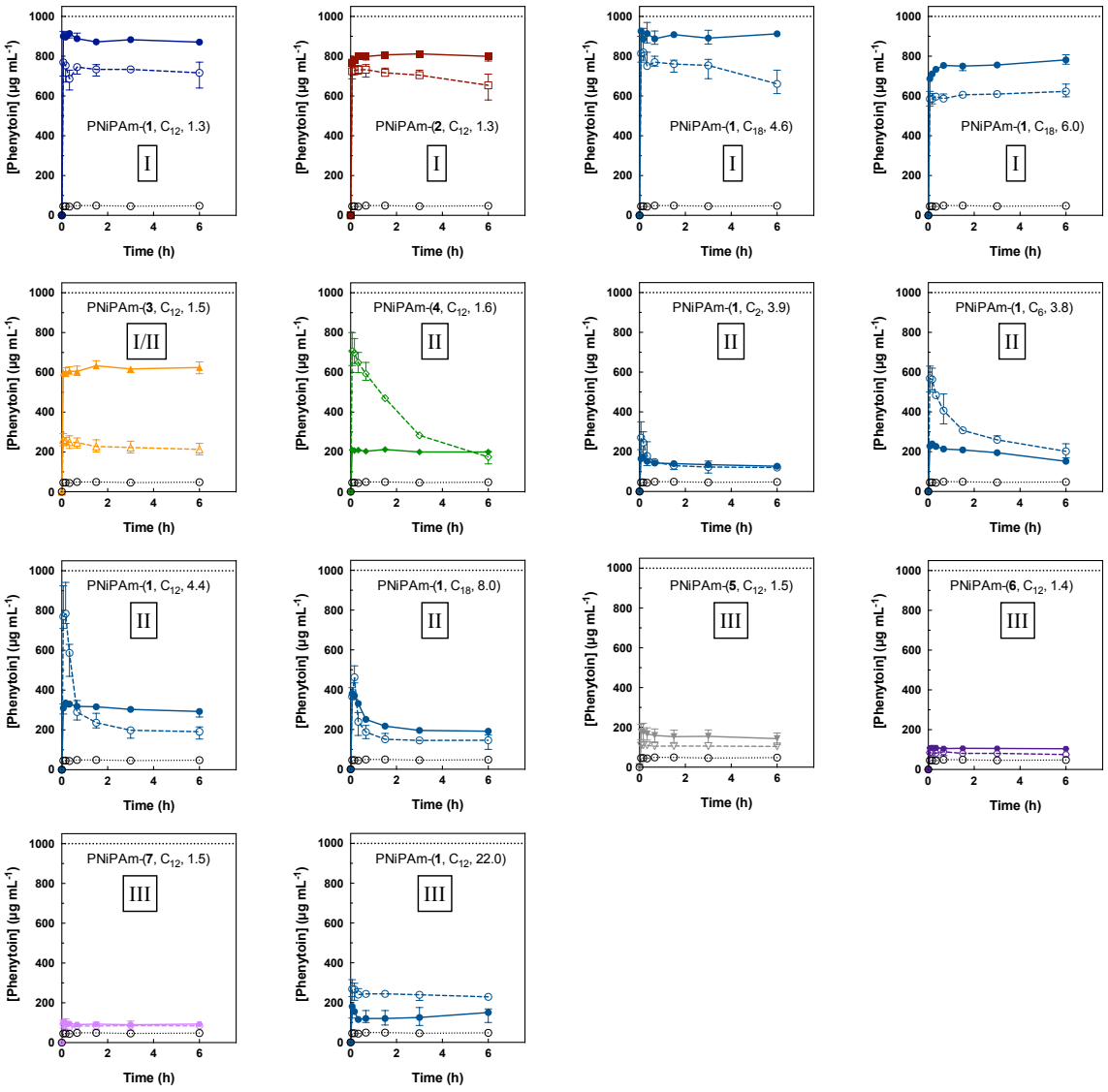

Figure S3.5. Solid dispersion dissolution vs. supersaturation maintenance as a function of polymer. Dissolution studies are shown with a solid line, and supersaturation maintenance studies are shown with a dashed line. All tests were performed with 9 mg mL^{-1} and 1,000 μg mL^{-1} phenytoin. In all plots, the dissolution profile of crystalline phenytoin was included as a reference (open circles, dotted line). Tests were run in triplicate. The data shown are the mean values, and the error bars represent the range of data.

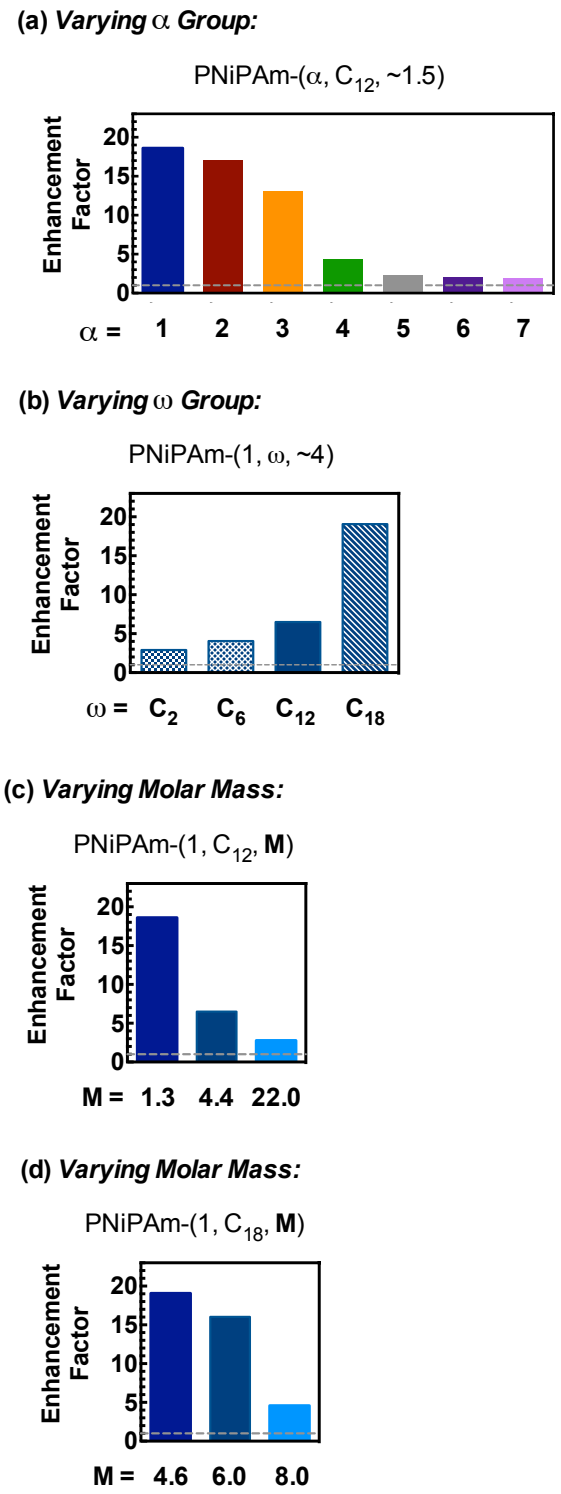

Figure S3.6. Enhancement factors from the dissolution profiles, as based on (a) varying α-end group; (b) varying molar mass with ω = C_{12}; (c) varying ω-end group; and (d) varying molar mass with ω = C_{18}. Enhancement factors defined as AUC_{6h}(solid dispersion)/AUC_{6h}(phenytoin).

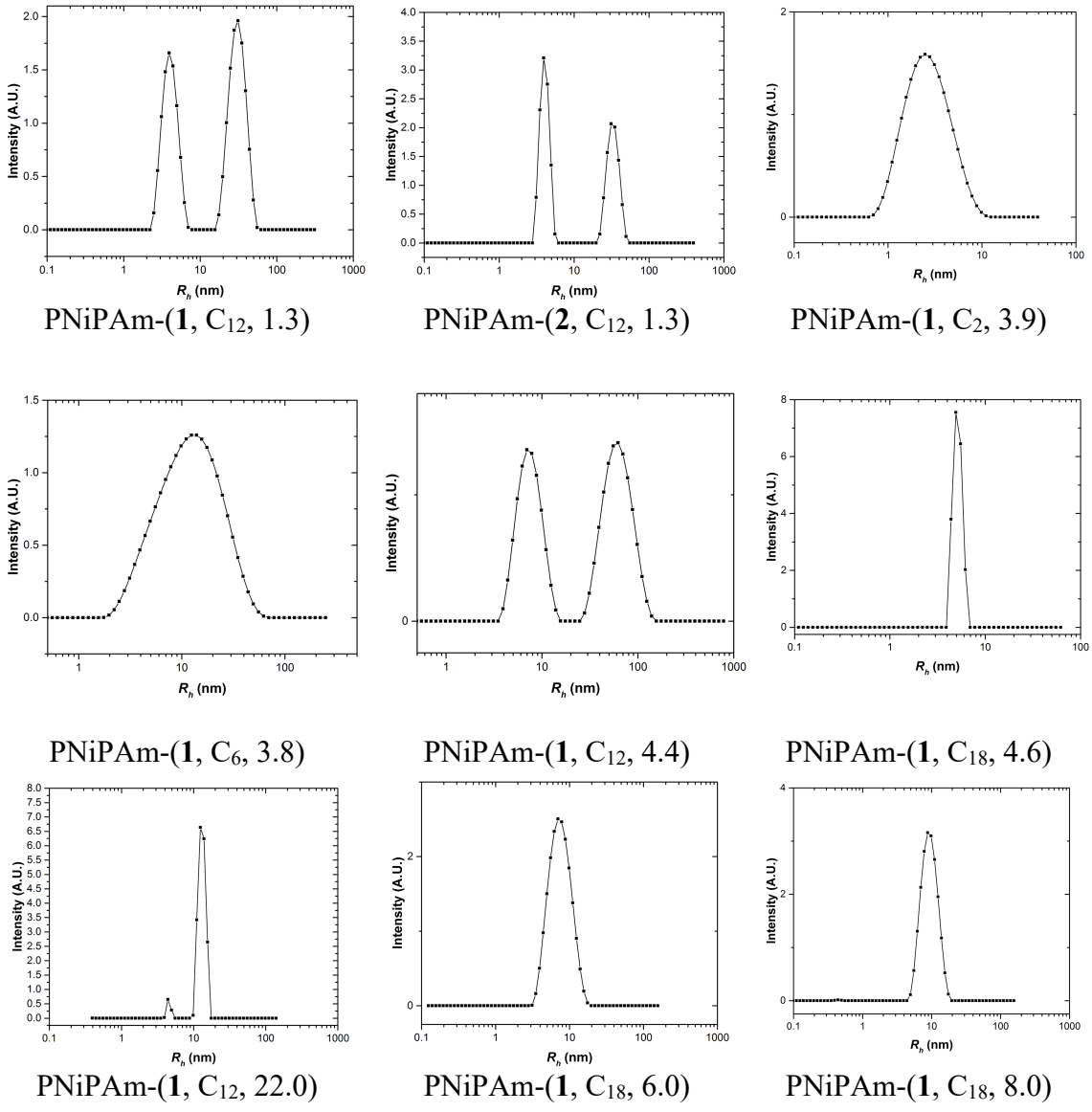

PNiPAm-(**1**, C_{12}, 1.3) PNiPAm-(**2**, C_{12}, 1.3) PNiPAm-(**1**, C_2, 3.9)

PNiPAm-(**1**, C_6, 3.8) PNiPAm-(**1**, C_{12}, 4.4) PNiPAm-(**1**, C_{18}, 4.6)

PNiPAm-(**1**, C_{12}, 22.0) PNiPAm-(**1**, C_{18}, 6.0) PNiPAm-(**1**, C_{18}, 8.0)

Figure S3.7. DLS REPES analyses.

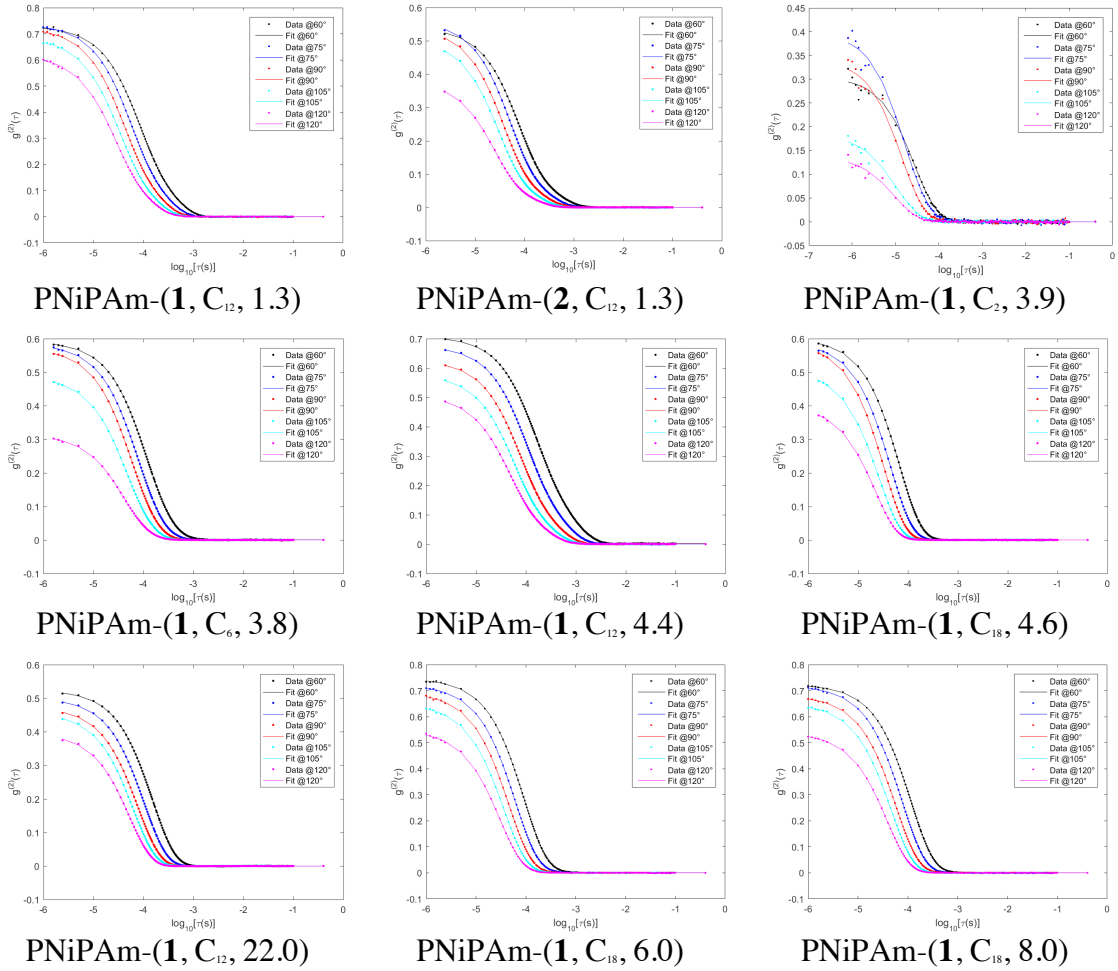

Figure S3.8. DLS autocorrelation functions and fits.

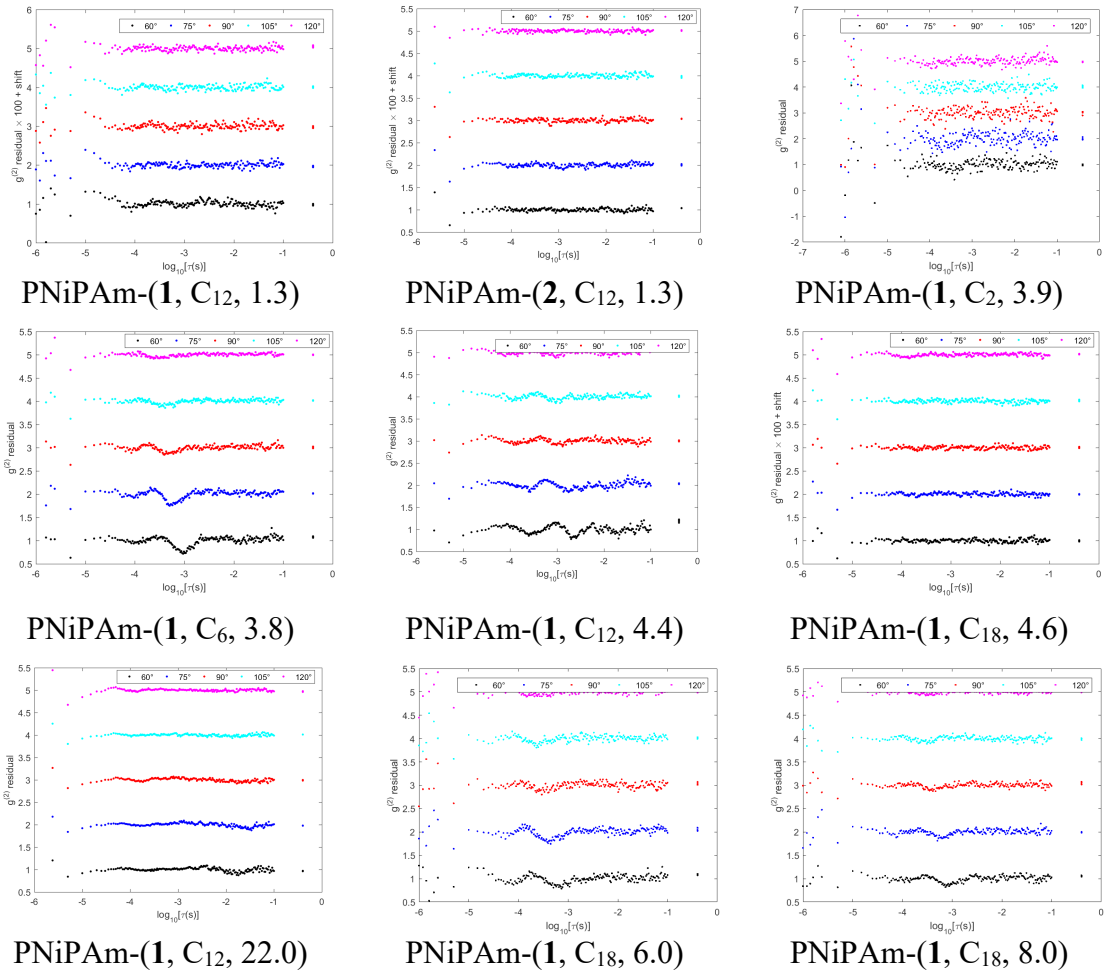

PNiPAm-(**1**, C_{12}, 1.3) PNiPAm-(**2**, C_{12}, 1.3) PNiPAm-(**1**, C_2, 3.9)

PNiPAm-(**1**, C_6, 3.8) PNiPAm-(**1**, C_{12}, 4.4) PNiPAm-(**1**, C_{18}, 4.6)

PNiPAm-(**1**, C_{12}, 22.0) PNiPAm-(**1**, C_{18}, 6.0) PNiPAm-(**1**, C_{18}, 8.0)

Figure S3.9. DLS autocorrelation function residuals.

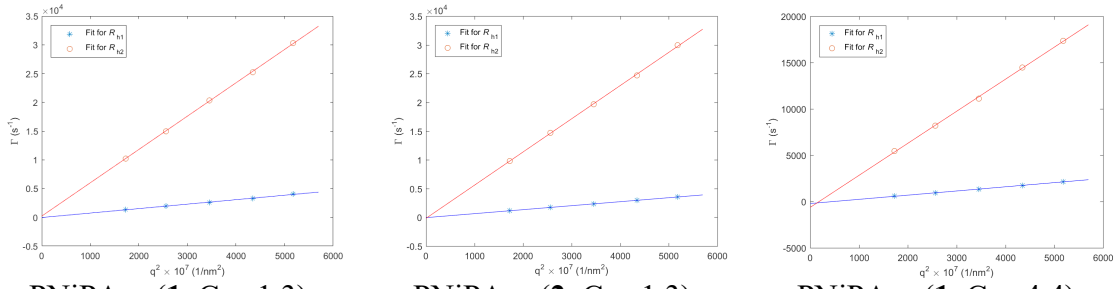

PNiPAm-(**1**, C_{12}, 1.3) PNiPAm-(**2**, C_{12}, 1.3) PNiPAm-(**1**, C_{12}, 4.4)

Figure S3.10. Plots of Γ versus q^2 from DLS for polymer samples fit with a double exponential decay model based on five angles from 60 to 120°.

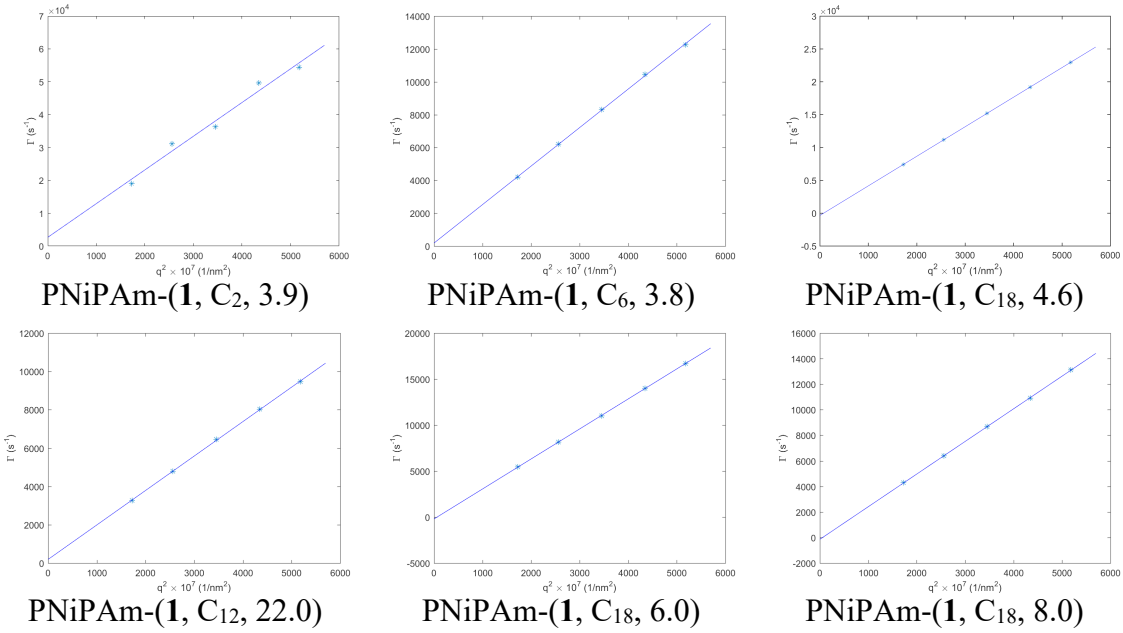

Figure S3.11. Plots of Γ versus q^2 from DLS for polymer samples fit with a second-order cumulant model based on five angles from 60 to 120°.

Table S3.1. **Atmospheric moisture uptake studies.**[a]

Polymer Sample	*Mass at t = 0 min (mg)*	*Mass at t = 0 min (mg)*	*Change in mass (mg)*
PNiPAm-(**1**, C_{12}, 1.3)	12	15	3
PNiPAm-(**2**, C_{12}, 1.3)	6	6	0
PNiPAm-(**3**, C_{12}, 1.5)	5	5	0
PNiPAm-(**4**, C_{12}, 1.6)	4	3	-1
PNiPAm-(**5**, C_{12}, 1.5)	4	4	0
PNiPAm-(**6**, C_{12}, 1.4)	9	10	1
PNiPAm-(**7**, C_{12}, 1.5)	9	10	1
PNiPAm-(**1**, C_2, 1.8)	19	19	0
PNiPAm-(**1**, C_2, 3.9)	12	11	-1
PNiPAm-(**1**, C_6, 2.1)	24	24	0
PNiPAm-(**1**, C_6, 3.8)	3	6	3
PNiPAm-(**1**, C_{18}, 4.6)	3	6	3
PNiPAm-(**1**, C_{12}, 4.4)	30	33	3
PNiPAm-(**1**, C_{12}, 22.0)	15	18	3
PNiPAm-(**1**, C_{18}, 6.0)	5	8	3
PNiPAm-(**1**, C_{18}, 8.0)	2	6	4

[a]Polymers were dried under vacuum overnight. After drying, small samples were massed into a vial, left on the bench for 20 min, and massed again. The change in mass is related to the readiness of the samples to absorb atmospheric moisture. Room temperature was 20 °C. Relative humidity was 16%.

Table S3.2. Hansen Solubility Parameters for CTAs[a]

CTA R group	δ_d	δ_p	δ_h
1	17.55	11.17	10.89
2	16.77	11.26	14.48
3	18.00	7.34	13.22
4	17.87	5.77	11.72
5	18.11	28.46	8.04
6	17.20	15.77	5.99
7	7.78	2.94	6.40
H_2O	15.64	16.03	42.39

[a]Hansen solubility parameter estimates using Hoftyzer-Van Krevelen group contribution method where δ_d is the dispersive Hansen parameter, δ_p is the polar Hansen parameter, and δ_h is the hydrogen bonding Hansen parameter.

Table S3.3. Elution times of CTAs from Reversed-Phase HPLC.[a]

CTA	Elution time (min)
1	11.8
2	13.4
3	13.5
4	14.2
5	18.1
6	31.9
7	47.9

[a]Increase elution time by reversed-phase high performance liquid chromatography was used as a measure of hydrophobicity of each CTA. Conditions were as follows: 10 μL injection of a roughly 1 mg mL^{-1} solution of CTA in MeOH, a mobile phase of 25/75 acetonitrile/H_2O with 0.05 wt% trifluoroacetic acid, UV detector at 309 nm (wavelength of maximum absorbance for trithiocarbonate).

Table S3.4. Fitting results from DLS for samples fitted with a double exponential decay model.

Polymer	Value of Correlation function[a] at $\tau = 10^{-6}$	$R_{h,1}$[b] (nm)	$R_{h,2}$[b] (nm)	Associated amplitude for $R_{h,1}$[a]	Associated amplitude for $R_{h,2}$[a]
PNiPAm-(**1**, C_{12}, 1.3)	0.708	30	4	0.49	0.36
PNiPAm-(**2**, C_{12}, 1.3)	0.506	33	4	0.34	0.40
PNiPAm-(**1**, C_{12}, 4.4)	0.609	51	7	0.45	0.35

[a]Values of the correlation function at $\tau = 10^{-6}$ s were taken using the double exponential decay fit modeled at 90°. Values of the associated amplitudes for $R_{h,1}$ and $R_{h,2}$ also based on the decay exponential decay modeled at 90°.

[b]R_h values based on diffusion coefficients found by plotting Γ versus q^2 based on five angles from 60 to 120°.

Table S3.5. Fitting results from DLS for samples fitted with a second-order cumulant model.

Polymer	Value of Correlation function[a] at $\tau = 10^{-6}$	Experimental R_h (nm)[b]	Average μ_2/Γ^{2b}
PNiPAm-(**1**, C_2, 3.9)	0.341	2	0.42
PNiPAm-(**1**, C_6, 3.8)	0.555	10	0.38
PNiPAm-(**1**, C_{18}, 4.6)	0.557	5	0.03
PNiPAm-(**1**, C_{12}, 22.0)	0.456	13	0.05
PNiPAm-(**1**, C_{18}, 6.0)	0.681	7	0.15
PNiPAm-(**1**, C_{18}, 8.0)	0.668	9	0.10

[a]Values of the correlation function at $\tau = 10^{-6}$ were taken using the second-order cumulant fit modeled at 90°.

[b]R_h values and average μ_2/Γ^2 values found by plotting Γ versus q^2 based on five angles from 60 to 120°.

3.13 References

(1) Liu, H.; Ilevbare, G. A.; Cherniawski, B. P.; Ritchie, E. T.; Taylor, L. S.; Edgar, K. J. *Carbohydr. Polym.* **2014**, *100*, 116–125.

(2) Abu-Diak, O. A.; Jones, D. S.; Andrews, G. P. *Mol. Pharm.* **2011**, *8* (4), 1362–1371.

(3) Warren, D. B.; Benameur, H.; Porter, C. J. H.; Pouton, C. W. *J. Drug Target.* **2010**, *18* (10), 704–731.

(4) Warren, D. B.; Bergström, C. A. S.; Benameur, H.; Porter, C. J. H.; Pouton, C. W. *Mol. Pharm.* **2013**, *10* (8), 2823–2848.

(5) Ilevbare, G. A.; Liu, H.; Edgar, K. J.; Taylor, L. S. *Mol. Pharm.* **2013**, *10* (6), 2381–2393.

(6) Ilevbare, G. A.; Liu, H.; Edgar, K. J.; Taylor, L. S. *Cryst. Growth Des.* **2012**, *12* (6), 3133–3143.

(7) Nakayama, M.; Okano, T. *Biomacromolecules* **2005**, *6* (4), 2320–2327.

(8) Furyk, S.; Zhang, Y.; Ortiz-Acosta, D.; Cremer, P. S.; Bergbreiter, D. E. *J. Polym. Sci. Part Polym. Chem.* **2006**, *44* (4), 1492–1501.

(9) Widanapathirana, L.; Tale, S.; Reineke, T. M. *Mol. Pharm.* **2015**, *12* (7), 2537–2543.

(10) Ting, J. M.; Tale, S.; Purchel, A. A.; Jones, S. D.; Widanapathirana, L.; Tolstyka, Z. P.; Li, G.; Guillaudeu, S. J.; Bates, F. S.; Reineke, T. M. *ACS Cent. Sci.*, **2016** *2* (10), 748–755.

(11) Curatolo, W.; Nightingale, J. A.; Herbig, S. M. *Pharm. Res.* **2009**, *26* (6), 1419–1431.

(12) Du, J.; Willcock, H.; Patterson, J. P.; Portman, I.; O'Reilly, R. K. *Small Weinh. Bergstr. Ger.* **2011**, *7* (14), 2070–2080.

(13) Fairbanks, B. D.; Gunatillake, P. A.; Meagher, L. *Adv. Drug Delivery Rev.* **2015**, *91*, 141–152.

(14) Pissuwan, D.; Boyer, C.; Gunasekaran, K.; Davis, T. P.; Bulmus, V. *Biomacromolecules* **2010**, *11* (2), 412–420.

(15) Chang, C.-W.; Bays, E.; Tao, L.; Alconcel, S. N. S.; Maynard, H. D. *Chem. Commun.* **2009**, *24*, 3580–3582.

(16) Ricarte, R. G.; Lodge, T. P.; Hillmyer, M. A. *Mol. Pharm.* **2015**, *12* (3), 983–990.

(17) Hiemenz, P. C.; Lodge, T. P. *Polymer Chemistry*, 2nd ed.; CRC Press: Boca Raton, FL, 2006.

(18) Yin, L.; Hillmyer, M. A. *Mol. Pharm.* **2014**, *11* (1), 175–185.

(19) Liu, P.; De Wulf, O.; Laru, J.; Heikkilä, T.; van Veen, B.; Kiesvaara, J.; Hirvonen, J.; Peltonen, L.; Laaksonen, T. *AAPS PharmSciTech* **2013**, *14* (2), 748–756.

(20) Donovan, M. D.; Flynn, G. L.; Amidon, G. L. *Pharm. Res. 7* (8), 863–868.

(21) Kubota, K.; Fujishige, S.; Ando, I. *Polym. J.* **1990**, *22* (1), 15–20.

(22) Tajarobi, F.; Larsson, A.; Matic, H.; Abrahmsén-Alami, S. *Eur. J. Pharm. Biopharm.* **2011**, *78* (1), 125–133.

(23) Ricarte, R. G.; Lodge, T. P.; Hillmyer, M. A. *Langmuir* **2016**.

(24) Zhou, C.; Hillmyer, M. A.; Lodge, T. P. *Macromolecules* **2011**, *44*, 1635–1641.

(25) Li, Z.; Johnson, L. M.; Ricarte, R. G.; Yao, L. J.; Hillmyer, M. A.; Bates, F. S.; Lodge, T. P. *Langmuir* **2017**, *33* (11), 2837–2848.

(26) Neslihan Gursoy, R.; Benita, S. *Biomed. Pharmacother.* **2004**, *58* (3), 173–182.

(27) Taylor, L. S.; Zhang, G. G. Z. *Adv. Drug Deliv. Rev.* **2016,** *101*, 122–142.

(28) Dalsin, M. C.; Tale, S.; Reineke, T. M. *Biomacromolecules* **2014**, *15* (2), 500–511.

(29) Friesen, D. T.; Shanker, R.; Crew, M.; Smithey, D. T.; Curatolo, W. J.; Nightingale, J. A. S. *Mol. Pharm.* **2008**, *5* (6), 1003–1019.

(30) Yakou, S.; Umehara, K.; Sonobe, T.; Nagai, T.; Sugihara, M.; Fukuyama, Y. *Chem. Pharm. Bull. (Tokyo)* **1984**, *32* (10), 4130–4136.

(31) Otsuka, N.; Ueda, K.; Ohyagi, N.; Shimizu, K.; Katakawa, K.; Kumamoto, T.; Higashi, K.; Yamamoto, K.; Moribe, K. *J. Pharm. Sci.* **2015**, *104* (8), 2574–2582.

(32) Moad, G.; Chong, Y. K.; Postma, A.; Rizzardo, E.; Thang, S. H. *Polymer* **2005**, *46* (19), 8458–8468.

Chapter 4: Understanding The Critical Excipient Properties for Dissolution Enhancement of Phenytoin

4.1 Introduction

Solubility-enhancing amorphous solid dispersions can aid in the oral delivery of hydrophobic, poorly soluble drugs. Effective solid dispersion excipients enable high supersaturation drug concentrations over biologically relevant time scales. The critical characteristics of an excipient that allow it to work well in a solid dispersion system are not well understood. We prepared poly(*N*-isopropylacrylamide), poly(*N*,*N*-dimethylacrylamide), and poly(*N*-hydroxyethylacrylamide) excipients of varying molar mass, and examined their ability to improve the aqueous solubility of phenytoin, a Biopharmaceutical Class System Class II drug. Binary and ternary solid dispersions of phenytoin and these excipients, along with hydroxypropyl methylcellulose acetate

succinate and hydroxypropyl methylcellulose, were prepared at 10 wt% drug loading. Dissolution behavior was studied at early time points (<1 minute) and over the course of 6 hours. Performance of the ternary solid dispersions was largely a function of the fraction of poly(*N*-isopropyl acrylamide) present in micellar structures. We present several systems that achieved significant improvement of phenytoin solubility over a wide composition range at enhancement factors among the highest seen to date for phenytoin.

Low aqueous solubility of emerging drugs poses an immense challenge to the pharmaceutical industry. A pharmaceutical active's bioavailability is often captured in two broad-stroke properties: permeability and solubility.[1,2] The Food and Drug Administration, and the pharmaceutical industry as a whole, classify most drugs by these two characteristics in a four-quadrant Biopharmaceutical Classification System (BCS).[1] Currently, 'ideal' drugs that exhibit high solubility and high permeability (Class I) make up roughly 35% of currently marketed drugs; however, only 10% of future drug candidates in the pipeline are Class I.[3] In contrast, the vast majority (~80 %) of future drug candidates are expected to have low aqueous solubility (Classes II and IV),[3,4] and this has driven extensive efforts towards formulation strategies for improving their aqueous solubility.[5]

Formulation of poorly soluble drugs into amorphous solid dispersions has been identified as a general solubility-enhancement method that does not compromise intestinal permeability of the pharmaceutical.[6,7] Dispersing the active pharmaceutical within a polymeric solid dispersion excipient provides several advantages for increasing drug solubility.[8,9] Polymer excipients are often designed to be hydrophilic, and as such, enhance the aqueous dispersibility of the poorly soluble drug.[10] Furthermore, by introducing the amorphous form of the drug in aqueous media upon dissolution, solid dispersions deliver

a higher-energy form of the drug with a higher solubility than the crystalline solubility of the drug.[11,12,13]

Unfortunately, the higher free energy of the amorphous compound relative to its crystalline counterpart thermodynamically favors crystallization of the drug. As such, the choice of a suitable excipient to stabilize the drug in both the solid and dissolved states is critical to the success of this solubilizing method.[14] While suitable excipient-drug pairs can be discovered through screening processes, our aim is to expand the foundational understanding of effective pharmaceutical excipients through systematic variations of key molecular and physical properties of the excipient.

As a model drug-excipient pair, this work focuses on phenytoin, a BCS Class II (low solubility, high permeability) antiepileptic, and poly(acrylamide)-based polymers. Previous work has shown several highly effective poly(acrylamide)-based excipients for the achievement and sustainment of high supersaturation levels of phenytoin (up to a 22-fold increase over crystalline solubility).[15,16,17,18,19] Specifically, low-molar-mass, micelle-forming poly(*N*-isopropylacrylamide) (PNiPAm) homopolymer has performed well, both on its own[18] and when blended with HPMCAS.[17] Poly(*N*,*N*-dimethylacrylamide-*co*-*N*-isopropylacrylamide) (PDMAm-*co*-PNiPAm) containing ~70 mol% *N*-isopropylacrylamide has also performed well, both as free chains and as in the corona of self-assembled micelles.[16,19]

This work probes the transferability of the conclusions of previous PNiPAm-phenytoin systems. Specifically, this work expanded on the understanding afforded by the study on low-molar-mass (<10 kDa) PNiPAm homopolymers that formed dispersed micelles in aqueous solution.[18] The current understanding and explanation for the effective solubilization behavior is that dissolved phenytoin is stabilized within local environments

of high NiPAm content.[17,18,19] In the case of low-molar-mass RAFT-synthesized homopolymers, micellization of PNiPAm homopolymer (NiPAm corona, alkyl chain hydrophobic core) increases the local PNiPAm concentration within the corona environment as compared to free chains.[17,18,19]

Stabilization of phenytoin in PNiPAm-rich environments may occur because PNiPAm offers a suitable hydrophilic/hydrophobic balance that encourages phenytoin partitioning in the corona.[19] PNiPAm may also offer favorable hydrophobic interactions between PNiPAm isopropyl groups and phenytoin aromatic rings[17,19] and/or specific secondary amide-secondary amide interactions that disrupt the fastest hydrogen-bond ribbon growth axis of phenytoin.[20] Indeed, Moghadam and Larson developed all-atom molecular dynamic simulations of NiPAm-based polymers in water in the presence of phenytoin.[21] They argue that an advantageous balance of hydrophilic/hydrophobic character can be accessed both in low-molar-mass PNiPAm homopolymers and in PNiPAm copolymers with other hydrophilic comonomers, and that an ideal hydrophilic/hydrophobic balance can maximize stabilizing excipient-phenytoin contacts.

We previously evaluated PNiPAm homopolymers of varying molar mass and end group for supersaturation achievement and maintenance of phenytoin.[18] By keeping many of the polymeric molecular details the same — *i.e.* the controlled synthesis by reversible addition-fragmentation chain transfer polymerization, the chain transfer agent, and the molar mass range — in this work, we test the generalizability of previous conclusions. These findings probed the role of the NiPAm repeat unit specifically. Through the investigation of binary and ternary solid dispersions of phenytoin formulated with two structurally similar homopolymers and two cellulosic polymers, we have increased our

understanding relating to the importance of NiPAm in the enhancement of phenytoin's solubility in aqueous media.

4.2 Synthesis and Characterization of Polymeric Excipients

The polymers highlighted here were studied as solid dispersion excipients in binary and ternary blends with phenytoin (Scheme 4.1). Synthetic solid dispersion excipients were prepared from three different acrylamide monomers via reversible addition-fragmentation chain transfer (RAFT) polymerization. Based on previous work demonstrating the effectiveness of *N*-isopropyl acrylamide as a monomer unit in several polymeric solid dispersion excipient systems with phenytoin, the acrylamide backbone structure was maintained in all of the synthetic polymers studied here.[15,16,17,18,19] Homopolymers of poly(*N*-isopropylacrylamide) (PNiPAm), poly(*N*,*N*-dimethylacrylamide) (PDMAm), and poly(*N*-hydroxyethylacrylamide) (PHEAm) all inherited a starting RAFT chain transfer agent (CTA) that possessed both a carboxylic acid terminus and a C_{12}-alkyl chain terminus. This specific CTA was chosen for its ability to drive micellization of low-molar-mass polymers, as previously demonstrated with low-molar-mass PNiPAm.[18] Additionally, two common commercially available cellulosic excipients were studied: hydroxypropyl methylcellulose acetate succinate (HPMCAS) and hydroxypropyl methylcellulose (HPMC) (See Experimental Section for more detail).

Scheme 4.1. Chemical structures of polymeric excipients and phenytoin. The cellulosic structures shown are representative, where actual placement of all substituents is without regioselective control, and the degree of substitution of each functionality is independently varied.

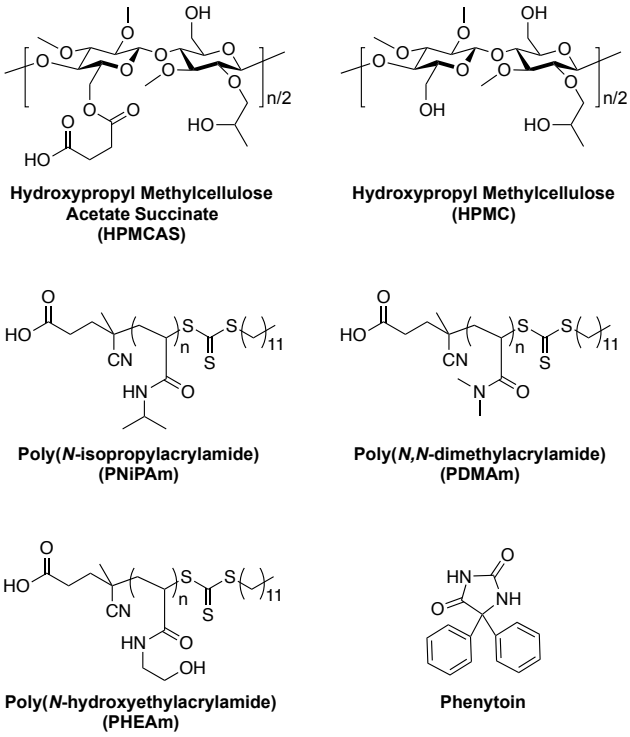

Phenytoin (Scheme 4.1) has a melting temperature (T_m) of 296 °C, a moderately lypophilic octanol-water partition coefficient (logP) value of 1.92, and a solubility for the crystalline form in DI water of 27.1 μg mL^{-1}.[22,23] The hydantoin ring of phenytoin offers two hydrogen bond donors and two hydrogen bond acceptors, and the two phenyl rings offer hydrophobic character to the molecule.

The molecular and thermal characteristics of all polymer samples are summarized in Table 4.1. Three series of low-molar-mass homopolymers were prepared based on each acrylamide monomer. Polymers are named by their polymer abbreviation, followed by their M_n value determined by NMR spectroscopy, in kDa, assuming one end group per

chain; for example, PNiPAm-(1.3) indicates a PNiPAm homopolymer with an M_n value of 1.3 kDa. M_n values as determined by SEC were equivalent or larger than M_n values by NMR spectroscopy. Dispersities for PDMAm samples were larger than typically seen for RAFT polymerizations. DSC was used to determine the glass transition temperatures (T_gs) of the polymers. Within each homopolymer series, T_g values generally increased with increasing molar mass. T_g values for the synthetic polymers ranged from 52 to 94 °C. The cellulosic polymers possessed T_g values over 120 °C.

Table 4.1. Molecular and thermal characteristics of polymer samples.

Sample	M_n NMR[a] (kg mol^{-1})	M_n SEC[b] (kg mol^{-1})	M_w SEC[b] (kg mol^{-1})	$Đ$ SEC[b]	T_g (°C)[c]
PNiPAm-(1.3)	1.3	1.8	1.8	1.0	71
PNiPAm-(4.4)	4.4	4.9	5.0	1.0	94
PDMAm-(2.0)	2.0	2.3	4.4	2.0	52
PDMAm-(3.3)	3.3	3.4	14	4.1	58
PDMAm-(5.6)	5.6	11	30	2.8	61
PDMAm-(6.5)	6.5	10	51	5.1	67
PDMAm-(11.3)	11.3	22	102	4.7	78
PHEAm-(1.7)	1.7	–	–	–	61
PHEAm-(2.9)	2.9	–	–	–	59
PHEAm-(4.3)	4.3	–	–	–	61
PHEAm-(5.6)	5.6	–	–	–	63
PHEAm-(8.8)	8.8	–	–	–	63
HPMCAS	–	60	142	2.38	121
HPMC	–	11.8	15.7	1.33	132

[a]M_n NMR determined by ^{1}H NMR spectroscopy in DMSO-d_6, 64 scans, d1 = 10 sec. [b]M_n SEC, M_w SEC, and $Đ$ determined by SEC using a light scattering detector. [c]Glass transition temperatures (T_gs) as determined by DSC in the second heating cycle at a heating rate of 10 °C min^{-1}.

To probe solubility, each polymer sample was dissolved at 9 mg mL^{-1} in phosphate buffered saline (PBS, pH 6.5) at 37 °C. All of the samples were dissolved at 9 mg mL^{-1} such that no chunks/particles of polymer were visually apparent (Figure S4.2). All PNiPAm and PDMAm samples gave clear solutions at this concentration. HPMCAS and

HPMC also formed clear solutions at this loading and temperature. The lowest molar mass PHEAm-(1.7) sample solution was clear, though all samples of higher molar mass appeared hazy, indicating the presence of larger solution structures.

The thermal phase transitions of the two PNiPAm samples were studied by turbidimetry.[24,25,26] Cloud points of PNiPAm-(1.3) and PNiPAm-(4.4) at 9 mg mL^{-1} in PBS-based dissolution media (pH 6.5) with 0.05 wt% simulated intestinal fluid powder (SIF) were determined by transmittance (T) measurements. The cloud point (50%T) of PNiPAm-(4.4) was 38 °C. No cloud point was detected for PNiPAm-(1.3), up to 50 °C (Figure S4.3). Thus, while thermoresponsive behavior may contribute to the performance of the PNiPAm-(4.4) sample during dissolution, no thermoresponsive behavior is expected to contribute to the performance of the PNiPAm-(1.3) sample.

Dynamic light scattering (DLS) was used to evaluate the presence, size, and size distribution of solution structures that the excipients formed in PBS (pH 6.5, w/o SIF). No SIF powder was added to the PBS used for DLS to limit scattering complexities arising from SIF lipids. Apparent size distributions are shown in Figure 4.1. Most samples showed random residuals of the autocorrelation functions to the fits (Figure S4.7), suggesting good reliability of the fitting models chosen. Systematic error was observed for the cellulosic polymers and the PHEAm-(4.3), -(5.6), and -(8.8) samples, indicating that the double exponential model used does not perfectly describe the size distributions within the solution. Plots of the mean decay rates (Γ) vs q^2 are linear with near-zero intercepts (Figure S4.8), which is consistent with the relaxation processes being diffusive. Key results from the DLS studies in PBS are summarized in Table 4.2.

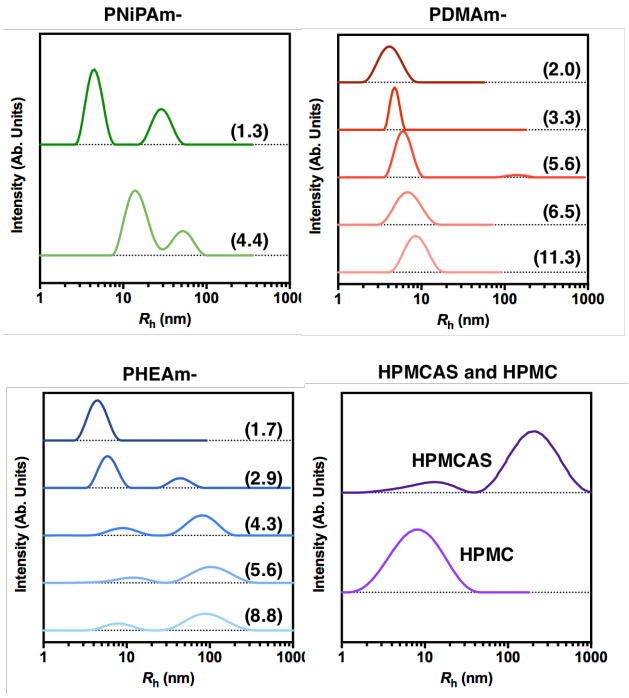

Figure 4.1. Apparent micellar distributions of polymer samples dissolved in PBS (pH 6.5, w/o SIF) at 9 mg mL^{-1}. The scattering angle is 90°.

Table 4.2. Hydrodynamic Radius (R_h) values determined by DLS in PBS buffer (pH 6.5, w/o SIF).

Polymer	**R_h (nm)**	**μ_2/Γ^{2a}**
PNiPAm-(1.3)[b]	5, 28	–
PNiPAm-(4.4)[b]	12, 49	–
PDMAm-(2.0)[c]	4	0.12
PDMAm-(3.3)[c]	6	0.09
PDMAm-(5.6)[c]	6	0.16
PDMAm-(6.5)[c]	7	0.06
PDMAm-(11.3)[c]	9	0.05
PHEAm-(1.7)[c]	5	0.16
PHEAm-(2.9)[b]	6, 66	–
PHEAm-(4.3)[b]	8, 68	–
PHEAm-(5.6)[b]	9, 85	–
PHEAm-(8.8)[b]	7, 69	–
HPMCAS[b]	9, 157	–
HPMC[b]	6	0.45

[a]Calculated from the average μ_2/Γ^2 values across five angles. [b]Determined by fitting with a double exponential decay function. [c]Determined by fitting with a second-order cumulant expansion.

Both PNiPAm samples showed two populations by REPES. The first population was indicative of micelles, and the second population indicated the presence of larger aggregates. All PDMAm samples showed a single peak, suggesting only the presence of micelles, without larger aggregates. The lowest molar mass PHEAm sample showed a single peak, though the larger molar mass samples also showed a second population at larger sizes of about 100 nm, which could explain the haziness seen in those samples. HPMCAS appeared as two broad distributions around 9 and 157 nm, and HPMC as a single broad distribution around 6 nm.

The lowest molar masses of each synthetic polymer, PNiPAm-(1.3), PDMAm-(2.0), and PHEAm-(1.7), form structures that have an R_h values of 5, 4, and 5 nm, respectively. Making the assumption that these micelles are dense water-free spheres, aggregation numbers (N_{agg}) can be roughly estimated from the respective R_h values, the total M_n found by NMR spectroscopy, and a bulk density. Estimated values of N_{agg} for the PNiPAm-(1.3), PDMAm-(2.0), and PHEAm-(1.7) micelles were found to be 200, 100, and 200, respectively (sample calculation included in Supporting Information).

4.3 Spray-Dried Solid Dispersions with Phenytoin

Solid dispersions were formulated as binary and ternary blends of phenytoin with either one or two polymeric excipients, respectively. The solid-state properties of the solid dispersions were analyzed by DSC. A single glass transition temperature (T_g) was seen for all of the solid dispersions, consistent with the drug being molecularly dispersed within the excipient, with T_g values in the range of 54 to 99 °C (Table S4.1).

During dissolution testing, the solid dispersions studied were introduced to PBS with SIF powder to mimic intestinal conditions. Under *in vitro* conditions, the

concentration of phenytoin loaded was kept constant at 1,000 μg mL^{-1} by loading the SDD at 10,000 μg mL^{-1} (polymer loading at 9 mg mL^{-1}). The loaded drug concentration is significantly above the aqueous solubility of crystalline phenytoin (27.1 μg mL^{-1}) and below its estimated amorphous solubility (1,280 μg mL^{-1}).[27] Sink dissolution conditions are met when the volume of dissolution medium is at least three to ten times the volume that would give the drug's saturation concentration at the given drug loading; at 1,000 μg mL^{-1} the target drug concentration is relatively close to its estimated amorphous solubility, and thus the conditions we use are considered non-sink.[28]

Under routine dissolution conditions, dissolution vials were loaded with solid dispersion; PBS (w/ SIF) was introduced (the addition of PBS marked t = 0) and the vials were immediately mixed using a vortex mixer for 60 s at room temperature. The samples were placed in an isothermal holder maintained at 37 °C. The concentration of dissolved phenytoin was then evaluated at 4, 10, 20, 40, 90, 180, and 360 min after initial placement in the isothermal holder. At each time point, the concentration of phenytoin was determined by centrifuging down any suspended solids, taking an aliquot of the supernatant, evaluating the concentration via reversed-phase HPLC (post dissolution in methanol), and resuspending any solids by mixing on the vortex mixer for 60 s. The dissolution vial was then placed back into the isothermal holder until the next time point.

Early-time-point data was added to the routine dissolution profiles to increase the temporal resolution of the dissolution experiments. In a similar manner to the routine dissolution conditions, dissolution vials were loaded with solid dispersion. PBS (w/ SIF) was added to the dissolution vials (this addition marked t = 0). The vials were then mixed using a vortex mixer for either 15, 30, or 60 s at room temperature (~22 °C). The vials were then immediately centrifuged, and the concentration of phenytoin was determined as

above. Each early-time-point sample was a singular time point from a separate sample, with no resuspension or later time points taken.

4.4 Dissolution of Binary Solid Dispersions with Micelle-Forming Homopolymers as Excipients

Binary solid dispersions of phenytoin with micelle-forming homopolymers as the solid dispersion excipients were studied to elucidate the effect of monomer type and molar mass on the dissolution performance of phenytoin. To enable a comparison against previous work, dissolution studies using PNiPAm-(1.3) and PNiPAm-(4.4) are shown in Figure 4.2a, with added early-time-point resolution in Figure S4.4.

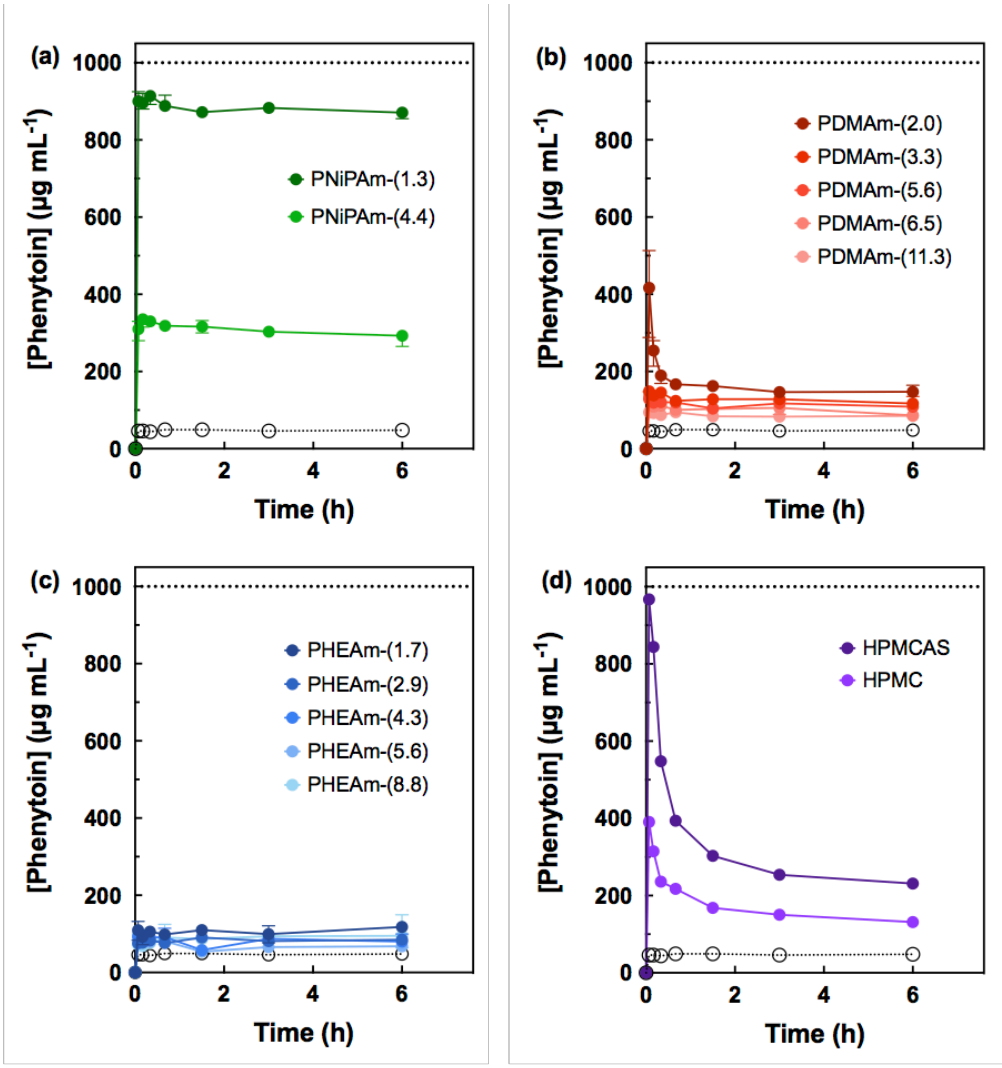

Figure 4.2. Dissolution of solid dispersions of 10 wt % phenytoin with 90 wt % (a) PNiPAm, (b) PDMAm, (c) PHEAm homopolymers, and (d) HPMCAS and HPMC. In all plots, the dissolution profile of crystalline phenytoin is also included as a reference (open circles). The loaded concentration of phenytoin was 1,000 µg mL^{-1} (indicated with the dashed line). Dissolution was run in triplicate. The data shown are the mean values, and the error bars represent the range of data. Figure 4.2a adapted from reference 18 pending permission (Copyright 2019 American Chemical Society).

The PDMAm homopolymer series was designed to probe the general ability of a micelle-forming homopolymer with an amide functionality to achieve and maintain a high

supersaturation of phenytoin. Dissolution of PDMAm samples (Figure 4.2b) showed a limited increase in apparent solubility of phenytoin over its crystalline form. These results suggest that < 500 μg mL^{-1} phenytoin was released into the dissolution media. However, early-time-point data for the PDMAm samples revealed full release of phenytoin (Figure 4.3) for the two lowest molar mass PDMAm samples at the shortest vortex times. Decreased phenytoin concentrations were seen at longer vortex times, indicating that crystallization is occurring rapidly, even during the vortexing process. At higher PDMAm molar masses, the effect of the hydrophobic alkyl tail is minimized, and the resultant polymer becomes more hydrophilic. Thus, while the higher molar mass samples did not show the same high initial concentrations of phenytoin as the lowest molar mass samples did, it is likely that these also fully released the phenytoin, but that phenytoin crystallized even before these early aliquots were taken.

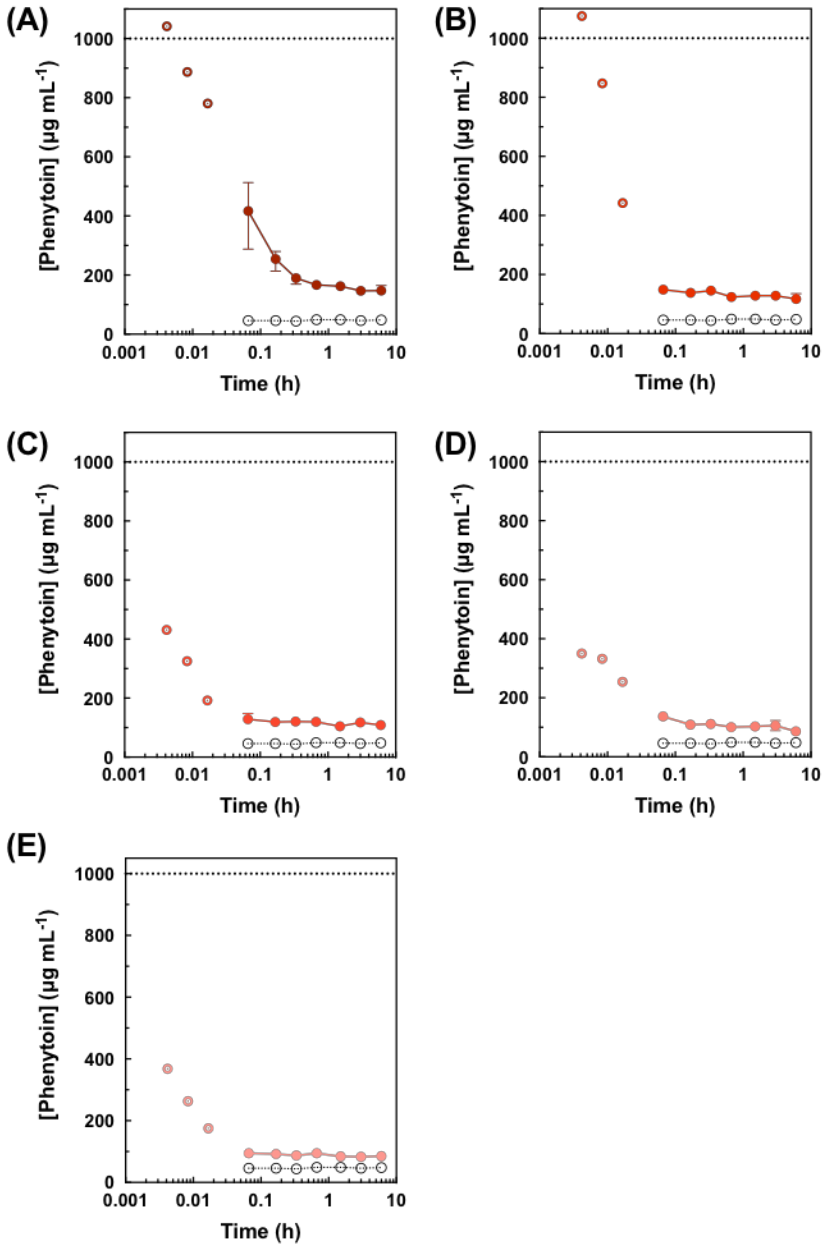

Figure 4.3. Early time point dissolution (open circles) and routine dissolution (filled circles) of solid dispersions of 10 wt % phenytoin and 90 wt % PDMAm: (A) PDMAm-(2.0), (B) PDMAm-(3.3), (C) PDMAm-(5.6), (D) PDMAm-(6.5), (E) PDMAm-(11.3). All x-axes are presented in log scale to make the initial time points easier to visualize. The dissolution profile of crystalline phenytoin was also included as a reference (black open circles). The loaded concentration of phenytoin was 1,000 µg mL^{-1} (indicated with the dashed line).

Although the PDMAm samples were fully dispersed at 9 mg mL^{-1}, formed micelles, and were able to achieve full supersaturation levels of phenytoin upon dissolution at short times, they were not able to maintain the high level of phenytoin concentration. Thus, those attributes alone along with amide functionality in the monomer structure do not lead to generalized excipient features that can maintain high supersaturation of phenytoin.

The PHEAm homopolymer series was designed to probe the generality of aqueous-dispersed, low-molar-mass excipients the formed micelles *and* possessed hydrogen bond donating abilities at the amide functionality (unlike PDMAm). This secondary amide character matched the secondary isopropyl acrylamide of the best performing excipient, and had the potential to probe the role of the combined amide carbonyl and hydrogen bond donor. Again, this series probed the potential effect across molar masses, ranging from 2 kDa to 9 kDa.

Dissolution of the PHEAm-based spray dried samples also revealed minimal solubility enhancement of phenytoin over its crystalline solubility (Figure 4.2c). Early-time-point data (Figure S4.5) was less revealing of early time dissolution than seen for the PDMAm series. Our efforts have revealed that the elements of small micelles, polymer solubility, hydrogen bond donors and secondary amide functionality are not generalizable to excipients beyond PNiPAm for maintaining supersaturation of phenytoin.

Phenytoin was also formulated into solid dispersions with HPMCAS and HPMC for comparative purposes. Together, routine dissolution and early-time-point studies (Figure 4.4) of these systems revealed peak dissolution within minutes, and subsequent crystallization over 6 hours. Notably, the complete dissolution seen in early time points for

HPMC was not detected in the routine dissolution studies (Figure 4.2d). This finding stresses the importance of capturing the full release mechanism when designing and drawing conclusions from dissolution experiments.

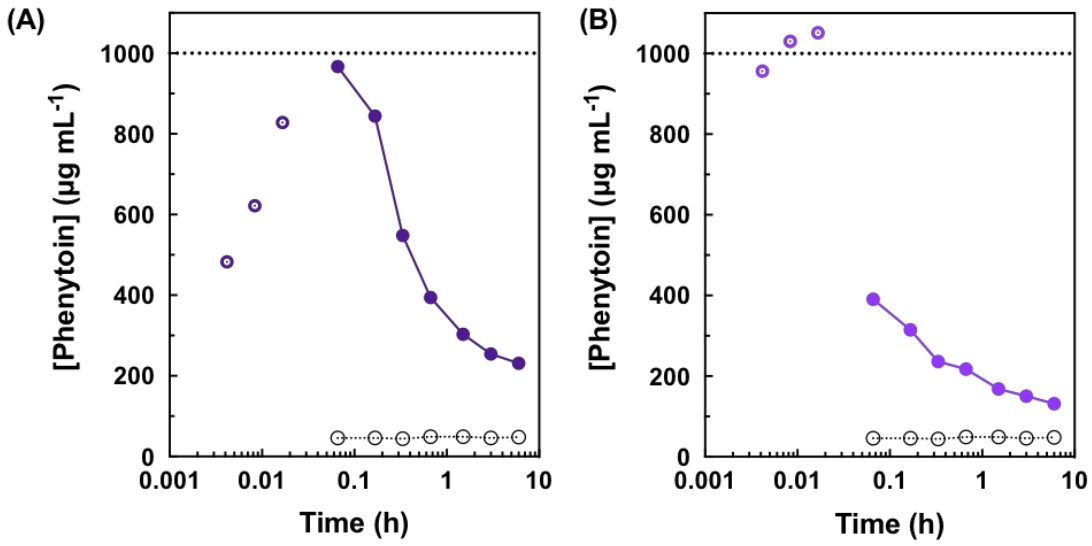

Figure 4.4. Early time point dissolution (open circles) of solid dispersions of 10 wt % phenytoin and 90 wt % (A) HPMCAS and (B) HPMC. All x-axes are presented in log scale to make the initial time points easier to visualize. In all plots, the routine dissolution profiles are included as filled in circles. The dissolution profile of crystalline phenytoin was also included as a reference. The loaded concentration of phenytoin was 1,000 µg mL^{-1}.

Area-under-the-curve (AUC) integrations are commonly used to quantitatively compare the effectiveness of a solid dispersion to increase the solubility of a drug. Enhancement factors (EFs) here are defined as a simple ratio of AUC over 6 h (AUC_{6h}) of the solid dispersion to the AUC_{6h} of pure phenytoin. Based on the engineering target of 1,000 µg mL^{-1} phenytoin for 6 h, the maximum EF possible is 22.1. The attained EFs can be related to the fraction of the engineering target, expressed as F_{ET}, or a percentage,

expressed as F_{ET} • 100%. The EFs and F_{ET} • 100% values for all binary blends are included in Figure 4.5. Only three samples achieved EF values above 5: PNiPAm-(1.3), PNiPAm-(4.4) and HPMCAS. In the case of PNiPAm-(1.3) the F_{ET} • 100% reached 97%.

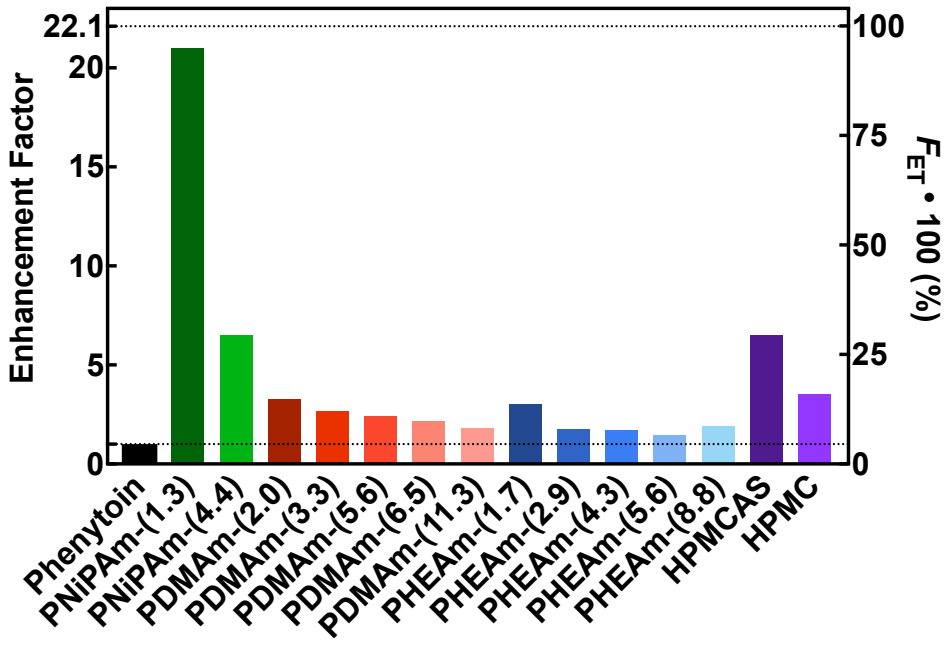

Figure 4.5. Enhancement factors and F_{ET} • 100 (%) values for all binary blends. The engineering target of 1,000 μg mL^{-1} phenytoin corresponds to a maximum EF possible of 22.1, which is represented by the top dotted line. The bottom dotted line represents an EF value of 1, as set by the solubility of crystalline phenytoin over 6 h.

4.5 Dissolution of Ternary Solid Dispersions: Phenytoing with Blends of Micelle-Forming Homopolymers

Given that PNiPAm-(1.3) was the highest performing material in the samples studied, ternary solid dispersions were formulated with PNiPAm-(1.3) and various diluent

excipients to probe importance of PNiPAm content within small micelles for the dissolution enhancement seen in the PNiPAm/phenytoin binary system. By blending phenytoin with PNiPAm and a diluent solid dispersion excipient, we were able to evaluate how the dissolution enhancement relates to the presence and density of NiPAm chains in micelle corona. The first two diluents used were PDMAm-(2.0) and PHEAm-(1.7). For these low-molar-mass synthetic polymers, the fully stretched length of the resultant micelle corona chains is roughly equivalent, given their similar degrees of polymerization. Also, since PNiPAm-(1.3), PDMAm-(2.0), and PHEAm-(1.7) are all synthesized from the same RAFT chain transfer agent, the micellization of these homopolymers, and mixtures of these homopolymers, is assumed to be similarly driven by the association of the common C_{12} alkyl tail.

For blends of A-B and B-C block polymers, where B is considered insoluble in solution and A and C are soluble, phase diagrams can describe and predict the thermodynamics favoring either mixed micelles with intermixed A and C coronas or mixtures of ordinary micelles with pure A and C coronas.[29] In these systems, we take A and C to be the repeating monomer units, and B to be the common C_{12} alkyl core. At these low molar masses, we posit that χN between A (PNiPAm) and C (either PDMAm or PHEAm as the diluent) is sufficiently low that A/C mixing is favorable, and that mixed micelles are formed. With the added compatiblizing effect of water, the enthalpic driving force for A/C segregation of these short blocks is likely insufficient to override the entropic driving force to mix. Thus, dissolved samples of PNiPAm:PDMAm and PNiPAm:PHEAm blends are presumed to exist as mixed micelles with a common C_{12} hydrophobic core and a mixed corona of PNiPAm and PDMAm or PHEAm. Thus, the amount of NiPAm within

the corona is expected to decrease for the mixed PNiPAm:PDMAm and PNiPAm:PHEAm systems.

To probe the solution structures formed in the absence of phenytoin, blends of the polymers at 100:0, 80:20, 70:30, 60:40, 40:60, 20:80, and 0:100 wt:wt PNiPAm:diluent were dissolved in PBS (w/o SIF, pH 6.5) (Figure 4.6) and evaluated by DLS. For both PNiPAm:PDMAm (Figure 4.6A) and PNiPAm:PHEAm blends (Figure 4.6B), a single structure with an R_h of 4 to 5 nm remained evident in all samples. The larger structure seen for PNiPAm alone remained in all blends, and the size increased over ~30 nm with increasing diluent present (R_h of 28 nm for pure PNiPAm, R_h of 57 nm for PNiPAm:PDMAm 20:80, R_h of 57 for PNiPAm:PHEAm 20:80). DLS results are summarized in Table 4.3.

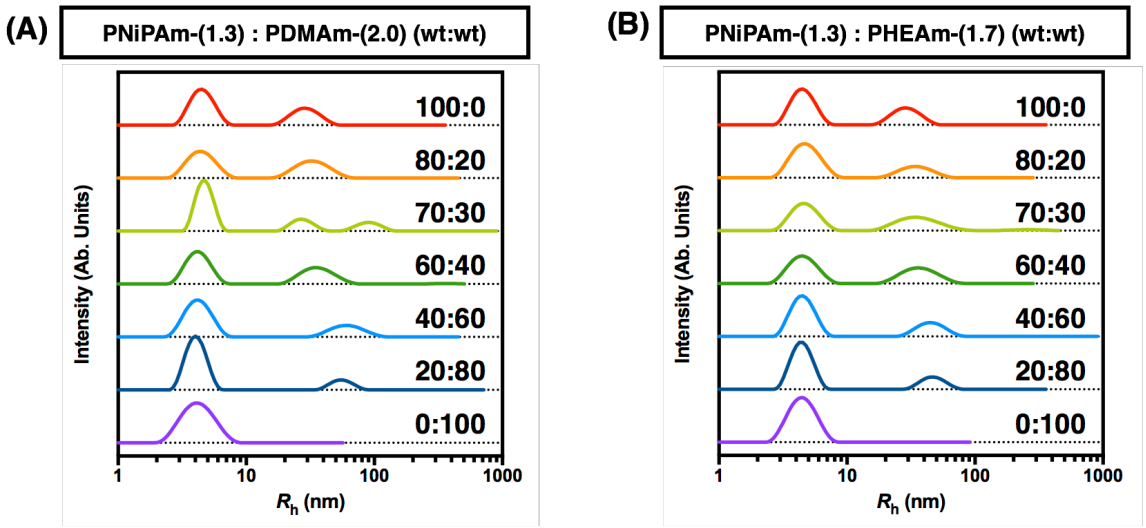

Figure 4.6. Apparent micellar distributions of polymer blends of (A) PNiPAm-(1.3) and PDMAm-(2.0), and (B) PNiPAm-(1.3) and PHEAm-(1.7), codissolved in PBS (pH 6.5) at a total polymer loading of 9 mg mL^{-1}. The scattering angle is 90°. Samples are given as wt:wt PNiPAm:diluent, where 100:0 and 0:100 samples are a single polymer.

Table 4.3. Hydrodynamic Radius (R_h) values determined by DLS in PBS buffer (pH 6.5).

Excipient Blends	(wt/wt)	R_h (nm)[a]
PNiPAm-(1.3)/PDMAm-(2.0)	80/20	5, 33
	70/30	4, 38
	60/40	4, 40
	40/60	4, 52
	20/80	4, 57
PNiPAm-(1.3)/PHEAm-(1.7)	80/20	5, 31
	70/30	5, 39
	60/40	5, 39
	40/60	5, 50
	20/80	5, 56
PNiPAm-(1.3)/HPMCAS	80/20	5, 49
	70/30	5, 55
	60/40	6, 77
	40/60	6, 100
	20/80	7, 121
PNiPAm-(1.3)/HPMC	80/20	5, 28
	70/30	5, 29
	60/40	5, 27
	40/60	5, 32
	20/80	5, 26

[a]Determined by fitting with a double exponential decay function.

Dissolution studies of the PNiPAm:PDMAm and PNiPAm:PHEAm ternary solid dispersions revealed that these two blend series showed nearly identical release profiles (Figures 4.7A and 4.7B). The similar abilities of these systems to achieve and maintain supersaturations of phenytoin over 6 h suggests similar mechanisms for phenytoin stability in solution. The performance was essentially mirrored for the same wt:wt values across both systems. Thus, the performance of these blends was likely related to the fraction of PNiPAm present in the micelles, and essentially independent of the diluent chains. When lowering the PNiPAm content relative to the diluent, crystallization was evident for both systems by the 6 h time point for the 60:40 PNiPAm:diluent composition. At all PNiPAm contents higher than 60:40 wt:wt PNiPAm:diluent, AUCs above 15 (F_{ET} • 100 (%) values

above 68%) were reached.

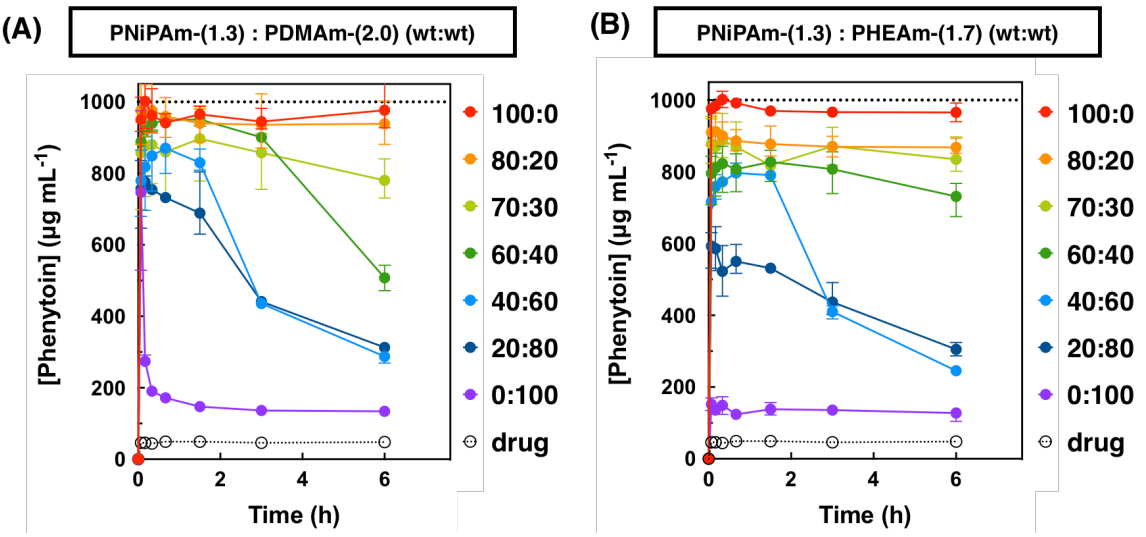

Figure 4.7. Dissolution of solid dispersions of 10 wt % phenytoin and blends of (A) PNiPAm-(1.3) and PDMAm-(2.0) and (B) PNiPAm-(1.3) and PHEAm-(1.7). In all plots, the dissolution profile of crystalline phenytoin was also included as a reference (open circles). The loaded concentration of phenytoin was 1,000 µg mL^{-1}. The data shown are the mean values, and the error bars represent the range of data.

Since both PDMAm and PHEAm are considerably more hydrophilic than PNiPAm, we hypothesize that the micelle coronae become too hydrophilic to encourage the partitioning of phenytoin within them. Thus, the stabilizing effect and solubilization enhancement of PNiPAm is decreased, regardless of whether that stabilizing effect is simply due to a hydrophobic/hydrophilic balanced environment that does not promote phenytoin crystallization, or if it is due to specific, crystallization-disrupting phenytoin-PNiPAm interactions.

4.6 Dissolution of Ternary Solid Dispersions: Phenytoin with Micelle-Forming PNiPAm and Cellulosic Polymers

Ternary mixtures of phenytoin with PNiPAm and either HPMCAS or HPMC were also prepared. Because of the difference in structure, mixing of the HPMCAS or HPMC into the PNiPAm micelle structure likely does not occur. Thus, for these systems, it is the total amount of PNiPAm available to form micelles that is affected, rather than the amount of PNiPAm within a mixed micelle coronae, as in the PNiPAm:PDMAm and PNiPAm:PHEAm systems.

REPES analysis of the PNiPAm:HPMCAS (Figure 4.8A) and PNiPAm:HPMC (Figure 4.8B) blends showed discrete populations contributed from each polymer. For PNiPAm:HPMCAS blends, three species were apparent by REPES. Each sample showed the presence of the population present in PNiPAm and two species present in HPMCAS. The intermediate-sized population seen for the blends likely captured both the larger PNiPAm aggregates and the smaller HPMCAS aggregates.

For the PNiPAm:HPMC blends, two populations from PNiPAm were seen, and the smaller one overlapped in size with the single peak seen for HPMC. With decreasing PNiPAm content, the presence of the larger PNiPAm-only aggregates decreased relative to the smaller, shared PNiPAm-and-HPMC peak. Summarized DLS results are included in Table 4.3. The autocorrelation functions of all blends were fit with a double exponential decay fitting. For the samples with three populations, the systematic error seen in the residuals suggest that the double exponential fitting was not completely appropriate. Scattering intensity scales with R_h^6, such that we expect the larger populations were present in very small amount relative to the smaller populations.[30]

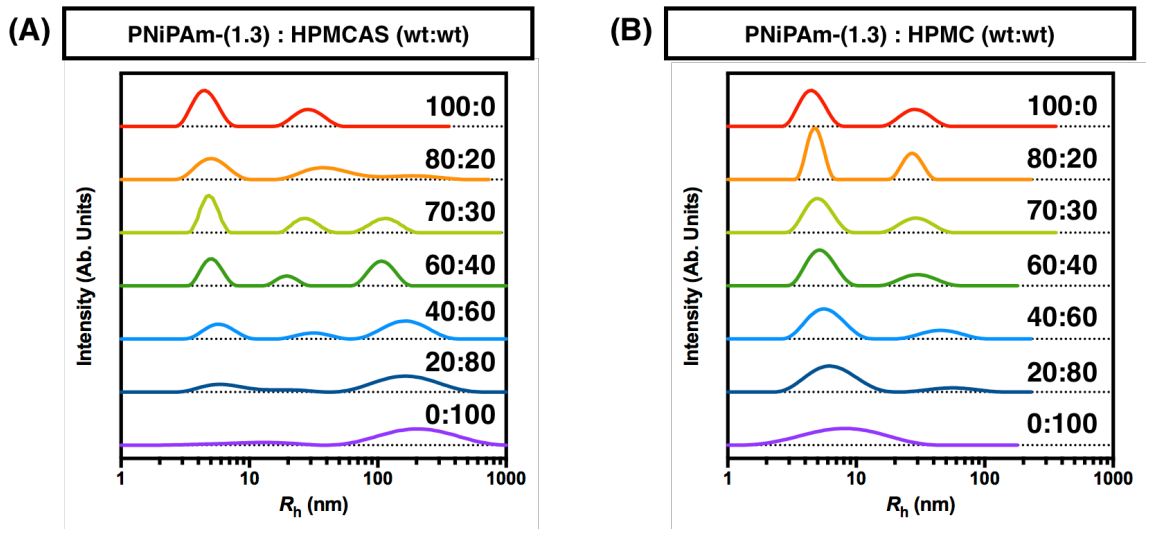

Figure 4.8. Apparent micellar distributions of polymer blends of (A) PNiPAm-(1.3) and HPMCAS, and (B) PNiPAm-(1.3) and HPMC, codissolved in PBS (pH 6.5) at a total polymer loading of 9 mg mL^{-1}. The scattering angle is 90°. Samples are given as wt:wt PNiPAm:diluent, where 100:0 and 0:100 samples are a single polymer.

The PNiPAm:HPMCAS and PNiPAm:HPMC ternary systems allowed us to probe how the dilution of PNiPAm micelles in general, not necessarily in a micelle corona as above, affected the ability of the ternary solid dispersions to achieve and maintain phenytoin supersaturation. Because HPMCAS and HPMC are hydrophilic polymers that achieve full release of phenytoin in binary blends (Figures 4.4A and 4.4B, respectively), they should not have an effect on the ability of a PNiPAm-based ternary solid dispersion to achieve high initial supersaturations. Dissolution studies of PNiPAm:HPMCAS and PNiPAm:HPMC are shown in Figures 4.9A and 4.9B. The PNiPAm:diluent cellulosic ternary systems were able to maintain supersaturation of phenytoin to a lower PNiPAm composition than seen for the mixed micelle ternary systems. AUCs above 15 (F_{ET} • 100

(%) values above 68%) were seen to down to a PNiPAm content of 40:60 PNiPAm:diluent. Even just 20:80 PNiPAm:HPMC offered significant solubility enhancement and delayed crystallization over pure HPMC.

Diluting the relative amount of PNiPAm micelles with HPMCAS and HPMC did less to invoke crystallization over 6 h than directly diluting NiPAm within the micelle coronas with PDMAm and PHEAm. The difference in observed crystallization in these systems suggests that it is the concentration of PNiPAm specifically within the micelles that is critical to the supersaturation sustainment seen for these systems.

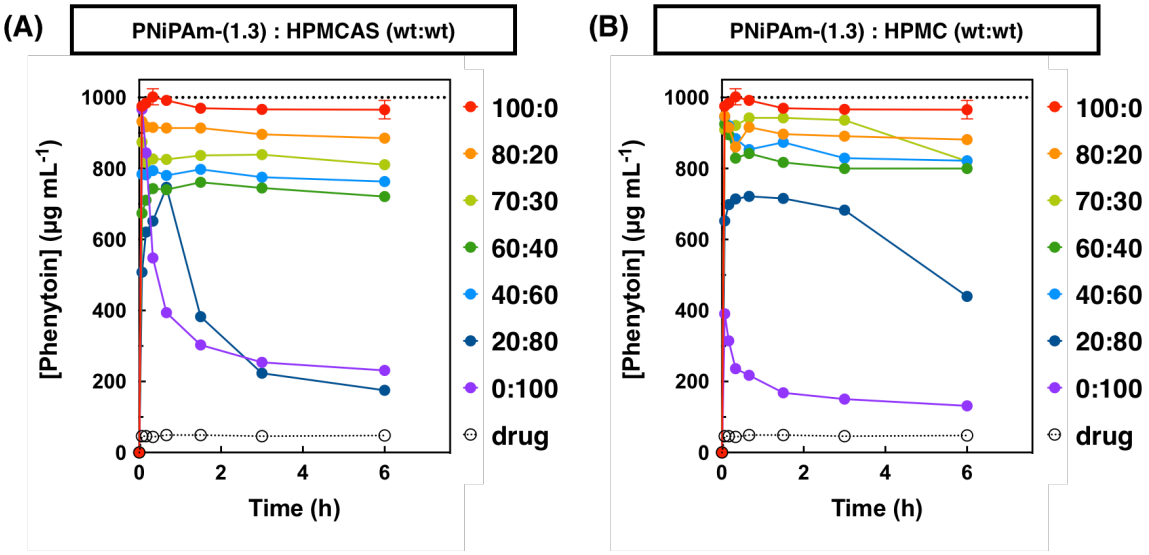

Figure 4.9. Dissolution of solid dispersions of 10 wt % phenytoin and blends of (A) PNiPAm-(1.3) and HPMCAS and (B) PNiPAm-(1.3) and HPMC. In all plots, the dissolution profile of crystalline phenytoin was also included as a reference (open circles). The loaded concentration of phenytoin was 1,000 µg mL^{-1}. The data shown are the mean values, and the error bars represent the range of data.

4.7 Solubility Enhancement Across Series

The EFs for all ternary blends are included in Figure 4.10. Within each ternary

series, four or five blends provided solubility enhancement factors over 15, among the highest seen to date for phenytoin. While the 80:20, 70:30, and 60:40 PNiPAm:diluent blends have near identical EFs across each diluent, differences can be seen at the 40:60 and 20:80 ratios.

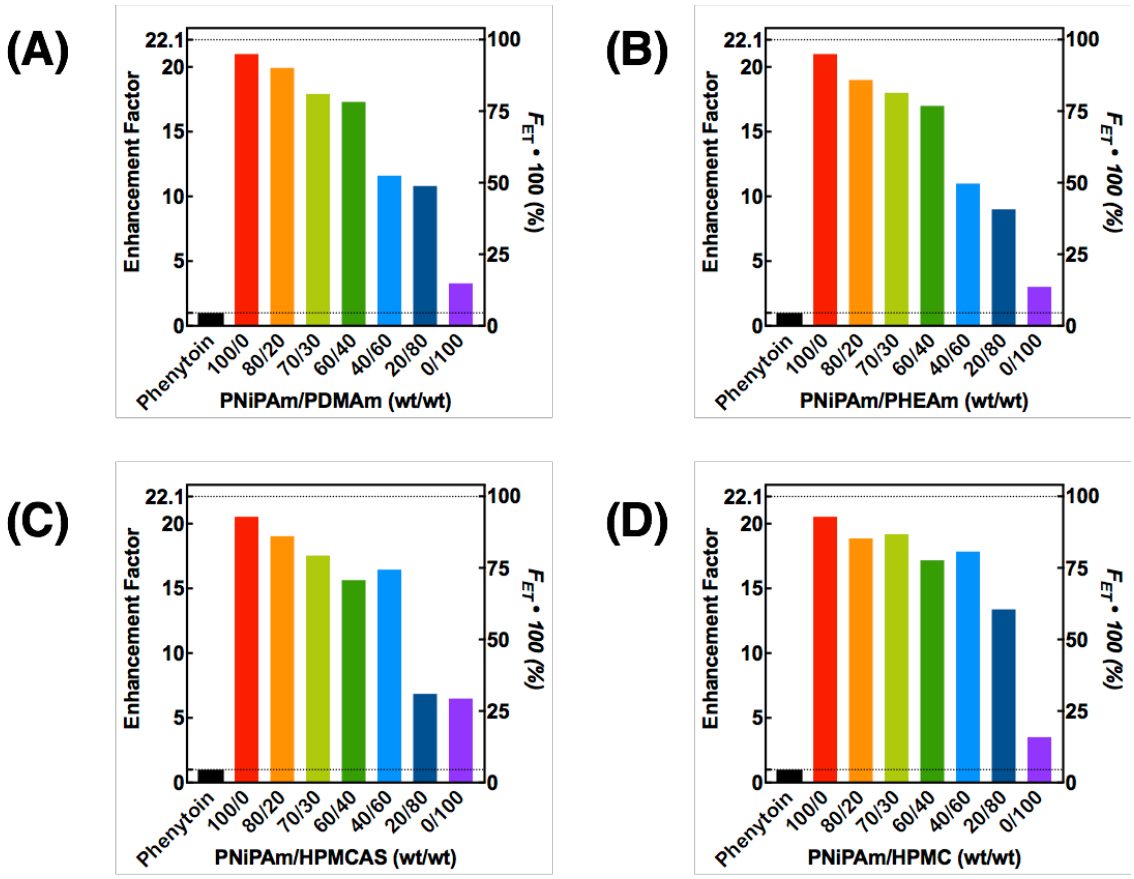

Figure 4.10. Enhancement factors (EF) and F_{ET} • 100 (%) values for ternary blends, of PNiPAm-(1.3), and a diluent of (A) PDMAm-(2.0), (B) PHEAm-(1.7), (C) HPMCAS, and (D) HPMC. Compositions are denoted by their respective PNiPAm/diluent wt/wt ratio. The engineering target of 1,000 μg mL^{-1} phenytoin corresponds to a maximum EF possible of 22.1.

Further illuminating the role of PNiPAm relative to the diluent, Figure 4.11 relates the mol of NiPAm per mol of phenytoin in the solid dispersion to the EFs seen for all ternary blends. All samples out perform a simple weighted mixing rule (with the exception of 20:80 PNiPAm:HPMCAS, which showed minimal crystallization retardation relative to a binary solid dispersion with HPMCAS). Although the EFs were generally above a simple averaging, it is unlikely that these effects were due to some synergistic behavior between PNiPAm and the diluent. Furthermore, since the performance of the PNiPAm:PDMAm and PNIPAm:PHEAm systems were nearly identical, the results seem to be independent of the diluent polymer, which also argues against synergy. Rather, there seems to be both a critical density of PNiPAm within micelles, and a critical amount of PNiPAm total, both are necessary to maintain high supersaturations of phenytoin in solution.

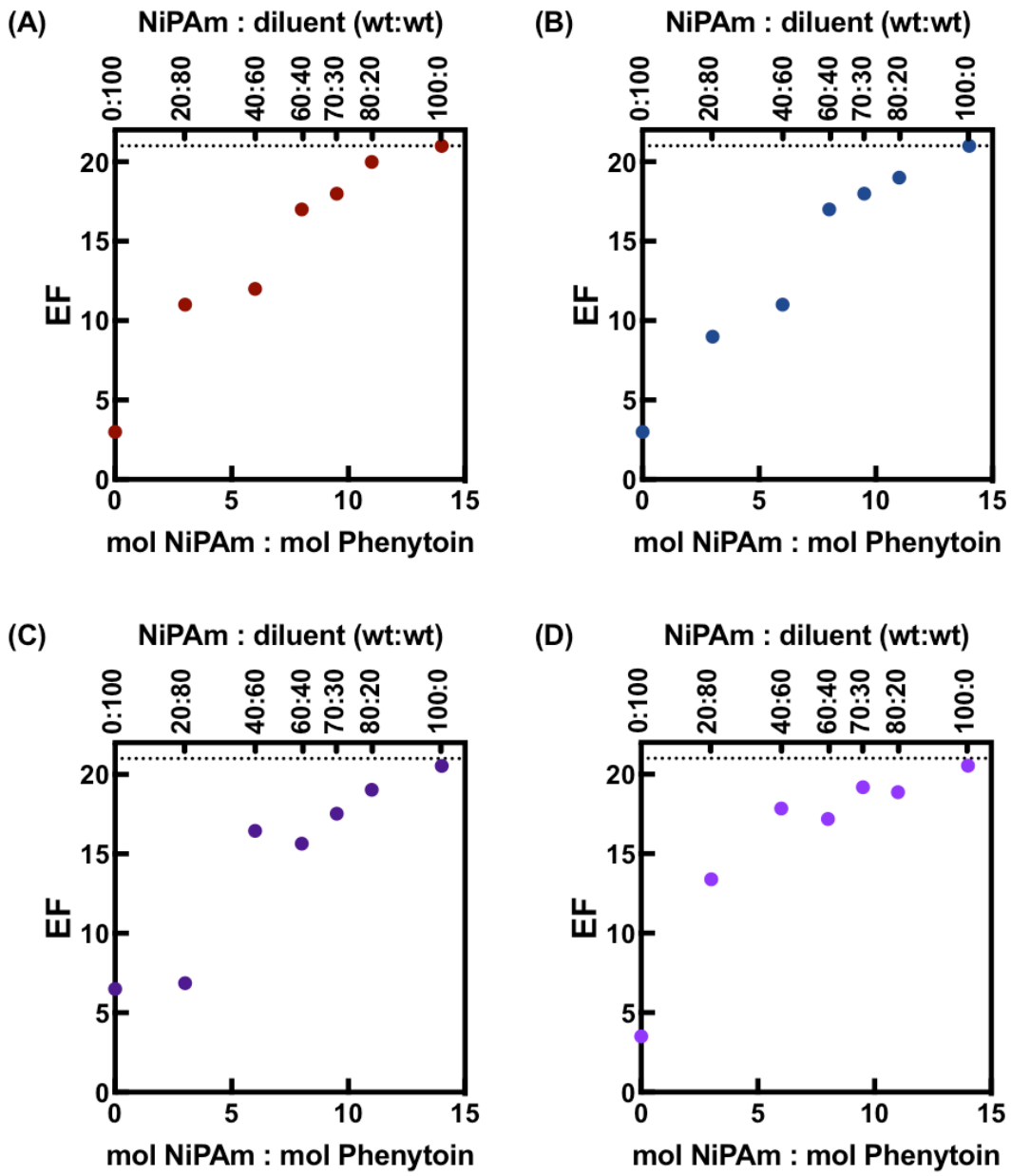

Figure 4.11. The enhancement factor of the blends as a function to the molar ratio of NiPAm to phenytoin in ternary solid dispersions of phenytoin, PNiPAm, and (A) PDMAm, (B) PHEAm, (C) HPMCAS, and (D) HPMC. The dotted horizontal line marks the maximum EF, if all phenytoin was fully dissolved for the 6 hours.

4.8 Discussion

Although BCS classifications give an indication of 'high' or 'low' (<100 μg mL^{-1})[2] solubility, the solubility of a solute, such as a drug molecule, in water largely depends on two independent characteristics: the crystallinity of the solute, and the ability of the solute to interact with water.[31] These two molecular characteristics are often captured in two physical properties, T_m and logP, respectively. Although these two physical properties can vary independently of each other, in combination they can be used to predict the solubility of the solid solute in water (S_W^{solid}) through an empirically derived general solubility equation:[32]

$$\log S_W^{solid} = 0.5 - 0.01(T_m - 25) - \log P \quad (1)$$

where T_m is the melting temperature in degrees Celsius.

This general solubility equation allows for the relative contribution of the crystallinity of the solute and its ability to interact with water to be weighed against each other with respect to overall solubility. Samples with high T_m values are often highly crystalline, and samples with high logP values strongly prefer non-polar environments over aqueous environments. These two qualities are in fact independent of each other, though, particularly in pharmaceuticals, there are often groupings of bioactive molecules within subspaces based on similar structural components.

Poorly soluble molecules with T_m values above 200 °C and with logP values below 2 are said to have "solid-state-limited solubility", because in their solid state, these molecules form dense crystal lattices with strong, tightly associated intermolecular interactions.[33,22] The poor solubility of these molecules is a mostly function of the crystallinity of the compound, rather than significant hydrophobic character. In this way, a moderately hydrophobic compound can have extremely poor aqueous solubility.

In contrast, poorly soluble molecules which are more lipophilic (logP > 3) and have lower T_m values often show solvation-limited solubility, where poor interactions of the compound with water means that hydration of the compound is unfavorable. The higher lipophilicity of these compounds promotes self-aggregation over mixing into water, also rendering them as poorly soluble in water.[34,33]

Unfortunately, while solubility-enhancement studies often look at poorly soluble compounds, we believe there should be a better separation between mechanisms of observed solubility enhancement based on these more underlying solubility-defining physical properties. While the terms "poorly soluble" in water and "hydrophobic" are often interchanged, these two qualities are not precisely synonymous. It is reasonable to posit that during the development of solubility-enhancing methods, compounds with solid-state solubility challenges would behave substantially differently from those with poor solvation-state solubility. In support of this, notably more solvation-limited-solubility drugs have been formulated and brought to the commercial market than solid-state-limited-solubility drugs.[35]

As mentioned, solid dispersions are known to offer several strategic advantages towards improving the solubility of a poorly soluble drug. These advantages include: (1) introducing the more-soluble amorphous form of the drug upon dissolution, and (2) improving wettability/solvation by using hydrophilic excipient. Between these two advantages, it has been noted that strong crystallizer compounds (sometimes referred to as "solid-state-limited solubility" compounds) benefit more from pre-dissolution amorphization than improved wettability.[33] In contrast, 'greasy' hydrophobic compounds are referred to as being solvation-limited, where improved wettability through excipient choice adds more benefit than pre-dissolution amorphization. We posit that the key to

dissolution improvement of solid-state-limited solubility molecules, like phenytoin, involves inhibiting the dissolved drug molecules from reforming intermolecular self-associations. The amorphous character afforded during spray drying inherently limits the crystalline character of the compound; the key is limiting crystallization-driving self-associations in solution once the drug is dispersed. In this work, solid dispersion excipients systems that offered a threshold amount of PNiPAm-dense micelle coronas were able to delay crystallization of phenytoin over 6 h, giving insight to a possible platform for similar solid-state-limited solubility molecules in the future.

4.9 Conclusions

In conclusion, we studied the relative importance of PNiPAm and its molecular properties for the dissolution enhancement of phenytoin. By specifically varying the chemical moieties of poly(acrylamide)-based homopolymers, we probed the relative importance of different properties with respect to solid dispersions achieving full release of phenytoin with prolonged supersaturation. We synthesized PDMAm and PHEAm homopolymers that formed aqueous-dispersed micelles in solution, with the aim of understanding the generality of poly(acrylamide)-based polymers to maintain phenytoin in solution. Although no further homopolymers were identified as high-performing excipients with respect to maintain supersaturation of phenytoin, we were able to design ternary systems that fully released phenytoin immediately upon dissolution. Through the formulation of ternary blends composed of phenytoin, PNiPAm, and a diluent of PDMAm, PHEAm, HPMCAS, or HPMC, it was revealed that two critical components were necessary for full sustainment of phenytoin supersaturations: (1) a high density of NiPAm within the micelle corona, and (2) a critical concentration of PNiPAm micelles in the

dissolution solution. These results will hopefully help guide future development of excipients with stabilizing functionalities in a highly dense formation, potentially for use with other solid-state-limited solubility drugs.

4.10 Supplemental Information

Materials

All chemicals were used as received from the manufacturer: *N*-isopropylacrylamide (Sigma, 99+%), *N*-hydroxyethyl acrylamide (Sigma, 97%), *N*,*N*-dimethylacrylamide (Sigma, 99%), 4,4′-azobis(4-cyanovaleric acid) (Sigma, 98+%), 4-cyano-4-(dodecylsulfanylthiocarbonyl)sulfanylpentanoic acid (Strem Chemical, 97+%), phenytoin (Sigma, 99+%), dioxane (Sigma-Aldrich), simulated intestinal fluid powder (Biorelevant) and dimethyl sulfoxide-d_6 (DMSO-d_6, Cambridge Isotope Laboratories, 99.9% D). The cellulosic HPMCAS and HPMC samples used were AFFINISOL™ HPMCAS 912 G and METHOCEL™ E3 LV, respectively, and were provided the Dow Chemical Company. Cellulosic materials are often characterized by the average number of substituent groups per glucose repeat unit, defined as the functional group degree of substitution. The HPMCAS sample had methoxy, hydroxypropyl, acetate, and succinate degrees of substitution of 1.94, 0.25, 0.57, and 0.28, respectfully. This HPMCAS grade was chosen because it was independently determined by the Dow Chemical Company to outperform all other commercial HPMCAS grades as a solid dispersion excipient for phenytoin at a loading of 10 wt % over 6 h. The HPMC sample had methoxy and hydroxypropyl degrees of substitution of 1.91 and 0.25, respectfully, and was chosen for its low viscosity in water when dissolved, and its intermediate hydrophobic/hydrophilic balance.

Synthesis of PNiPAm, PDMAm, and PHEAm

The syntheses of PNiPAm, PDMAm, and PHEAm were all performed via similar methods. A sample polymerization is given here: NiPAm (1.275 g, 0.01127 mol), 4-cyano-4-[(octadecylsulfanylthiocarbonyl) sulfanyl]pentanoic acid (0.500 g, 0.00102 mol), and 4,4′-azobis(4-cyanopentanoic acid) (0.0286 g, 0.000102 mol) were added to a round-

bottom flask. Dioxane (25 mL) was added. The reaction mixture was sparged with nitrogen gas for 45 min, and then placed in an oil bath at 72 °C. After 5 h, the reaction was exposed to air. The resultant polymer was isolated and purified by precipitation (2 times). The polymer was dried under vacuum at 40 °C overnight. Solubility of the polymers in phosphate buffered saline (PBS, 82 mM sodium chloride, 20 mM sodium phosphate dibasic, 47 mM potassium phosphate monobasic, pH 6.5), was tested by visually examining solutions at 9 mg mL^{-1}.

Molecular Characterization

Nuclear magnetic resonance (NMR) was performed on a 500 MHz Varian INOVA-500 spectrometer in DMSO-d_6 with a d1 relaxation time of 10 sec.

Size exclusion chromatography (SEC) was used to determine molar masses and molar mass distributions, using LS detectors. Full traces (Figure S1) were plotted from RI signals, relative to polystyrene detectors. PNiPAm and PDMAm samples were analyzed using THF as the mobile phase, PHEAm samples were analyzed using DMF as the mobile phase, and HPMC was analyzed using a mobile phase of 0.1 M Na_2SO_4 aqueous solution supplemented with 1% acetic acid. Molar mass data for HPMCAS was provided by The Dow Chemical Company.

Thermal Analysis

Differential scanning calorimetry (DSC) was performed on a Discovery DSC (TA Instruments, New Castle, DE) equipped with a refrigerated cooling system. A dry N_2 purge flowed through the cell at 50 mL min^{-1}, and samples were run in hermetically sealed TZero aluminum pans. Polymer samples were dried under vacuum before DSC analysis; samples (2-10 mg) were heat-cool-heat cycled at 10 °C min^{-1} between −85 and 150 °C. T_g values were taken from the second heating scan. Spray-dried dispersions were dried under vacuum

before DSC analysis; samples (2-6 mg) were ramped at 5 °C min^{-1} from −85 and 140 °C; T_g values were taken from the first heating scan.

Turbidity Analysis of PNiPAm Thermoresponsiveness

The cloud points of PNiPAm-(1.3) and PNiPAm-(4.4) in PBS solution (w/ SIF, pH 6.5) was determined by transmittance measurements. Solutions were prepared in glass ampules at 9 mg mL^{-1} and placed in the holding cell of a heating block (±1 °C). A 10 mW helium-neon laser (λ = 633 nm) passed through a neutral density filter and then through the sample ampule. The transmitted light was focused by a lens and the signal was collected by a photodiode detector. Heating rate was kept constant at 2.5 °C min^{-1}. The cloud point was taken as the 50% transmittance point (50%T).

Spray-Dried Dispersion Preparation

Spray-dried dispersions were prepared at lab-scale using a mini-spray dryer (Bend Research, Bend, OR). Solid dispersions were made either as binary blends of a homopolymer and phenytoin, or ternary solid dispersions of two homopolymers and phenytoin. For dispersion preparation, a total-solids loading of 2.0 wt% drug and polymer were dissolved in 90/10 v/v MeOH/H_2O. Samples were sprayed at a constant inlet temperature (75 °C), N_2 flow rate (28.6 sL min^{-1}), and solution flow rate (1.3 mL min^{-1}). Spray-dried dispersions were collected and immediately dried under vacuum overnight, and further stored at room temperature in a vacuum desiccator.

Solid dispersions were all made at 10 wt% phenytoin (90 wt% excipient). Binary solid dispersions were 10 wt% phenytoin and 90 wt% of a homopolymer. Ternary solid dispersions were 10 wt% phenytoin, and 90 wt% excipient, where the composition of the excipient was varied across 80:20, 70:30, 60:40, 40:60, and 20:80 wt:wt PNiPAm:diluent, where the diluent was PDMAm-(2.0), PHEAm-(1.7), HPMCAS, or HPMC. Samples that

are labelled as either “100:0” or “0:100” are the binary blends of phenytoin with a single excipient, either PNiPAm or the diluent.

Standard Dissolution Tests

Dissolution tests were performed in phosphate buffered saline solution (PBS, 82 mM sodium chloride, 20 mM sodium phosphate dibasic, 47 mM potassium phosphate monobasic) with 0.5 wt % simulated intestinal fluid (SIF) powder (FaSSIF, Biorelevant) at 37 °C. In a 1.5-mL microcentrifuge tube, an appropriate amount of spray-dried dispersion and PBS were added to target a total drug concentration of 1,000 μg mL^{-1}. Samples were mixed on a vortex mixer (Scientific Industries Vortex-Genie 2 on a setting of 10) for 1 min to suspend all solids and then placed (t = 0) in an isothermal sample holder held at 37 °C. At set time points (4, 10, 20, 40, 90, 180, 360 min), the samples were centrifuged at 13,000 g for 1 min, a 50-μL aliquot was removed from the supernatant, and the aliquot was diluted with 300 μL of HPLC-grade methanol. The samples were then vortexed for 30 s to re-suspend the centrifuged solids, and the tubes were returned to the isothermal sample holder. The drug concentration was determined by reversed-phase high performance liquid chromatography in 60/40 (v/v) H_2O/MeCN. Samples were analyzed on an Agilent 1260 liquid chromatograph with a multi-wavelength UV-Vis detector, 1260 MWD, at 225 nm. Separation occurred on an Agilent Poroshell 120 EC-C18 column with 120 Å pores. A calibration curve from 12.5 μg mL^{-1} to 500 μg mL^{-1} was prepared, with an R^2 value of 0.9986.

Early-Time-Point Dissolution Tests

Early-time-point dissolution tests were performed similarly to standard dissolution tests. Rather than the first instance of vortex mixing being for a 1 min, the solution was vortexed for 15, 30, or 60 seconds, and the sample was then immediately centrifuged at

13,000 g for 1 min. An aliquot was taken and the concentration of phenytoin was determined as described above.

Dynamic Light Scattering

Dynamic light scattering (DLS) measurements were conducted using a Brookhaven Instruments BI-200SM light scattering system equipped with a 637-nm laser. Samples were prepared at a concentration of 9 mg mL^{-1} polymer in phosphate buffered saline (PBS). Samples were passed through a 0.2-μm filter to remove dust, loaded into glass tubes, and placed in a temperature-controlled, index-matching bath. The temperature was held at 37 °C during measurements. Intensity autocorrelation functions (Figure S6) spanning 1 μs to 1 s were collected at five scattering angles of 60°, 75°, 90°, 105°, and 120°, with an acquisition time of 10 min per angle. For each sample, a REPES analysis was performed on the autocorrelation function from 90°. The autocorrelation functions for samples that showed a single population by REPES were fitted to a second-order cumulant model, and for samples that showed two populations by REPES were fitted to a double exponential decay model. Residuals (Figure S7) between the intensity correlation functions and the selected fits were plotted to determine the quality of the chosen fit. The mutual diffusion coefficient, D_m, was extracted from linear fits of the mean decay rate (Γ) vs q^2 (Figure S8). Mean hydrodynamic radii (R_h) were obtained via the Stokes-Einstein relationship. Dispersities for the samples fit to a second-order cumulant model are given as the average μ_2/Γ^2 value across all five angles.

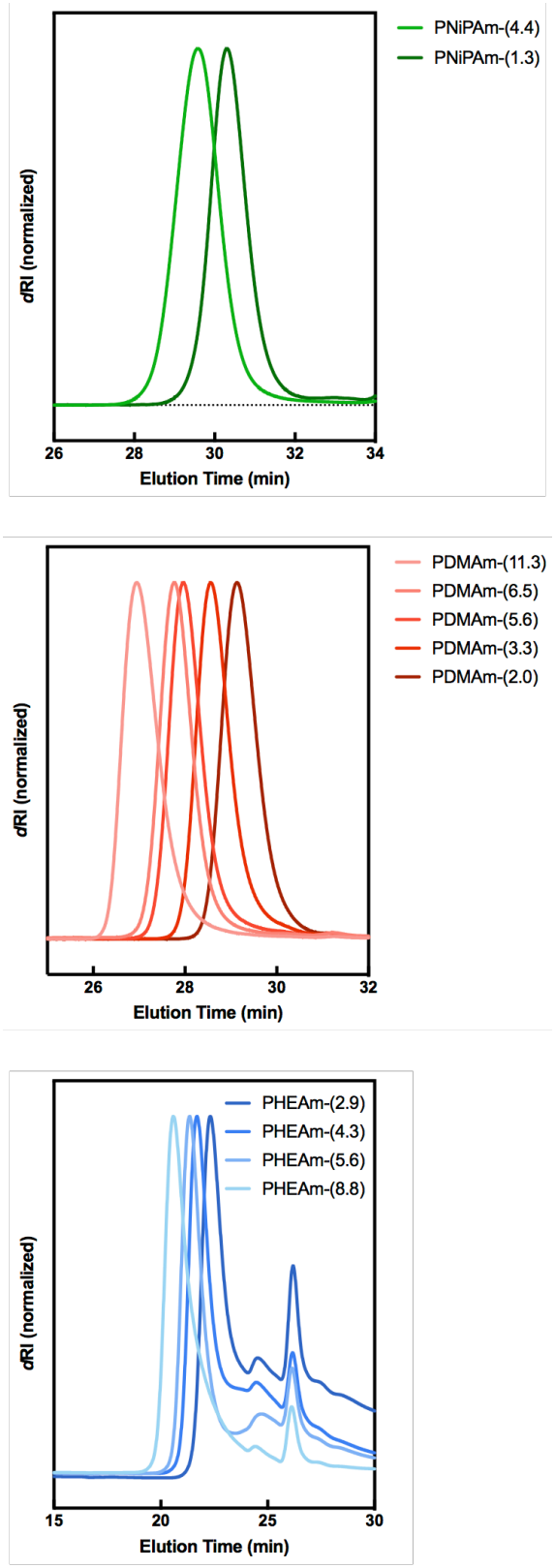

Figure S4.1. SEC traces of PNiPAm, PDMAm, and PHEAm samples.

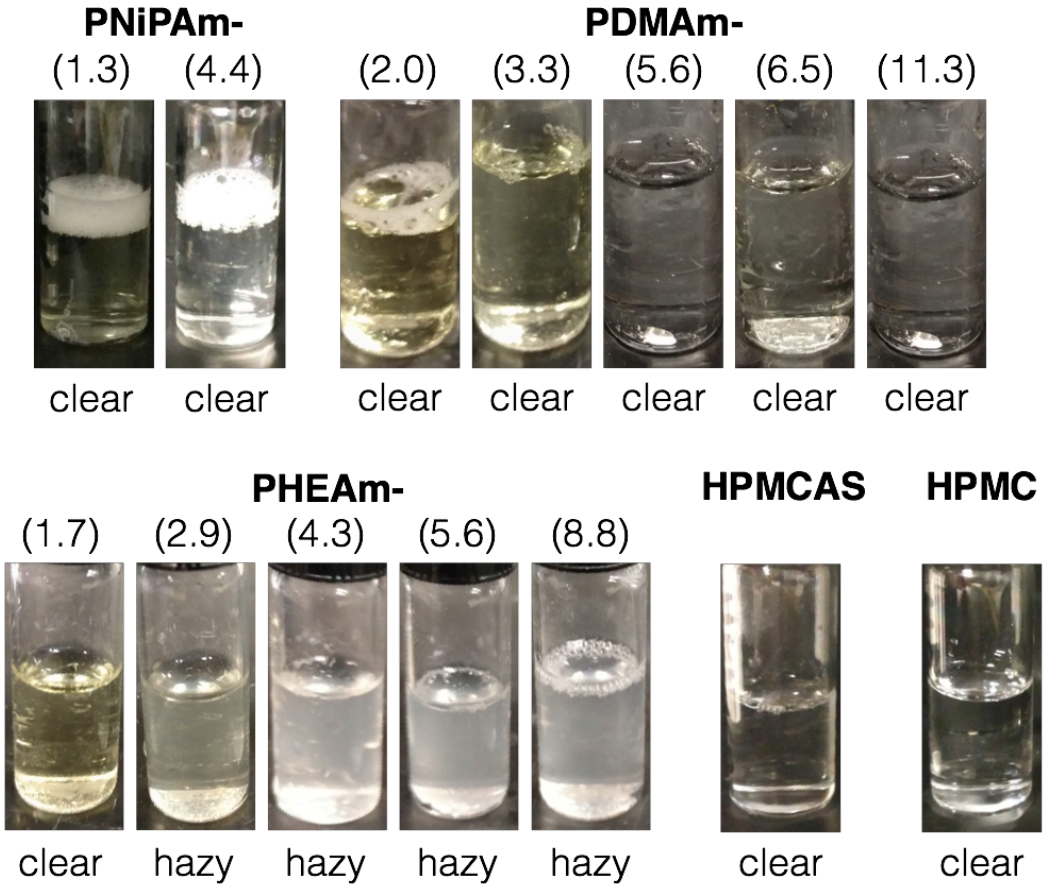

Figure S4.2. Pictures of polymer samples dissolved in PBS (pH 6.5) at 9 mg mL^{-1} and 37 °C.

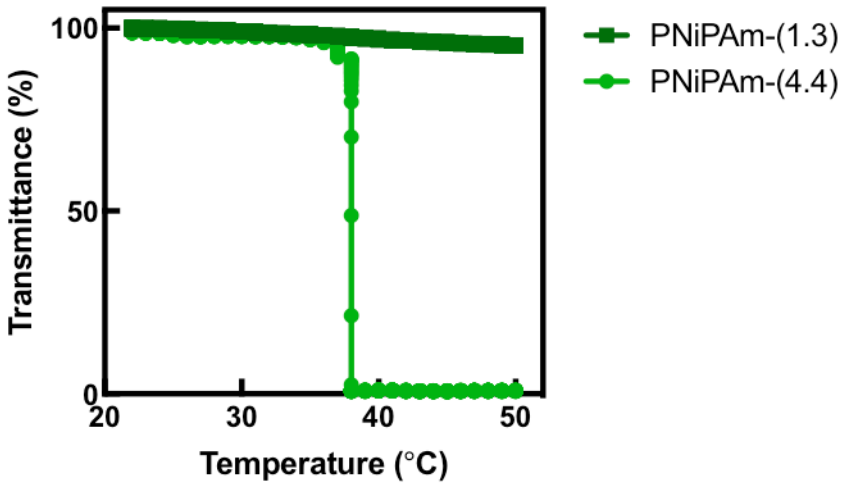

Figure S4.3. Transmittance versus temperature measurements of PNiPAm samples at 9 mg mL^{-1} in PBS (w/ SIF, pH 6.5).

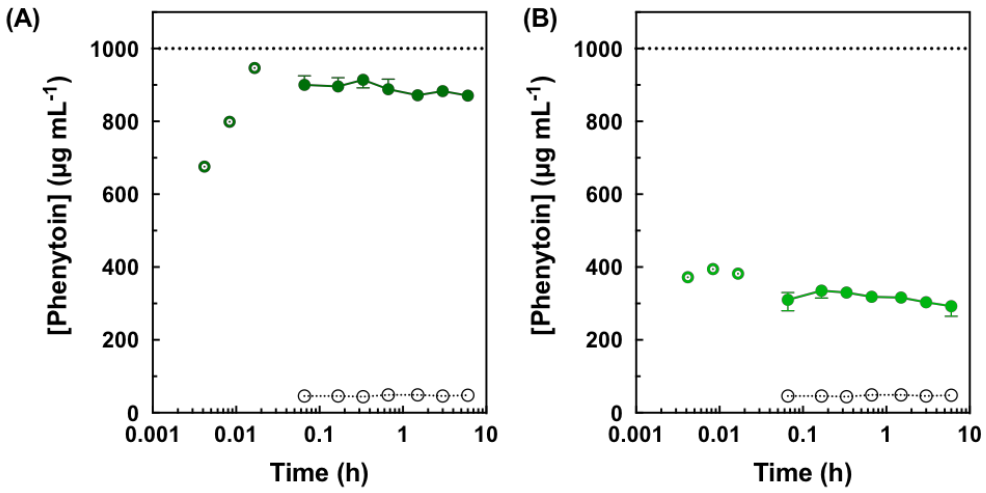

Figure S4.4. Early-time-point dissolution (open circles) and routine dissolution (filled circles) of solid dispersions of 10 wt% phenytoin and 90 wt% PNiPAm: (A) PNiPAm-(1.3), (B) PNiPAm-(4.4). All x-axes are presented in log scale to make the initial time points easier to visualize. The dissolution profile of crystalline phenytoin was also included as a reference (black open circles). The loaded concentration of phenytoin was 1,000 µg mL^{-1}. Routine dissolution curves (filled circles) were adapted with permission from reference 1. Copyright 2019 American Chemical Society.

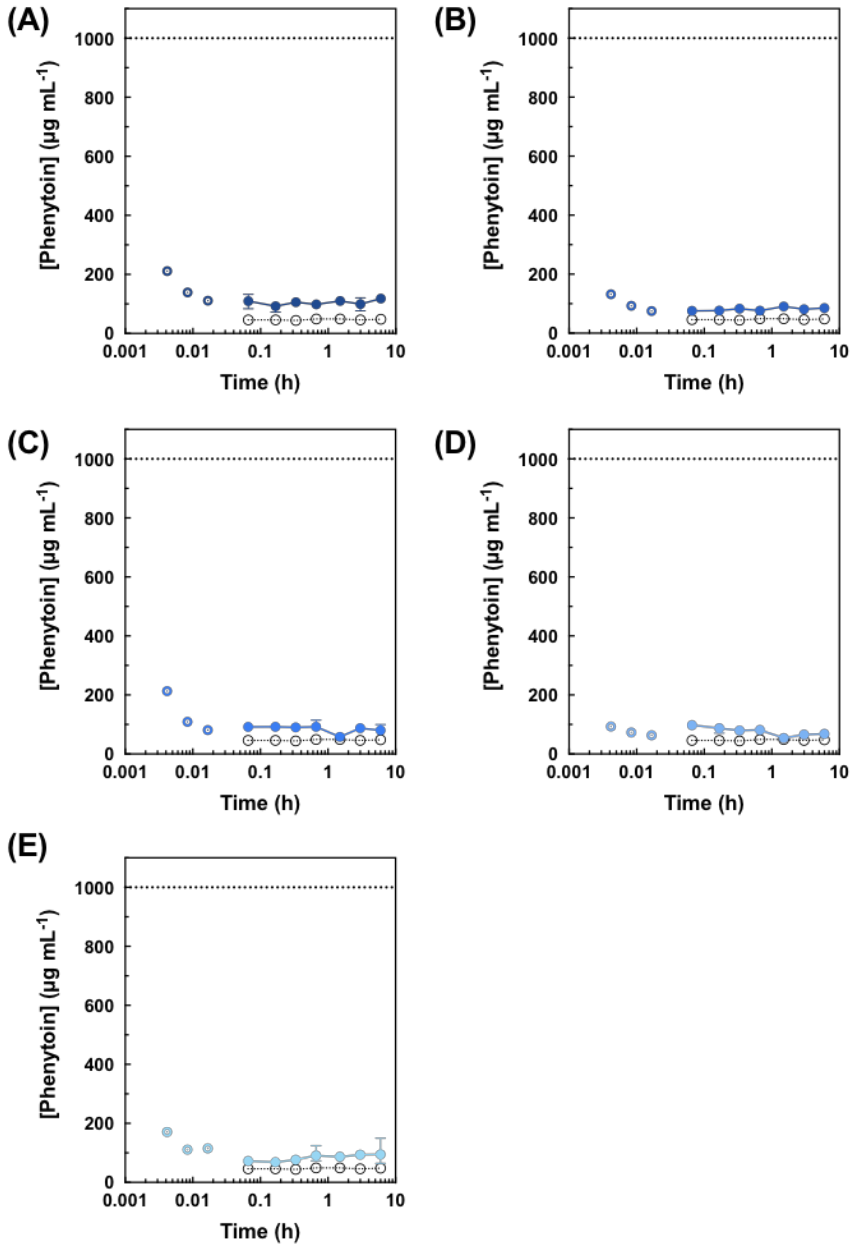

Figure S4.5. Early-time-point dissolution (open circles) of solid dispersions of 10 wt % phenytoin and 90 wt % PHEAm: (A) PHEAm-(1.7), (B) PHEAm-(2.9), (C) PHEAm-(4.3), (D) PHEAm-(5.6), (E) PHEAm-(8.8). All x-axes are presented in log scale to make the initial time points easier to visualize. In all plots, the routine dissolution profiles are included as filled in circles. The dissolution profile of crystalline phenytoin was also included as a reference. The loaded concentration of phenytoin was 1,000 µg mL^{-1} (indicated with the dashed line).

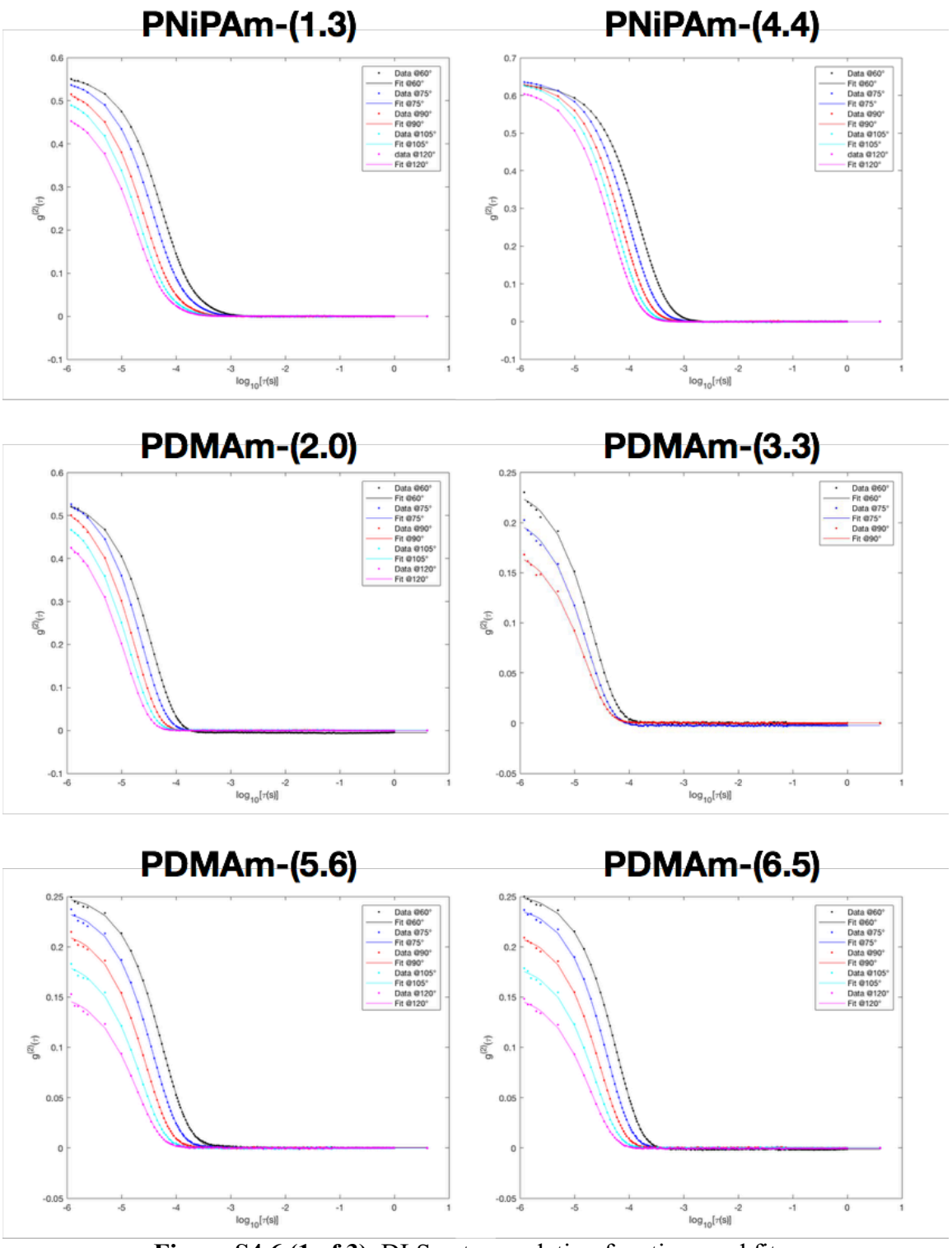

Figure S4.6 (1 of 3). DLS autocorrelation functions and fits.

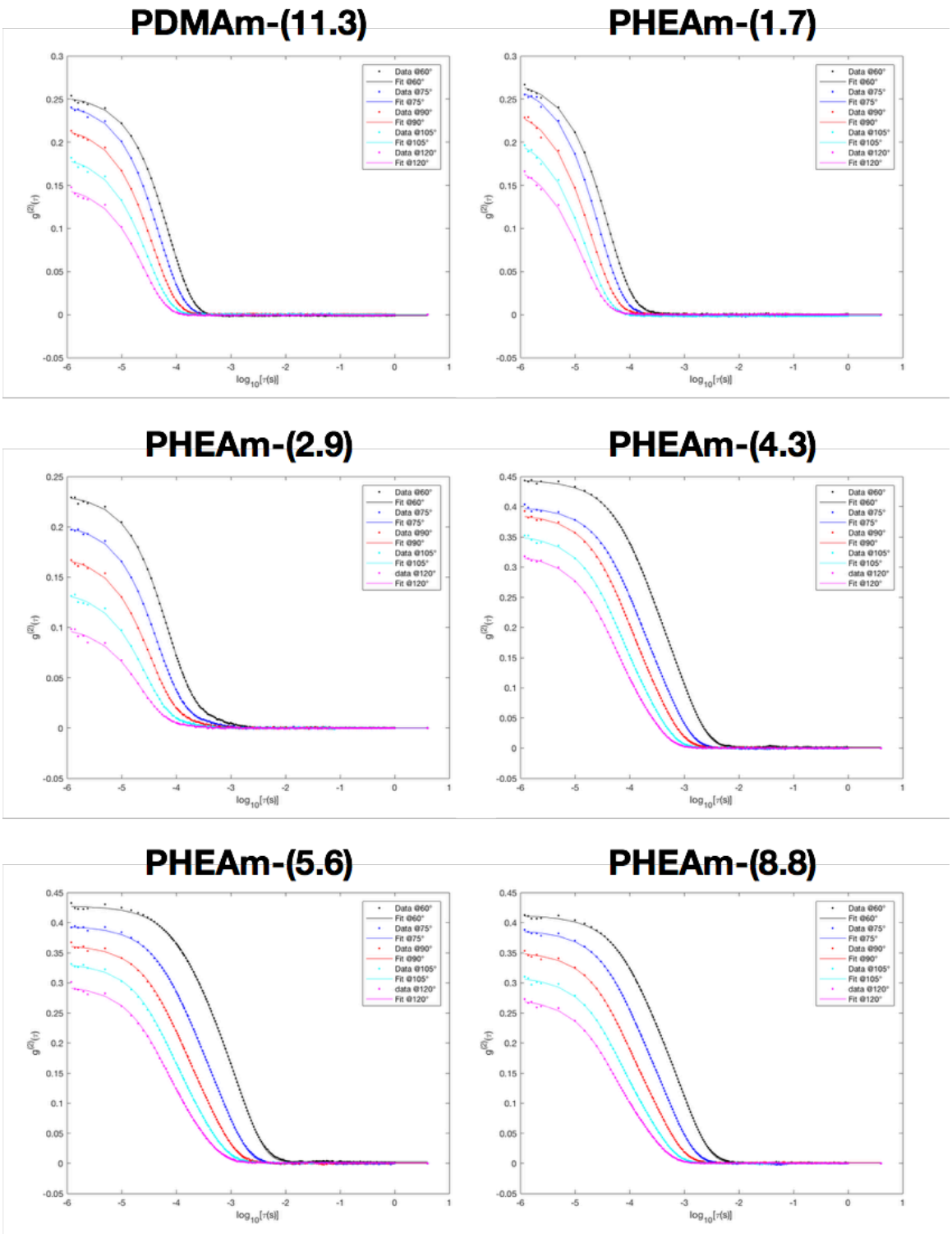

Figure S4.6 (2 of 3). DLS autocorrelation functions and fits.

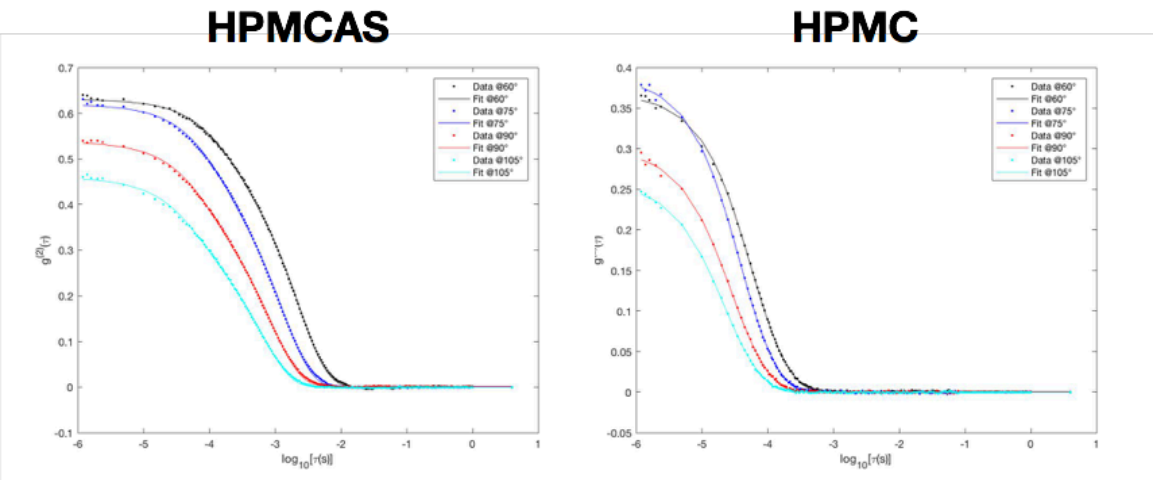

Figure S4.6 (3 of 3). DLS autocorrelation functions and fits.

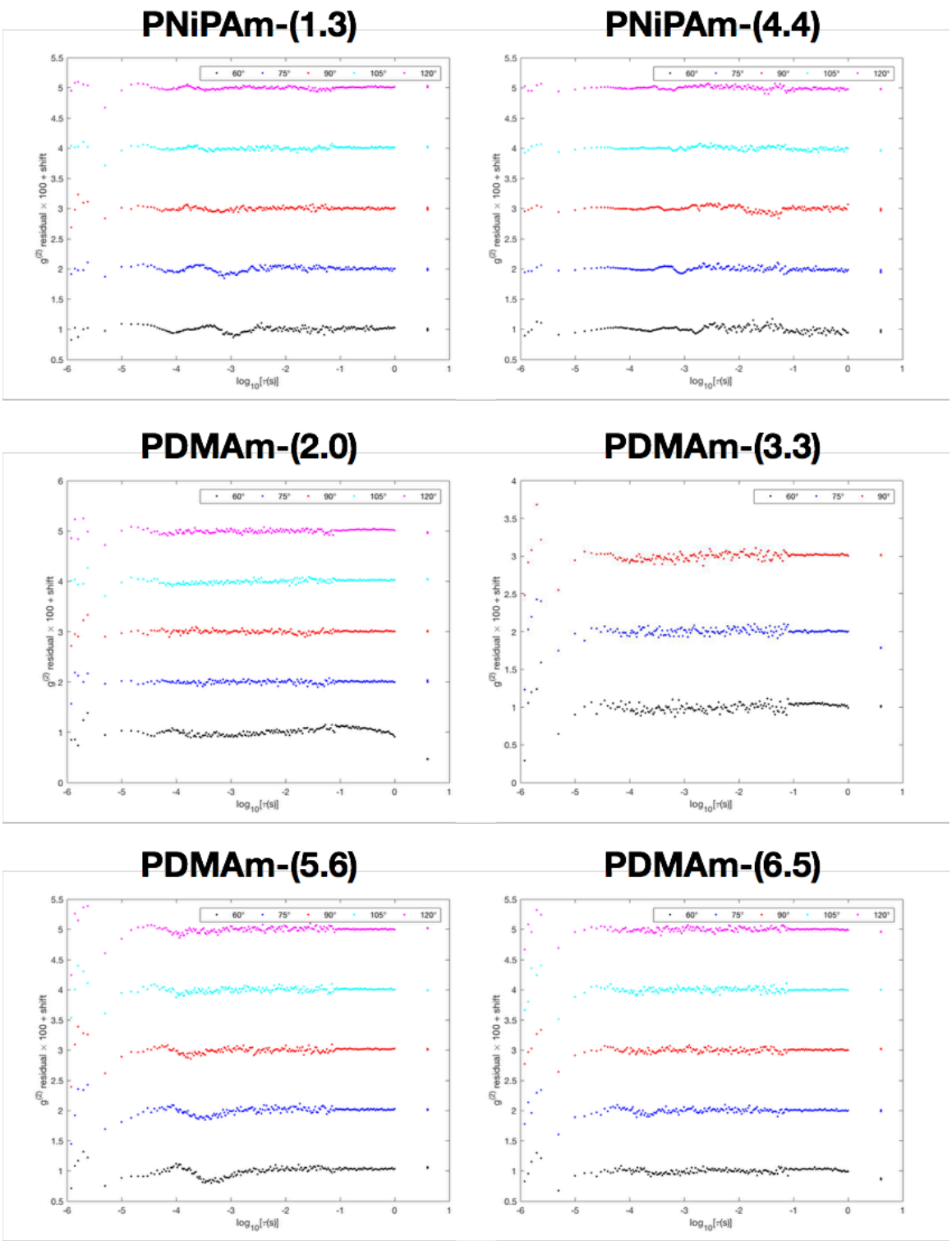

Figure S4.7 (1 of 3). DLS autocorrelation function/fit residuals.

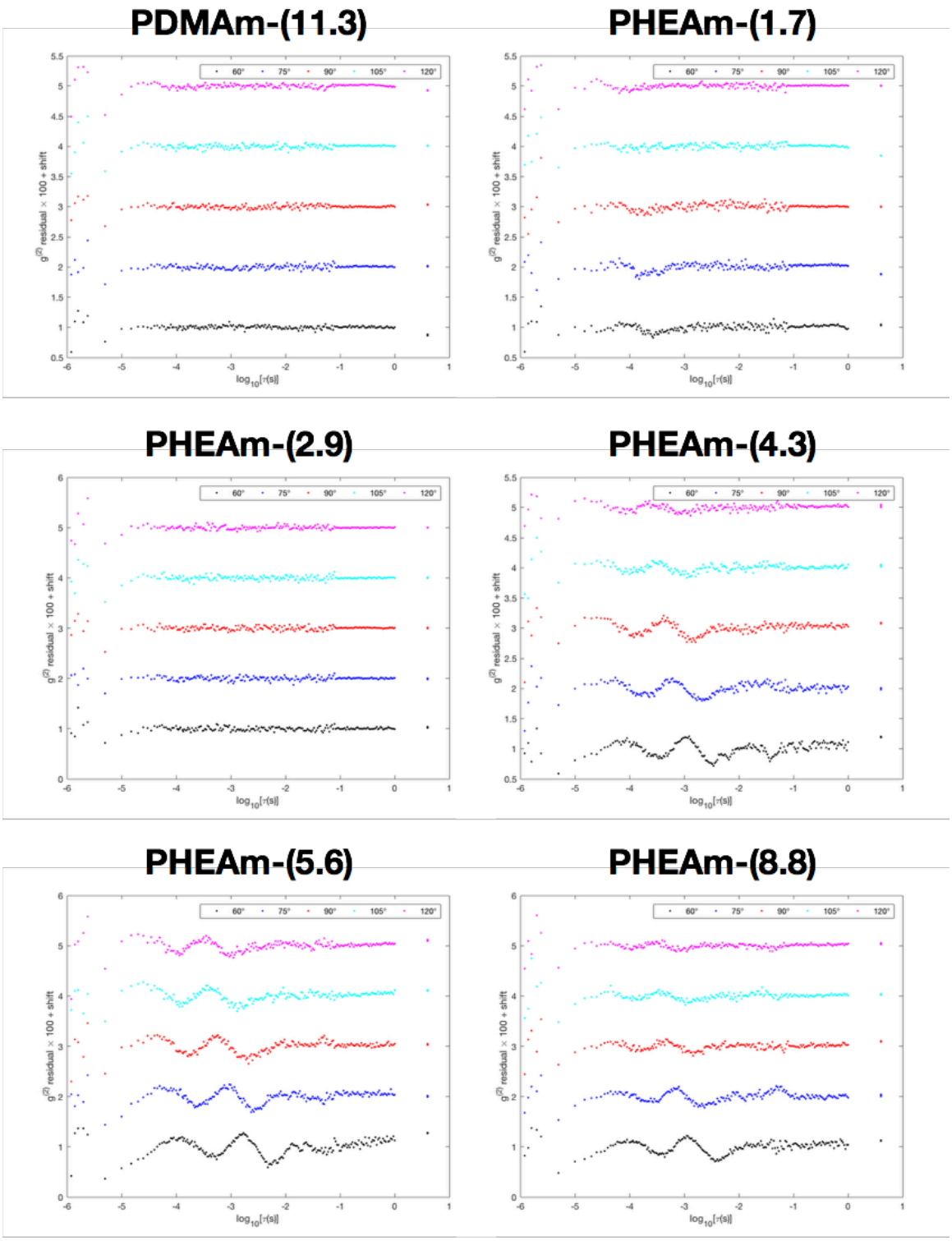

Figure S4.7 (2 of 3). DLS autocorrelation function/fit residuals.

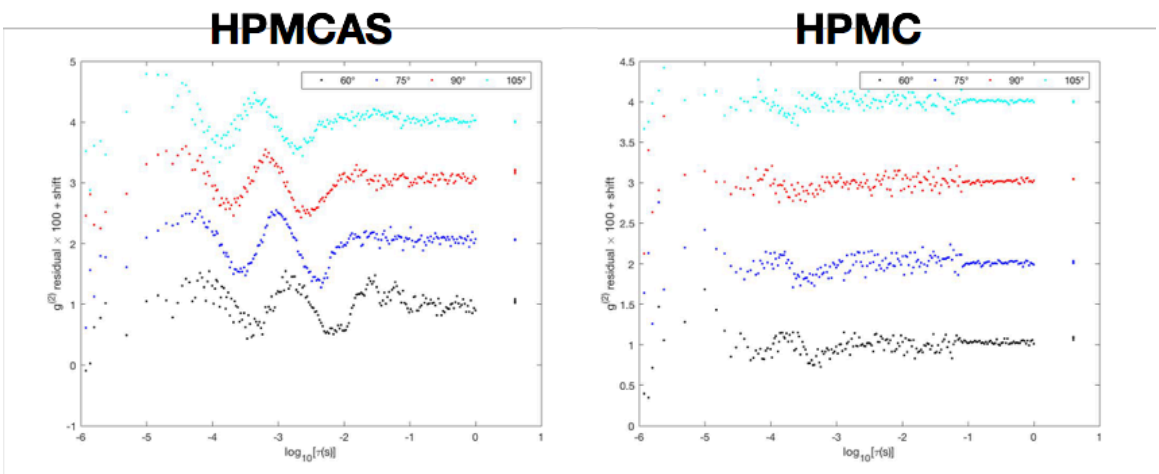

Figure S4.7 (3 of 3). DLS autocorrelation function/fit residuals.

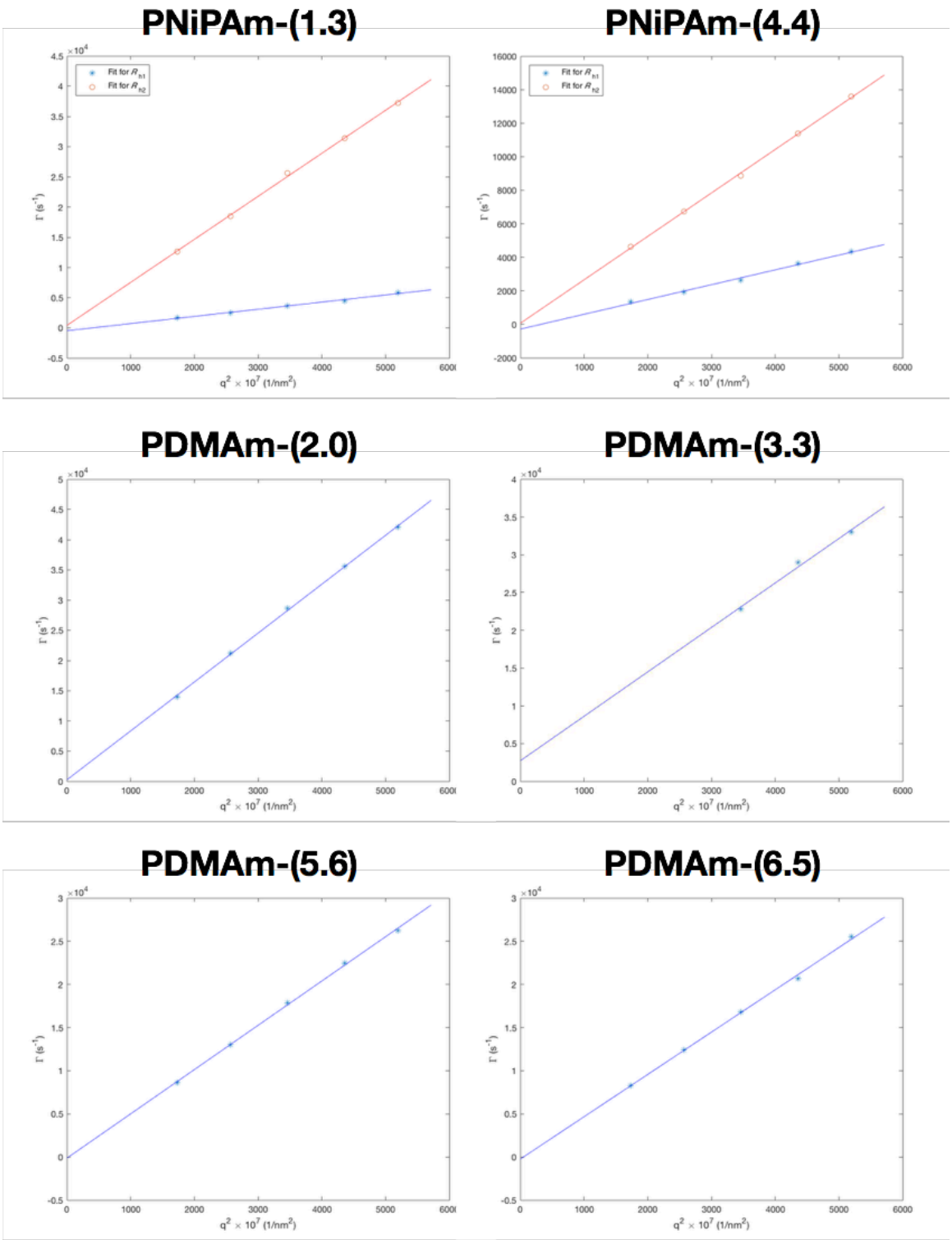

Figure S4.8 (1 of 3). Plots of Γ versus q^2 from DLS for polymer samples based on angles from 60 to 120°.

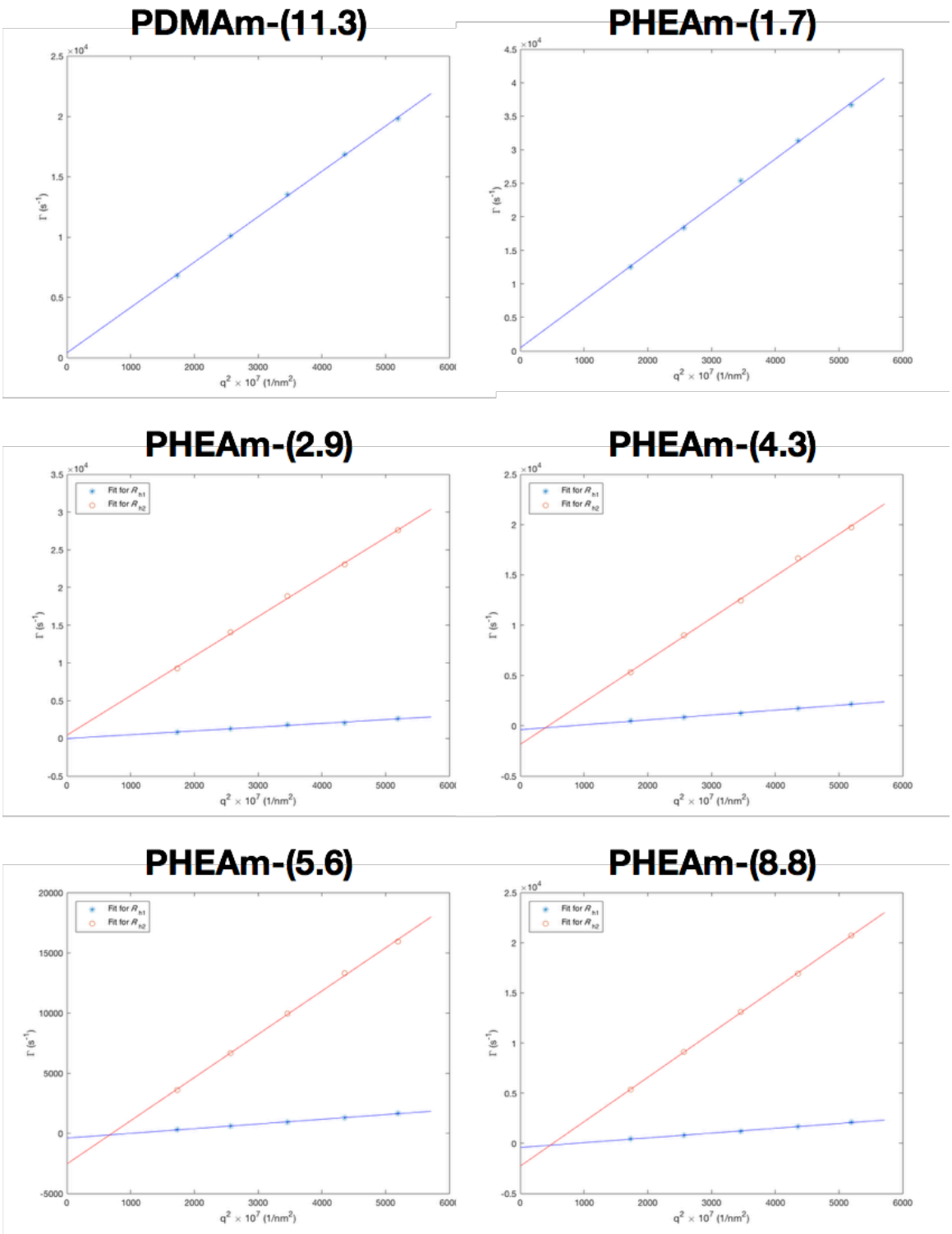

Figure S4.8 (2 of 3). Plots of Γ versus q^2 from DLS for polymer samples based on angles from 60 to 120°.

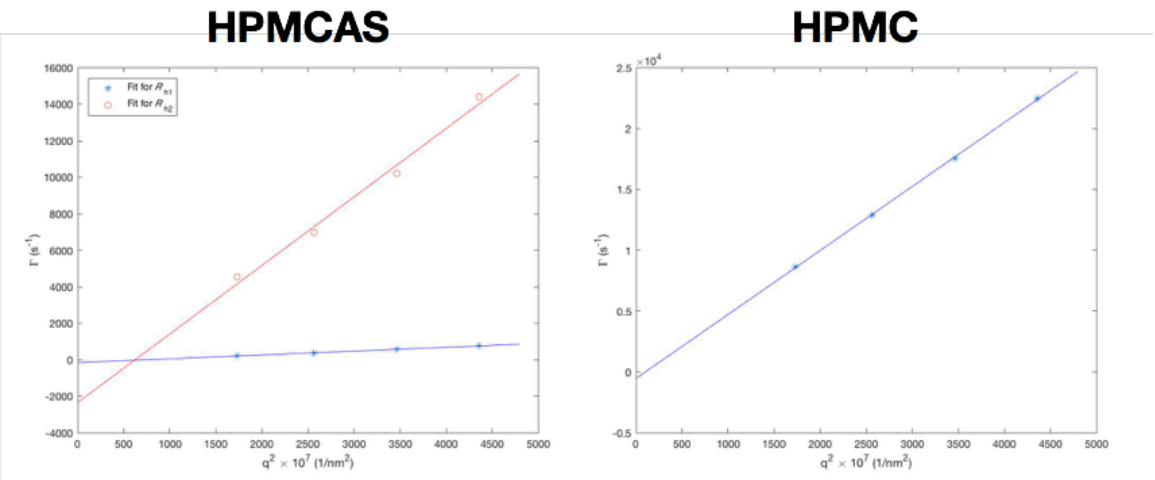

Figure S4.8 (3 of 3). Plots of Γ versus q^2 from DLS for polymer samples based on angles from 60 to 120°.

DSC is routinely used to quantify the crystallinity of solid dispersions; however, the melting temperature of phenytoin is 296 °C, which is above the degradation temperature of these polymer samples. Thus, it is not possible to directly probe crystallinity of these solid dispersions by DSC. DSC can also be used to probe the miscibility of the drug within the polymer. A single glass transition temperature (T_g) of the solid dispersion between the drug and the polymer typically indicates that the drug is molecularly dispersed within the polymer matrix. A single T_g was seen for all of the solid dispersions (Table S1).

Table S4.1. Glass transition temperatures (T_gs) of binary and ternary solid dispersions with 10 wt % phenytoin and 90 wt % excipient(s). All dispersions are denoted by their respective excipient(s).

Binary Blend Excipients		**Solid Dispersion T_g (°C)**
PNiPAm-(1.3)		78
PNiPAm-(4.4)		97
PDMAm-(2.0)		54
PDMAm-(3.3)		64
PDMAm-(5.6)		68
PDMAm-(6.5)		72
PDMAm-(11.3)		72
PHEAm-(1.7)		57
PHEAm-(2.9)		57
PHEAm-(4.3)		58
PHEAm-(5.6)		59
PHEAm-(8.8)		60
HPMCAS		95
HPMC		93
Ternary Blend Excipients	**(wt/wt)**	**Solid Dispersion T_g (°C)**
PNiPAm-(1.3)/PDMAm-(2.0)	80/20	63
	70/30	60
	60/40	61
	40/60	58
	20/80	52
PNiPAm-(1.3)/PHEAm-(1.7)	80/20	68
	70/30	70
	60/40	67
	40/60	68
	20/80	65
PNiPAm-(1.3)/HPMCAS	80/20	86
	70/30	96
	60/40	87
	40/60	95
	20/80	82
PNiPAm-(1.3)/HPMC	80/20	87
	70/30	99
	60/40	85
	40/60	88
	20/80	96

Sample Calculation for N_{agg}

Assuming a dense sphere, the aggregation number (number of chains in a micelle) can be estimated from the volume of the micelle by:

$$\frac{M_{micelle}}{\rho N_A} = \frac{4\pi}{3} R^3$$

where $M_{micelle}$ is the molar mass of the micelle, ρ is a bulk density of the polymer, and R is taken to be R_h.

Then, we relate the aggregation number (N_{agg}) to the molar mass of the micelle ($M_{micelle}$) and the molar mass of a polymer chain (M_n) through $M_n \bullet N_{agg} = M_{micelle}$, to establish:

$$\frac{M_n \bullet N_{agg}}{\rho N_A} = \frac{4\pi}{3} R_h^3$$

Using the values for the smallest populations of the lowest-molar-mass samples, and assuming a density of 1 g/cm^3, we estimate N_{agg} values as summarized in Table S2.

Table S4.2. Estimated N_{agg} values for lowest-molar-mass samples of synthetic polymers.

Polymer	**R_h of smallest population (nm)**	**Estimated N_{agg}**
PNiPAm-(1.3)	5	200
PDMAm-(2.0)	4	100
PHEAm-(1.7)	5	200

4.11 References

(1) Ku, M. S. Use of the Biopharmaceutical Classification System in Early Drug Development. *AAPS J.* **2008**, *10* (1), 208–212.

(2) Kawabata, Y.; Wada, K.; Nakatani, M.; Yamada, S.; Onoue, S. Formulation Design for Poorly Water-Soluble Drugs Based on Biopharmaceutics Classification System: Basic Approaches and Practical Applications. *Int. J. Pharm.* **2011**, *420* (1), 1–10.

(3) Thayer, A. M. (**2010**) Finding solutions *Chem. Eng. News* 88, 13– 18.

(4) Babu, N. J.; Nangia, A. Solubility Advantage of Amorphous Drugs and Pharmaceutical *Cocrystals. Cryst. Growth Des*. **2011**, *11*, 2662− 2679.

(5) Liu, H.; Taylor, L. S.; Edgar, K. J. The role of polymers in oral bioavailability enhancement; a review. *Polymer* **2015**, *77*, 399−415.

(6) Miller, J. M.; Beig, A.; Carr, R. A.; Spence, J. K.; Dahan, A. A Win–Win Solution in Oral Delivery of Lipophilic Drugs: Supersaturation via Amorphous Solid Dispersions Increases Apparent Solubility without Sacrifice of Intestinal Membrane Permeability. *Mol. Pharm.* **2012**, *9* (7), 2009–2016.

(7) Chiou, W. L.; Riegelman, S. Pharmaceutical Applications of Solid Dispersion Systems. *J. Pharm. Sci.* **1971**, *60* (9), 1281–1302.

(8) Brouwers, J.; Brewster, M. E.; Augustijns, P. Supersaturating Drug Delivery Systems: The Answer to Solubility-limited Oral Bioavailability? *J. Pharm. Sci.* **2009**, *98* (8), 2549–2572.

(9) Hancock, B. C.; Parks, M. What is the true solubility advantage for amorphous pharmaceuticals? *Pharm. Res*. **2000**, *17*, 397−404.

(10) Craig, D. Q. M. The Mechanisms of Drug Release from Solid Dispersions in Water-Soluble Polymers. *Int. J. Pharm.* **2002**, *231* (2), 131–144.

(11) Murdande, S. B.; Pikal, M. J.; Shanker, R. M.; Bogner, R. H. Solubility Advantage of Amorphous Pharmaceuticals: I. A Thermodynamic Analysis. *J. Pharm. Sci.* **2010**, *99* (3), 1254–1264.

(12) Murdande, S. B.; Pikal, M. J.; Shanker, R. M.; Bogner, R. H. Solubility advantage of amorphous pharmaceuticals: II. Application of quantitative thermodynamic relationships for prediction of solubility enhancement in structurally diverse insoluble pharmaceuticals. *Pharm. Res*. **2010**, *27*, 2704−2714.

(13) Murdande, S. B.; Pikal, M. J.; Shanker, R. M.; Bogner, R. H. Solubility advantage of amorphous pharmaceuticals, part 3: Is maximum solubility advantage experimentally attainable and sustainable? *J. Pharm. Sci.* **2011**, *100*, 4349−4356.

(14) Ting, J. M.; Porter, W. W.; Mecca, J. M.; Bates, F. S.; Reineke, T. M. Advances in Polymer Design for Enhancing Oral Drug Solubility and Delivery. *Bioconjugate Chem.* **2018**.

(15) Widanapathirana, L.; Tale, S.; Reineke, T. M. Dissolution and Solubility Enhancement of the Highly Lipophilic Drug Phenytoin via Interaction with Poly(*N*-Isopropylacrylamide-*Co*-Vinylpyrrolidone) Excipients. *Mol. Pharm.* **2015**, *12* (7), 2537–2543.

(16) Ting, J. M.; Tale, S.; Purchel, A. A.; Jones, S. D.; Widanapathirana, L.; Tolstyka, Z. P.; Li, G.; Guillaudeu, S. J.; Bates, F. S.; Reineke, T. M. High–Throughput

Excipient Discovery Enables Oral Delivery of Poorly Soluble Pharmaceuticals. *ACS Cent. Sci.*, **2016** *2* (10), 748–755.

(17) Li, Z.; Johnson, L. M.; Ricarte, R. G.; Yao, L. J.; Hillmyer, M. A.; Bates, F. S.; Lodge, T. P. Enhanced Performance of Blended Polymer Excipients in Delivering a Hydrophobic Drug through the Synergistic Action of Micelles and HPMCAS. *Langmuir* **2017**, *33* (11), 2837–2848.

(18) Johnson, L. M.; Li, Z.; LaBelle, A. J.; Bates, F. S.; Lodge, T. P.; Hillmyer, M. A. Impact of Polymer Excipient Molar Mass and End Groups on Hydrophobic Drug Solubility Enhancement. *Macromolecules* **2017**, *50* (3), 1102–1112.

(19) Li, Z.; Lenk, T. I.; Yao, L. J.; Bates, F. S.; Lodge, T. P. Maintaining Hydrophobic Drug Supersaturation in a Micelle Corona Reservoir. *Macromolecules* **2018**, *51* (2), 540–551.

(20) Zipp, G. L.; Rodriguez-Hornedo, N. Growth Mechanism and Morphology of Phenytoin and Their Relationship with Crystallographic Structure. *J. Phys. Appl. Phys.* **1993**, *26* (8B), B48.

(21) Moghadam, S.; Larson, R. G. Assessing the Efficacy of Poly(N-Isopropylacrylamide) for Drug Delivery Applications Using Molecular Dynamics Simulations. *Mol. Pharmaceutics* **2017**, *14* (2), 478–491.

(22) Wassvik, C. M.; Holmén, A. G.; Draheim, R.; Artursson, P.; Bergström, C. A. S. Molecular Characteristics for Solid-State Limited Solubility. *J. Med. Chem.* **2008**, *51* (10), 3035–3039.

(23) Mithani, S. D.; Bakatselou, V.; TenHoor, C. N.; Dressman, J. B. Estimation of the Increase in Solubility of Drugs as a Function of Bile Salt Concentration. *Pharm. Res.* **1996**, *13* (1), 163–167.

(24) Platé, N. A.; Lebedeva, T. L.; Valuev, L. I. Lower Critical Solution Temperature in Aqueous Solutions of *N*-Alkyl-Substituted Polyacrylamides. *Polymer Journal* **1999**, *31* (1), 21–27.

(25) Xia, Y.; Burke, N. A. D.; Stöver, H. D. H. End Group Effect on the Thermal Response of Narrow-Disperse Poly(N-Isopropylacrylamide) Prepared by Atom Transfer Radical Polymerization. *Macromolecules* **2006**, *39* (6), 2275–2283.

(26) Furyk, S.; Zhang, Y.; Ortiz-Acosta, D.; Cremer, P. S.; Bergbreiter, D. E. Effects of End Group Polarity and Molecular Weight on the Lower Critical Solution Temperature of poly(*N*-Isopropylacrylamide). *J. Polym. Sci. Part Polym. Chem.* **2006**, *44* (4), 1492–1501.

(27) Yin, L.; Hillmyer, M. A. Preparation and Performance of Hydroxypropyl Methylcellulose Esters of Substituted Succinates for in Vitro Supersaturation of a Crystalline Hydrophobic Drug. *Mol. Pharm.* **2014**, *11* (1), 175–185.

(28) Liu, P.; De Wulf, O.; Laru, J.; Heikkilä, T.; van Veen, B.; Kiesvaara, J.; Hirvonen, J.; Peltonen, L.; Laaksonen, T. Dissolution Studies of Poorly Soluble Drug Nanosuspensions in Non-Sink Conditions. *AAPS PharmSciTech* **2013**, *14* (2), 748–756.

(29) Palyulin, V. V.; Potemkin, I. I. Mixed versus Ordinary Micelles in the Dilute Solution of AB and BC Diblock Copolymers. *Macromolecules* **2008**, *41* (12), 4459–4463.

(30) Barnett, C. E. Some Applications of Wave-Length Turbidimetry in the Infrared. *The Journal of Physical Chemistry* **1942**, *46* (1), 69–75.

(31) Yalkowsky, S. H.; Valvani, S. C. Solubility and Partitioning I: Solubility of Nonelectrolytes in Water. *J Pharm Sci* **1980**, *69* (8), 912–922.

(32) Jain, N.; Yalkowsky, S. H. Estimation of the Aqueous Solubility I: Application to Organic Nonelectrolytes. *J. Pharm. Sci.* **2001**, *90* (2), 234–252.

(33) Edueng, K.; Mahlin, D.; Bergström, C. A. S. The Need for Restructuring the Disordered Science of Amorphous Drug Formulations. *Pharm Res* **2017**, *34* (9), 1754–1772.

(34) Bergström, C. A. S.; Wassvik, C. M.; Johansson, K.; Hubatsch, I. Poorly Soluble Marketed Drugs Display Solvation Limited Solubility. *J. Med. Chem.* **2007**, *50* (23), 5858–5862.

(35) Mao, F.; Kong, Q.; Ni, W.; Xu, X.; Ling, D.; Lu, Z.; Li, J. Melting Point Distribution Analysis of Globally Approved and Discontinued Drugs: A Research for Improving the Chance of Success of Drug Design and Discovery. *ChemistryOpen* **2016**, *5* (4), 357–368.

Bibliography

Abu-Diak, O. A.; Jones, D. S.; Andrews, G. P. *Mol. Pharm.* **2011**, *8* (4), 1362–1371.

Almeida e Sousa, L.; Reutzel-Edens, S. M.; Stephenson, G. A.; Taylor, L. S. *Mol. Pharm.* **2015**, *12*, 484–495.

Alonzo, D. E.; Gao, Y.; Zhou, D.; Mo, H.; Zhang, G. G. Z.; Taylor, L. S. *J. Pharm. Sci.* **2011**, *100*, 3316–3331.

Amidon, G. L.; Lennernäs, H.; Shah, V. P.; Crison, J. R. *Pharm. Res.* **1995**, *12*, 413–420.

Babu, N. J.; Nangia, A *Cocrystals. Cryst. Growth Des*. **2011**, *11*, 2662− 2679.

Babu, N. J.; Nangia, A. *Cryst. Growth Des.* **2011**, *11*, 2662–2679.

Baghel, S.; Cathcart, H.; O'Reilly, N. J. *Journal of Pharmaceutical Sciences* **2016**, *105* (9), 2527–2544.

Barnett, C. E. *The Journal of Physical Chemistry* **1942**, *46* (1), 69–75.

Bergström, C. A. S.; Wassvik, C. M.; Johansson, K.; Hubatsch, I. *J. Med. Chem.* **2007**, *50* (23), 5858–5862.

Bhattacharya, S.; Suryanarayanan, R. *J. Pharm. Sci.* **2009**, *98*, 2935–2953.

Brick, M.C.; Palmer, H.J.; Whitesides, T.H. *Langmuir* **2003**, *19* (16), 6367–6380.

Brouwers, J.; Brewster, M. E.; Augustijns, P. *J. Pharm. Sci.* **2009**, *98* (8), 2549–2572.

Center for Drug Evaluation, USFDA. Guidance for industry: Waiver of *In vivo* bioavailability and bioequivalence for immediate release solid oral dosage forms based on a biopharmaceutics classification system. August 2000.

Chang, C.-W.; Bays, E.; Tao, L.; Alconcel, S. N. S.; Maynard, H. D. *Chem. Commun.* **2009**, *24*, 3580–3582.

Chavda, H.; Patel, C.; Anand, I. *Systematic Reviews in Pharmacy* **2010**, *1* (1), 62–69.

Chen, H.; Pui, Y.; Liu, C.; Chen, Z.; Su, C.-C.; Hageman, M.; Hussain, M.; Haskell, R.; Stefanski, K.; Foster, K.; Gudmundsson, O.; Qian, F. *Journal of Pharmaceutical Sciences* **2017**.

Chen, R. *Int. J. Polym. Anal. Charact.* **2009**, *14*, 617–630.

Chiou, W. L.; Riegelman, S. *J. Pharm. Sci.* **1971**, *60* (9), 1281–1302.

Coan, K.E.D; Maltby, D.A.; Burlingame, A.L; Shoichet, B.K. *J. Med. Chem.* **2009**, *52* (7), 2067–2075.

Coan, K.E.D.; Shoichet, B.K. *J. Am. Chem. Soc.* **2008**, *130* (29), 9606–9612.

Committee for Medicinal Products for Human Use. Guideline on the Investigation of Bioequivalence (CPMP/EWP/QWP/1401/98 Rev. 1), July 2008.

Craig, D. Q. M. *Int. J. Pharm.* **2002**, *231* (2), 131–144.

Curatolo, W.; Nightingale, J. A.; Herbig, S. M. *Pharm. Res.* **2009**, *26* (6), 1419–1431.

Dalsin, M. C.; Tale, S.; Reineke, T. M. *Biomacromolecules* **2014**, *15* (2), 500–511.

Dengale, S. J.; Grohganz, H.; Rades, T.; Löbmann, K. *Advanced Drug Delivery Reviews* **2016**, *100* (Supplement C), 116–125.

Donovan, M. D.; Flynn, G. L.; Amidon, G. L. *Pharm. Res. 7* (8), 863–868.

Du, J.; Willcock, H.; Patterson, J. P.; Portman, I.; O'Reilly, R. K. *Small Weinh. Bergstr. Ger.* **2011**, *7* (14), 2070–2080.

Edgar, K. J.; Li, B.; Taylor, L.; Ilevbare, G.; Williams, S. M.; Liu, H. Cellulose derivatives for inhibiting crystallization of poorly water-soluble drugs. WO 2013/106433, July 18, 2013.

Edueng, K.; Mahlin, D.; Bergström, C. A. S. *Pharm Res* **2017**, *34* (9), 1754–1772.

Elkhabaz, A.; Sarkar, S.; Dinh, J. K.; Simpson, G. J.; Taylor, L. S. *Mol. Pharmaceutics* **2017**.

Fairbanks, B. D.; Gunatillake, P. A.; Meagher, L. *Adv. Drug Delivery Rev.* **2015**, *91*, 141–152.

Fedors, R. F. *Polym. Eng. Sci.* **1974**, *14*, 147–154.

Feng, B.Y.; Simeonov, A.; Jadhav, A.; Babaoglu, K.; Inglese, J.; Shoichet, B.K.; Austin, C.P. *J. Med. Chem.* **2007**, *50* (10), 2385– 2390.

Fleer, G. J.; Cohen Stuart, M. A.; Scheutjens, M. H. M.; Cosgrove, T.; Vincent, B. *Polymers at Interfaces*; 1st ed.; Chapman & Hall: London, 1993.

Fox, S. C.; Li, B.; Xu, D.; Edgar, K. J. *Biomacromolecules* **2011**, *12* (6), 1956–1972.

Frenkel, Y.V.; Clark, A.D.; Das, K.; Wang, Y-H.; Lewi, P.J.; Janssen, P.A.J.; Arnold, E. *J Med Chem.* **2005**, *48* (6), 1974–1983.

Friesen, D. T.; Shanker, R.; Crew, M.; Smithey, D. T.; Curatolo, W. J.; Nightingale, J. A. S. *Mol. Pharm.* **2008**, *5*, 1003–1019.

Furyk, S.; Zhang, Y.; Ortiz-Acosta, D.; Cremer, P. S.; Bergbreiter, D. E. *J. Polym. Sci. Part Polym. Chem.* **2006**, *44* (4), 1492–1501.

Hancock, B. C.; Parks, M. *Pharm. Res.* **2000,** *17*, (4), 397–404.

He, Y.; Ho, C. *Journal of Pharmaceutical Sciences* **2015**, *104* (10), 3237–3258.

Hiemenz, P. C.; Lodge, T. P. *Polymer Chemistry*, 2nd ed.; CRC Press: Boca Raton, FL, 2006.

Hoffman, J. D. *J. Chem. Phys.* **1958,** *29*, 1192–3.

Hsieh, Y.L.; Ilevbare, G.A.; Van Eerdenbrugh, B.; Box, K.J.; Sanchez-Felix, M.V.; Taylor, L.S. *Pharm. Res.* **29**, *2012*, 2738–2753.

Ilevbare, G. A.; Liu, H.; Edgar, K. J.; Taylor, L. S. *Cryst. Growth Des.* **2013**, *13*, 740–751.

Ilevbare, G. A.; Liu, H.; Edgar, K. J.; Taylor, L. S. *Cryst. Growth Des.* **2012**, *12* (6), 3133–3143.

Ilevbare, G. A.; Liu, H.; Edgar, K. J.; Taylor, L. S. *Mol. Pharm.* **2013**, *10* (6), 2381–2393.

Ilevbare, G. A.; Liu, H.; Pereira, J.; Edgar, K. J.; Taylor, L. S. *Mol. Pharm.* **2013**, *10*, 3392–3403.

Indulkar, A. S.; Box, K. J.; Taylor, R.; Ruiz, R.; Taylor, L. S. *Mol. Pharm.* **2015**, *12*, 2365–2377.

Jackson, M. J.; Kestur, U. S.; Hussain, M. A.; Taylor, L. S. *Mol. Pharm.* **2016**, *13*, 223–231.

Jain, N.; Yalkowsky, S. H. *J. Pharm. Sci.* **2001**, *90* (2), 234–252.

Jermain, S. V.; Brough, C.; Williams, R. O. *International Journal of Pharmaceutics* **2017**.

Johnson, L. M.; Li, Z.; LaBelle, A. J.; Bates, F. S.; Lodge, T. P.; Hillmyer, M. A. *Macromolecules* **2017**, *50* (3), 1102–1112.

Kanig, J. L. *J. Pharm. Sci.* **1964**, *53*, 188–92.

Kar, N.; Liu, H.; Edgar, K. J. *Biomacromolecules* **2011**, *12*, 1106–1115.

Kawabata, Y.; Wada, K.; Nakatani, M.; Yamada, S.; Onoue, S. *Int. J. Pharm.* **2011**, *420* (1), 1–10.

Klemm, D.; Heinze, T.; Stein, A.; Liebert, T. *Macromol. Symp.* **1995**, *99* (1), 129–140.

Ku, M. S. *AAPS J.* **2008**, *10* (1), 208–212.

Ku, M. S.; Dulin, W. *Pharm. Dev. Technol.* **2012**, *17*, 285–302.

Kubota, K.; Fujishige, S.; Ando, I. *Polym. J.* **1990**, *22* (1), 15–20.

Laitinen, R.; Löbmann, K.; Grohganz, H.; Priemel, P.; Strachan, C. J.; Rades, T. *International Journal of Pharmaceutics* **2017**, *532* (1), 1–12.

Lehmkemper, K.; Kyerematen, S. O.; Heinzerling, O.; Degenhardt, M.; Sadowski, G. *Mol. Pharmaceutics* **2017**.

Leuner, C.; Dressman, J. *Eur. J. Pharm. Biopharm.* **2000**, *50*, 47–60.

Levy, G. *Am. J. Pharm. 1835-1936* **1963**, *135*, 78–92.

Li, B.; Konecke, S.; Harich, K.; Wegiel, L.; Taylor, L. S.; Edgar, K. J. *Carbohydr. Polym.* **2013**, *92*, 2033–2040.

Li, B.; Liu, H.; Amin, M.; Wegiel, L. A.; Taylor, L. S.; Edgar, K. J. *Cellul. Dordr. Neth.* **2013**, *20*, 2137–2149.

Li, B.; Wegiel, L. A.; Taylor, L. S.; Edgar, K. J. *Cellul. Dordr. Neth.* **2013**, *20*, 1249–1260.

Li, Z.; Johnson, L. M.; Ricarte, R. G.; Yao, L. J.; Hillmyer, M. A.; Bates, F. S.; Lodge, T. P. *Langmuir* **2017**, *33* (11), 2837–2848.

Li, Z.; Lenk, T. I.; Yao, L. J.; Bates, F. S.; Lodge, T. P. *Macromolecules* **2018**, *51* (2), 540–551.

Lipinski, C. A. *J. Pharmacol. Toxicol. Methods* **2001**, *44*, 235–249.

Lipinski, C. A.; Lombardo, F.; Dominy, B. W.; Feeney, P. J. *Adv. Drug Deliv. Rev.* **2001**, *46*, 3–26.

Liu, H.; Ilevbare, G. A.; Cherniawski, B. P.; Ritchie, E. T.; Taylor, L. S.; Edgar, K. J. *Carbohydr. Polym.* **2014**, *100*, 116–125.

Liu, H.; Kar, N.; Edgar, K. J. *Cellulose* **2012**, *19*, 1279–1293.

Liu, H.; Taylor, L. S.; Edgar, K. J. *Polymer* **2015**, *77*, 399−415.

Liu, P.; De Wulf, O.; Laru, J.; Heikkilä, T.; van Veen, B.; Kiesvaara, J.; Hirvonen, J.; Peltonen, L.; Laaksonen, T. *AAPS PharmSciTech* **2013**, *14* (2), 748–756.

M. Gordon, J. S.; Taylor, *J. Appl. Chem.* **1952**, *2* (9), 493–500.

Mao, F.; Kong, Q.; Ni, W.; Xu, X.; Ling, D.; Lu, Z.; Li, J. *ChemistryOpen* **2016**, *5* (4), 357–368.

Miller, J. M.; Beig, A.; Carr, R. A.; Spence, J. K.; Dahan, A. *Mol. Pharm.* **2012**, *9* (7), 2009–2016.

Miller, J. M.; Beig, A.; Carr, R. A.; Webster, G. K.; Dahan, A. *Mol. Pharm.* **2012**, *9*, 581–590.

Miller, J. M.; Beig, A.; Krieg, B. J.; Carr, R. A.; Borchardt, T. B.; Amidon, G. E.; Amidon, G. L.; Dahan, A. *Mol. Pharm.* **2011**, *8*, 1848–1856.

Miller, J. M.; Dahan, A. *Int. J. Pharm.* **2012**, *430*, 388–91.

Mithani, S. D.; Bakatselou, V.; TenHoor, C. N.; Dressman, J. B. *Pharm. Res.* **1996**, *13* (1), 163–167.

Moad, G.; Chong, Y. K.; Postma, A.; Rizzardo, E.; Thang, S. H. *Polymer* **2005**, *46* (19), 8458–8468.

Moghadam, S.; Larson, R. G. *Mol. Pharmaceutics* **2017**, *14* (2), 478–491.

Mosquera-Giraldo, L. I.; Taylor, L. S. *Mol. Pharm.* **2015**, *12*, 496–503.

Mugheirbi, N. A.; Marsac, P. J.; Taylor, L. S. *Mol. Pharmaceutics* **2017**.

Multisource (generic) pharmaceutical products: Guidelines on registration requirements to establish interchangeability. In: WHO Expert Committee on Specifications for Pharmaceutical Preparations, Fortieth Report. Geneva, World Health Organization. WHO Technical Report Series, No. 937, Annex 7: 2000. p. 347-390.

Murdande, S. B.; Pikal, M. J.; Shanker, R. M.; Bogner, R. H. *J. Pharm. Sci.* **2010**, *99* (3), 1254–1264.

Murdande, S. B.; Pikal, M. J.; Shanker, R. M.; Bogner, R. H. *J. Pharm. Sci.* **2011**, *100*, 4349−4356.

Murdande, S. B.; Pikal, M. J.; Shanker, R. M.; Bogner, R. H. *Pharm. Res*. **2010**, *27*, 2704−2714.

Nakayama, M.; Okano, T. *Biomacromolecules* **2005**, *6* (4), 2320–2327.

Narasimhan, B.; Peppas, N. A. *J. Pharm. Sci.* **1997**, *86*, 297–304.

Neslihan Gursoy, R.; Benita, S. *Biomed. Pharmacother.* **2004**, *58* (3), 173–182.

Otsuka, N.; Ueda, K.; Ohyagi, N.; Shimizu, K.; Katakawa, K.; Kumamoto, T.; Higashi, K.; Yamamoto, K.; Moribe, K. *J. Pharm. Sci.* **2015**, *104* (8), 2574–2582.

Pacheco, L.F.; Carmona-Ribeiro, A.M. *J. Colloid Interface Sci.* **2003**, *258* (1), 146–154.

Padden, B. E.; Miller, J. M.; Robbins, T.; Zocharski, P. D.; Prasad, L.; Spence, J. K.; LaFountaine, J. Amorphous Solid Dispersions as Enabling Formulations for Discovery and Early Development http://www.americanpharmaceuticalreview.com.

Palyulin, V. V.; Potemkin, I. I. *Macromolecules* **2008**, *41* (12), 4459–4463.

Philipp, B.; Klemm, D.; Stein, A. *Papier (Darmstadt)* **1995**, *49*, 102–103, 106–108.

Philipp, B.; Klemm, D.; Wagenknecht, W. *Papier (Darmstadt)* **1995**, *49*, 58–64.

Philipp, B.; Wagenknecht, W.; Wagenknecht, M.; Nehis, I.; Klemm, D.; Stein, A.; Heinze, T.; Heinze, U.; Helbig, K.; et, al. *Papier (Darmstadt)* **1995**, *49*, 3–7.

Pissuwan, D.; Boyer, C.; Gunasekaran, K.; Davis, T. P.; Bulmus, V. *Biomacromolecules* **2010**, *11* (2), 412–420.

Platé, N. A.; Lebedeva, T. L.; Valuev, L. I. *Polymer Journal* **1999**, *31* (1), 21–27.

Prudic, A.; Lesanik, A.; Ji, Y.; Sadowski, G. *Eur J Pharm Biopharm.* **2015**, *93*, 88–94.

Purohit, H. S.; Taylor, L. S. *Pharm Res* **2017**, 1–20.

Raina, S. A.; Zhang, G. G. Z.; Alonzo, D. E.; Wu, J.; Zhu, D.; Catron, N. D.; Gao, Y.; Taylor, L. S. *Journal of Pharmaceutical Sciences* **2014**, *103* (9), 2736–2748.

Raina, S.; Alonzo, D.; Zhang, G.Z.; Gao, Y.; Taylor, L. *Pharm. Res.* **2015**, *32,* 3660-3673.

Ricarte, R. G.; Li, Z.; Johnson, L. M.; Ting, J. M.; Reineke, T. M.; Bates, F. S.; Hillmyer, M. A.; Lodge, T. P. *Macromolecules* **2017**, *50* (8), 3143–3152.

Ricarte, R. G.; Lodge, T. P.; Hillmyer, M. A. *Langmuir* **2016**, *32* (29), 7411–7419.

Ricarte, R. G.; Lodge, T. P.; Hillmyer, M. A. *Mol. Pharm.* **2015**, *12* (3), 983–990.

Seidler, J.; McGovern, S.L.; Doman, T.N.; Shoichet, B.K. *J. Med. Chem.* **2003**, *46* (21), 4477–4486.

Sekiguchi, K.; Obi, N. *Chem. Pharm. Bull. (Tokyo)* **1961**, *9*, 866–872.

Simonelli, A. P.; Mehta, S. C.; Higuchi, W. I. *J. Pharm. Sci.* **1969**, *58*, 538–549.

Song, Y.; Yang, X.; Chen ,X.; Nie, H.; Byrn, S.; Lubach, J. *Mol Pharm.* **2015**, *12*, 857–866.

Sun, D. D.; Lee, P. I. *Journal of Controlled Release* **2015**, *211* (Supplement C), 85–93.

Tajarobi, F.; Larsson, A.; Matic, H.; Abrahmsén-Alami, S. *Eur. J. Pharm. Biopharm.* **2011**, *78* (1), 125–133.

Taylor, L. S.; Zhang, G. G. Z. *Adv. Drug Deliv. Rev.* **2016,** *101*, 122–142.

Thayer, A. M. (**2010**) *Chem. Eng. News* 88, 13– 18.

Tian, B.; Wang, X.; Zhang, Y.; Zhang, K.; Zhang, Y.; Tang, X. *Pharm Res*. **2015**, *32*, 840–851.

Ting, J. M.; Porter, W. W.; Mecca, J. M.; Bates, F. S.; Reineke, T. M. *Bioconjugate Chem.* **2018**.

Ting, J. M.; Tale, S.; Purchel, A. A.; Jones, S. D.; Widanapathirana, L.; Tolstyka, Z. P.; Li, G.; Guillaudeu, S. J.; Bates, F. S.; Reineke, T. M. *ACS Cent. Sci.*, **2016** *2* (10), 748–755.

Ting, J. M.; Tale, S.; Purchel, A. A.; Jones, S. D.; Widanapathirana, L.; Tolstyka, Z. P.; Li, G.; Guillaudeu, S. J.; Bates, F. S.; Reineke, T. M. *ACS Cent. Sci.*, **2016** *2* (10), 748–755.

Using Dow Excipients for Controlled Release of Drugs in Hydrophilic Matrix Systems **2006**.

Vasconcelos, T.; Sarmento, B.; Costa, P. *Drug Discov. Today* **2007**, *12*, 1068–1075.

Waldmann, S.; Almukainzi, M.; Bou-Chacra, N. A.; Amidon, G. L.; Lee, B.-J.; Feng, J.; Kanfer, I.; Zuo, J. Z.; Wei, H.; Bolger, M. B.; Löbenberg, R. *Mol. Pharm.* **2012**, *9*, 815–822.

Warren, D. B.; Benameur, H.; Porter, C. J. H.; Pouton, C. W. *J. Drug Target.* **2010**, *18* (10), 704–731.

Warren, D. B.; Bergström, C. A. S.; Benameur, H.; Porter, C. J. H.; Pouton, C. W. *Mol. Pharm.* **2013**, *10* (8), 2823–2848.

Wassvik, C. M.; Holmén, A. G.; Draheim, R.; Artursson, P.; Bergström, C. A. S. *J. Med. Chem.* **2008**, *51* (10), 3035–3039.

Widanapathirana, L.; Tale, S.; Reineke, T. M. *Mol. Pharm.* **2015**, *12* (7), 2537–2543.

Xia, Y.; Burke, N. A. D.; Stöver, H. D. H. *Macromolecules* **2006**, *39* (6), 2275–2283.

Yakou, S.; Umehara, K.; Sonobe, T.; Nagai, T.; Sugihara, M.; Fukuyama, Y. *Chem. Pharm. Bull. (Tokyo)* **1984**, *32* (10), 4130–4136.

Yalkowsky, S. H.; Valvani, S. C. *J Pharm Sci* **1980**, *69* (8), 912–922.

Yin, L.; Hillmyer, M. A. *Mol. Pharm.* **2014**, *11* (1), 175–185.

Zhou, C.; Hillmyer, M. A.; Lodge, T. P. *Macromolecules* **2011**, *44*, 1635–1641.

Zienty, F. B.; Vineyard, B. D.; Schleppnik, A. A. *J. Org. Chem.* **1962**, *27*, 3140–3146.

Zipp, G. L.; Rodriguez-Hornedo, N. *J. Phys. Appl. Phys.* **1993**, *26*, B48.

Appendix 1: Graft Polymers and Blends of Hydroxypropyl Methylcellulose for the Dissolution Enhancement of Phenytoin

A1.1 Introduction

Hydroxypropyl methylcellulose (HPMC) graft polymers were approached as a strategy to combine two platforms: cellulosic ethers and poly(*N*-isopropyl acrylamide)-based polymers. Previous studies showed that HPMC could be modified with hydrophobic succinic anhydride derivatives to yield HPMC esters that, as solid dispersion excipients, enhanced the dissolution performance of phenytoin in aqueous buffer.[1] Other studies showed *N*-isopropylacrylamide (NiPAm)-based copolymers[2] and blends[3] to be effective solid dispersion excipients for the dissolution and supersaturation enhancement of

phenytoin. The targeted synthesis of HPMC-*graft*-poly(NiPAm) (HPMC-*g*-PNiPAm) polymers was a way to combine these two platforms while conceivably maintaining the individual benefits of each component. These graft polymers were evaluated as solid dispersion excipients for phenytoin, and blends at the respective equivalent compositions were also evaluated. Serendipitous results that showed great performance of low molar mass PNiPAm homopolymer were later pursued, as described in Chapter 3.

A1.2 Cellulosic Graft Polymers

Graft polymers can be generated via approaches ranging from grafting 'from', 'to', or 'through'. Each of these strategies have independent pro and con considerations on synthetic and characterization feasibility. Cellulosics are characteristically known by their repeating anhydroglucose backbone, so the possibility for grafting 'through' is null. However, many examples of both grafting 'from' and 'to' cellulosic polymers have been well-documented. [4] For example, Das et al generated pH-responsive HPMC-*g*-poly(acrylamide) polymers via microwave irradiation, where radical formation on the HPMC backbone was initiated by potassium persulphate.[5] Kim et al. grafted NiPAm onto ethylcellulose through the use of ammonium persulphate for the use of spray drying with an xanthine oxidase inhibitor, allopurinol.[6] Other more complicated structures have also been accessed via grafting from. For example, Hufendiek et al. functionalized cellulose to incorporate trithiocarbonate moieties that were in turn used to polymerize NiPAm and *N*,*N*-dimethylacrylamide via a controlled reversible addition chain transfer polymerization mechanism.[7] Grafting 'to' approaches using cellulosic backbones are also documented. For example, Bokias et al. made carboxymethylcellulose (CMC)-*g*-PNiPAm through carbodiimide coupling of amine-terminated PNiPAm with the pendant carboxylic acids off

the CMC backbone.[8] In this study, we chose to use a similar carbodiimide coupling approach, where the inherited chain transfer agent acid functionality of RAFT-synthesized PNiPAm would react with the primary and secondary alcohols of HPMC (Scheme 1).

Scheme A1.1. Synthetic approach towards hydroxypropyl methycellulose-*g*-poly(*N*-isopropyl acrylamide) (HPMC-g-PNiPAm) through 4-dimethylaminopyridine (DMAP)-catalyzed carbodiimide coupling of HPMC and PNiPAm with *N*,*N'*-diisopropylacrylamide (DIC). Attachment of the PNiPAm side chain would be without regioselective control, and is shown at the C6 position only as a random representative.

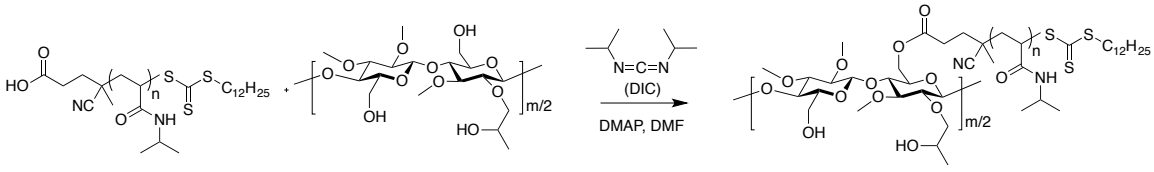

A1.3 Synthesis of Hydroxypropyl Methylcellulose-*graft*-Poly(*N*-isopropyl acrylamide)s

Hydroxypropyl methylcellulose from the METHOCEL™ E3 (The Dow Chemical Company) was used as received. Characterized by light-scattering SEC, this starting HPMC was dissolved in a mobile phase of 0.1 M Na_2SO_4 with 1% acetic acid, with M_n = 11.8 kg mol^{-1}, M_w = 15.7 kg mol^{-1}, $Đ$ = 1.33. On average, per anhydroglucose unit, this material possessed a degree of methyl ether substitution of 1.91, a hydroxypropyl ether substitution of 0.25, and a free hydroxyl substitution of 1.09. At this molar mass and substitution pattern, there are, on average, 74 substituted anhydroglucose units per chain.

Poly(*N*-isopropyl acrylamide) (PNiPAm) was synthesized as described in Chapter 3. Characterized by light-scattering SEC in THF, the PNiPAm used for this study had M_n = 2.3 kg mol^{-1}, M_w = 2.4 kg mol^{-1}, $Đ$ = 1.04. Based on the chain transfer agent (CTA) used

during the polymerization of this low-molar-mass PNiPAm sample, the inherited acid functionality provided an easy handle for carbodiimide coupling.

A series of HPMC-*g*-PNiPAm samples were synthesized via 4-dimethylaminopyridine (DMAP)-catalyzed carbodiimide coupling chemistry with the use of *N*,*N'*-diisopropylacrylamide (DIC) in dimethylformamide (DMF). Different conditions were evaluated to maximize coupling efficiency between the HPMC hydroxyls and the PNiPAm carboxylic acid (Table A1.1).

Table A1.1. HPMC-*g*-PNiPAm reaction conditions and final PNiPAm incorporation.

Entry	PNiPAm loaded (g)	HPMC loaded (g)	Time (h)	Temp (°C)	DIC : PNiPAm-COOH[a]	DIC : DMAP[b]	wt% PNi-PAm loaded[c]	wt% PNi-PAm by NMR[d]
1	0.4	0.2	72	65	2:1	2:0.2	67	1.4
2	0.4	0.2	72	65	30:1	2:0.2	67	5.8
3	0.4	0.2	72	25	10:1	2:0.2	67	7.7
4	0.4	0.2	72	25	60:1	2:0.2	67	16
5	0.4	0.2	72	65	10:1	2:0.4	67	3.5
6	0.4	0.2	48	65	10:1	2:0.2	67	2.4
7	0.2	1.8	72	25	100:1	2:0.4	10	1.0
8	0.8	1.2	72	25	100:1	2:0.4	40	1.7
9	1.4	0.6	72	25	100:1	2:0.4	70	10
10	2.0	1.0	72	25	60:1	2:0.2	67	25

[a]mol ratio of loaded DIC to PNiPAm terminal carboxylic acid.

[b]mol ratio loaded DIC to DMAP.

[c]wt% of PNiPAm loaded relative to HPMC, assuming complete incorporation of PNiPAm in the final product.

[d]wt% of PNiPAm loaded relative to HPMC in the final product as determined by ^{1}H NMR spectroscopy, after crude product was purified by precipitation from DMF in diethyl ether (2X), d1 = 20 sec, 500 MHz instrument, 64 scans.

^{1}H NMR spectroscopy was used to quantitatively evaluate PNiPAm incorporation, where the triplet of the terminal methyl on the $C_{12}H_{25}$ alkyl tail (0.84 – 0.88 ppm) was integrated and compared to backbone HPMC protons, as well as an internal standard. Using mesitylene as an internal standard, linear relationships were established between the amount of PNiPAm loaded, both as simple PNiPAm homopolymers (Figure A1.1a) and as a blend with HPMC (Figure A1.1b), and the amount of PNiPAm detected by ^{1}H NMR. The linear relationships (Figure A1.1) with a slope near 1 (and $R^2 \approx 1$) between the amount of loaded PNiPAm and the amount of PNiPAm detected by NMR confirms this as a valid characterization tool.

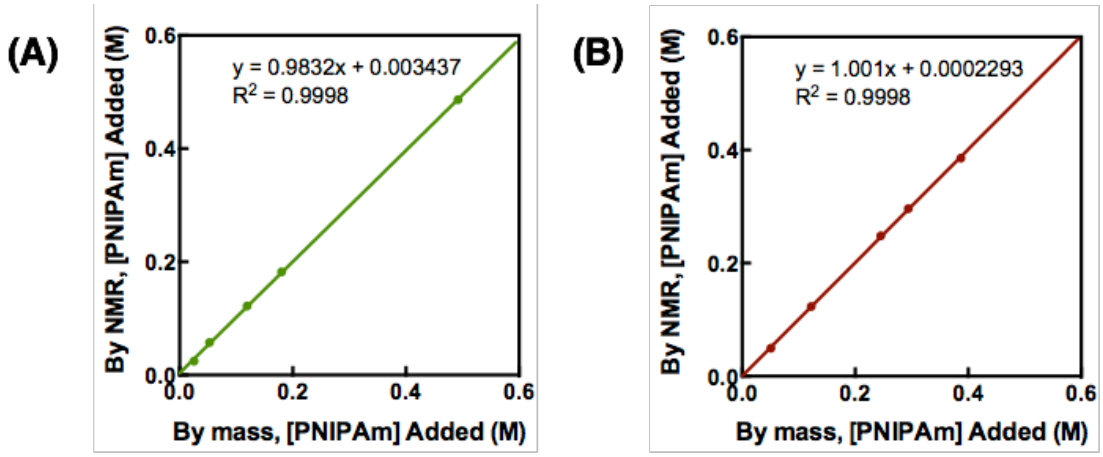

Figure A1.1. Comparison of PNiPAm added to an NMR sample and the amount of PNiPAm detected, when using an internal standard of mesitylene. The validity of this characterization method was established both when observing (A) PNiPAm homopolymer and (B) PNiPAm in a blend with HPMC.

A separation strategy was developed to ensure full removal of free, uncoupled PNiPAm homopolymer. From DMF, PNiPAm was removed from HPMC-*g*-PNiPAm by two precipitations from DMF into diethyl ether. To validate this separation strategy, a 50/50 wt/wt blend of HPMC and PNiPAm was dissolved in DMF and precipitated twice

into diethyl ether (Figure A1.2). No residual PNiPAm hompolymer was observed in the HPMC after two precipitations.

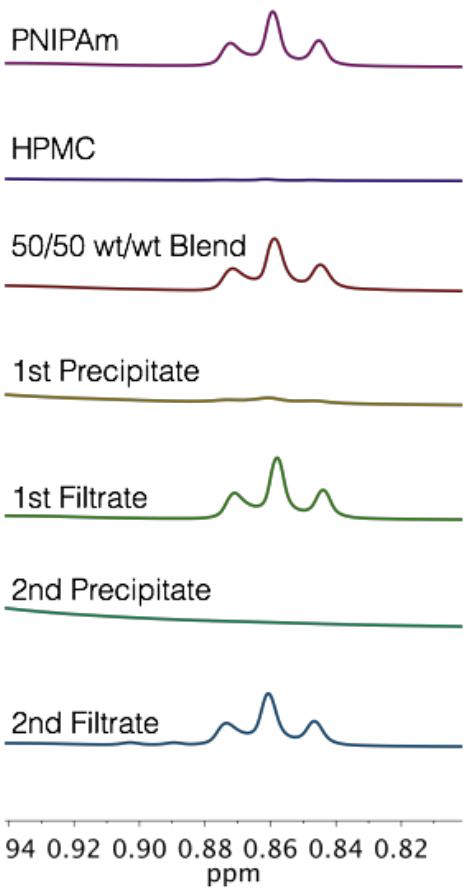

Figure A1.2. Verification of the utilized precipitation purification strategy as a way to quantitatively remove unincorporated PNiPAm from starting HPMC. All spectra were normalized to an HPMC backbone peak. After two precipitations, complete removal of PNiPAm is evident by the disappearance of the terminal CTA methyl at 0.86 ppm (triplet).

HPMC-*g*-PNiPAm (entry 10) was isolated (83% yield) and purified as described above. As the sample with the highest incorporation of PNiPAm, at a grafting efficiency of 38%, this sample possessed a final 25 wt% PNiPAm and 75 wt% HPMC. This final

product represented an average of four PNiPAm grafts per HPMC backbone chain, with one graft per every 19 anhydroglucose units.

A1.4 Spray-Dried Dispersions with Phenytoin

Spray dried dispersions loaded with 10 wt% phenytoin were fabricated at standard conditions (see Chapter 2). Excipients in this study included HPMC-*g*-PNiPAm (entry 10), HPMC as a control, PNiPAm as a control, and HPMC/PNiPAm wt/wt blends as a control comparison to probe the affect of the graft tethering. Dissolution studies were conducted under conditions previously described (PBS, pH 6.5, 37 °C, [phenytoin] target of 1,000 μg mL^{-1}) (Figure A1.3). In comparison to the control of HPMC and PNiPAm, the dissolution profile of the 75/25 wt/wt HPMC/PNiPAm blend showed an averaging behavior, where as the 75/25 wt/wt HPMC-*g*-PNiPAm graft polymer (entry 10) showed a limited release profile. Although the HPMC-*g*-PNiPAm excipient did not perform significantly better than the control HPMC, it is worth noting the difference in profile shape between the two. It is hypothesized that the functionalization of the free hydroxyls on HPMC with the $C_{12}H_{25}$-terminated PNiPAm significantly impacts overall excipient solubility. Thus, the dissolution profile no longer hints at a burst release with rapid crystallization, but rather a limited release, likely as a function of lower excipient solubility. Of remarkable note, the low-molar-mass PNiPAm sample produced a dissolution profile of near-full release with no observed crystallization over the 6 h time period.

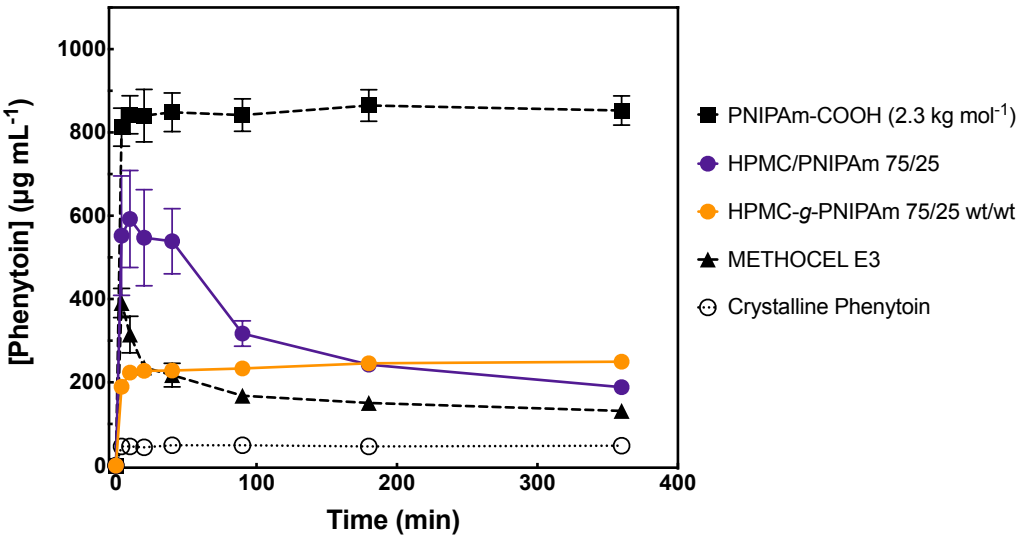

Figure A1.3. Dissolution profiles of solid dispersions of 10 wt% phenytoin with HPMC-*g*-PNiPAm (75 wt% HPMC, 25 wt% PNiPAm), PNiPAm homopolymer, HPMC, and HPMC/PNiPAm (75/25 wt/wt).

Switching away from graft polymers and towards more simple formulations, the potential of HPMC/PNiPAm blends as solid dispersion excipients were probed using a series wt/wt ratios (Figure A1.4). Across the full span of evaluated blends, an averaging dissolution behavior was seen that weighted towards the majority component. With increasing PNiPAm content, an increase in the achieved concentration of phenytoin was seen, as well as an increased delay of crystallization.

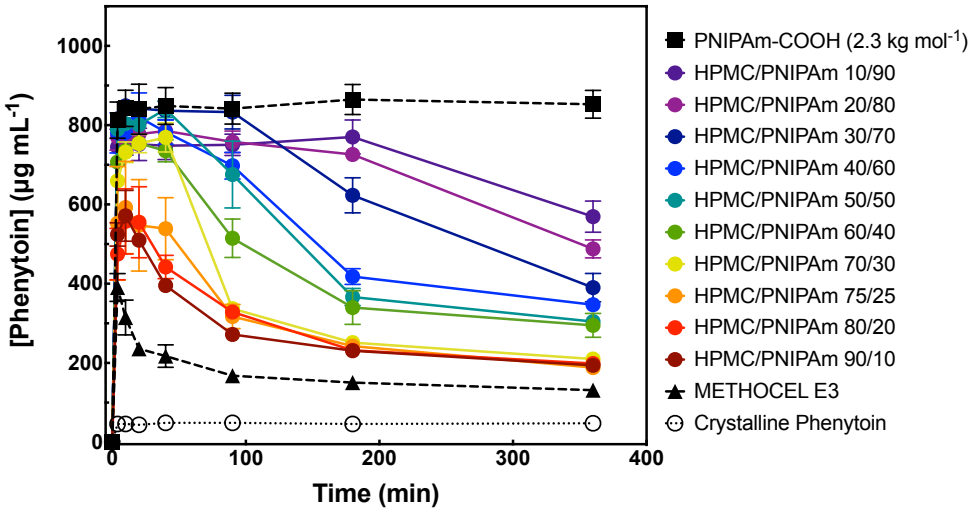

Figure A1.4. Dissolution profiles of solid dispersions of 10 wt% phenytoin with HPMC/PNiPAm wt/wt blends.

A1.5 Conclusions

This micro-study on HPMC-*g*-PNiPAm polymers as solid dispersion excipients for phenytoin yielded several key conclusions that were used to direct future studies. First, although graft polymers enhanced the dissolution performance of phenytoin, this enhancement was minimal, and gave little indication as a promising direction. Second, blends of HPMC and PNiPAm showed an averaging behavior that trended with the relative amounts of each excipient. Third, and most significantly, the low-molar-mass PNiPAm graft as a control solid dispersion excipient gave a dissolution profile that nearly met the engineering target of 1,000 µg mL^{-1} phenytoin for the full 6 h. This serendipitous find was used to motivate Chapter 3, which probed the influence of different features of this low molar mass sample, including end group and molar mass.

A1.6 References

(1) Yin, L.; Hillmyer, M. A. Preparation and Performance of Hydroxypropyl Methylcellulose Esters of Substituted Succinates for in Vitro Supersaturation of a Crystalline Hydrophobic Drug. *Mol. Pharm.* **2014**, *11* (1), 175–185.

(2) Ting, J. M.; Tale, S.; Purchel, A. A.; Jones, S. D.; Widanapathirana, L.; Tolstyka, Z. P.; Li, G.; Guillaudeu, S. J.; Bates, F. S.; Reineke, T. M. High–Throughput Excipient Discovery Enables Oral Delivery of Poorly Soluble Pharmaceuticals. *ACS Cent. Sci.*, **2016** *2* (10), 748–755.

(3) Li, Z.; Johnson, L. M.; Ricarte, R. G.; Yao, L. J.; Hillmyer, M. A.; Bates, F. S.; Lodge, T. P. Enhanced Performance of Blended Polymer Excipients through the Synergistic Action of Micelles and HPMCAS. *Langmuir* **2017**, *33* (11), 2837–2848.

(4) Roy, D.; Semsarilar, M.; Guthrie, J. T.; Perrier, S. Cellulose modification by polymer grafting: a review. *Chem. Soc. Rev.* **2009**, *38*, 2046–2064.

(5) Das, R.; Das, D.; Ghosh, P.; Ghosh, G.; Dhara, S. Novel pH-responsive graft copolymer based on HPMC and poly(acrylamide) synthesised by microwave irradiation: application in controlled release of ornidazole *Cellulose* **2015,** *22*, 313-327.

(6) Kim, B.Y.; Kang, H.S.; Kim, J.D. Thermo-sensitive microparticles of PNIPAM-grafted ethylcellulose by spray-drying method *J. Microencapsulation* **2002,** *19*, 661-669.

(7) Hufendiek, A.; Trouillet, V.; Meier, M.; Barner-Kowollik, C. Temperature Responsive Cellulose-*graft*-Copolymers via Cellulose Functionalization in an Ionic Liquid and Raft Polymerization *Biomacromolecules* **2014,** *15*, 2563-2572.

(8) Bokias, G.; Mylonas, Y.; Staikos, G. Synthesis and Aqueous Solutions Properties of Novel Thermoresponsive Graft Copolymers Based on a Carboxymethylcellulose Backbone *Macromolecules* **2001,** *34*, 4958-4964.